4967

NAME OF AUTHOR.....*PEEPLES, WAYNE JACOBSON*

TITLE OF THESIS.....*MAGNETO-TELLURIC Profiling*

.....*OVER A DEEP STRUCTURE*..

....

UNIVERSITY.....*Univ. of ALBERTA   Edmonton*

DEGREE.....*Ph.D.*.............YEAR GRANTED.....*1969 Fall*

(Signed).....*Wayne J. Peeples*

PERMANENT ADDRESS:

#302- 11130 57 Ave

Edmonton, Alta

Canada

DATED.....*Oct 28*.....1969

NL-91

THE UNIVERSITY OF ALBERTA

MAGNETO-TELLURIC PROFILING

OVER A DEEP STRUCTURE

by

Ⓒ WAYNE JACOBSON PEEPLES

A THESIS

SUBMITTED THE FACULTY OF GRADUATE STUDIES

IN PARTIAL FULFILMENT OF THE REQUIREMENTS FOR THE DEGREE

OF DOCTOR OF PHILOSOPHY

DEPARTMENT OF PHYSICS

EDMONTON, ALBERTA

FALL, 1969

UNIVERSITY OF ALBERTA

FACULTY OF GRADUATE STUDIES

The undersigned certify that they have read,
and recommend to the Faculty of Graduate Studies for
acceptance, a thesis entitled MAGNETO - TELLURIC
PROFILING OVER A DEEP STRUCTURE submitted by Wayne
Jacobson Peeples in partial fulfilment of the require-
ments for the degree of Doctor of Philosophy.

....
Supervisor

....

....

....

....
External Examiner

Date   September 19, 1969
       ....

ABSTRACT

Measurements of the surface electric and magnetic fields
in the period range 1 - 1,000 seconds were made along two
profiles in central and southern Alberta, Canada to determine
the crustal resistivities of this region. The analog data
obtained was electronically converted to digital form and
computer programs were written to analyse large amounts of
data using the Fast Fourier transform technique. Calculations
were made of the power spectra, the magnetotelluric impedance
tensor and the polarization characteristics of geomagnetic
micropulsations. The magnetotelluric impedance tensor
elements were computationally rotated into the principal
directions of resistivity and converted to apparent resistiv-
ities which exhibit a strong resistivity anisotropy. This
anisotropy is tentatively identified with inhomogenieties in
the basement composition and/or the lateral inhomogeniety
represented by the Rocky Mountain system. The magnetotelluric
results were compared with other geophysical results and
indicate the existence of deep lying structure slightly to
the south of a fault associated with a graben investigated by
Clowes, Kanasewich and Cumming (1968).

ACKNOWLEDGEMENTS

Finally I would like to acknowledge the contribution of my wife, Joanne, for her extreme patience, work, and understanding during the last months of deadline pressure.

TABLE OF CONTENTS

LIST OF ILLUSTRATIONS

Figure

Figure

CHAPTER I

INTRODUCTION

1.1 Purpose of the Investigation

Measurements of the electric and orthogonal magnetic fields at the surface of the earth were made at a series of stations forming the profile shown in Figure 1.3b. These measurements were made during the summer months of 1966 through 1968 as part of a program to determine the electrical properties of the earth's crust under the sedimentary basin of western Canada.

The original purpose of this research was to develop the technology of analysis in order to use the magnetotelluric method as a tool for the study of the crust and upper mantle which together with other geophysical methods could provide a more coherent picture of the subsurface structure. The recent seismic studies of Clowes, Kanasewich and Cumming (1968) have revealed a target for the application of the method. Kanasewich (1968) has proposed a large scale deeply buried structure trending north-east from the Kimberley region of British Columbia into Saskatchewan. The study of this structure by magnetotelluric methods will be the geological goal of this work.

1.2 A Historical Review of the Magnetotelluric Method

Although Clement as early as 1859 noted the coincidence

of telluric currents in North American and European telegraph lines with auroral activity, G. B. Airy (1868) was the first to make a systematic study of the telluric and magnetic field relationships. Terada (1917), Hirayama (1934) and Hatakeyama (1938) measured the dependence of the magnetic and telluric field relationships on the conductivity of the ground.

In 1950, Tikhonov first suggested using natural electromagnetic disturbances for crustal "sounding", and Cagnaird in 1953 published a comprehensive paper on the theory and graphical interpretation of the magnetic and telluric field relationships to determine subsurface electrical resistivities. By assuming the disturbance fields were plane electromagnetic waves, harmonically varying in time, which impinged on a horizontally stratified medium, Cagnaird presented a simple technique for matching theoretical apparent resistivity curves derived from layered models with measured apparent resistivities. Investigations by Wait (1954) and Price (1962) showed the effect of finite source dimensions on the measured apparent resistivities. However, Madden and Nelson (1964) showed that for reasonable earth conductivity models, the plane wave assumption appeared to be valid in the frequency range of interest to the magnetotelluric method.

Neves (1957) extended the theory to consider more complicated models with particular emphasis on two dimensional geometries using the method of finite differences. Several other workers have considered special two dimensional models,

the vertical contact fault within a layer over a uniform basal half space was solved analytically by d'Erceville and Kunetz (1962) and this solution was extended by Rankin (1962) to the case of the vertical dike problem. Cantwell (1960), and Bostick and Smith (1962) proposed techniques to obtain the directions of the principal axes of a conductivity structure for an anisotropic earth while O'Brien and Morrison (1967) solved analytically the general n-layer anisotropic boundary value problem. Madden and Nelson (1964), Sims and Bostick (1969), Morrison et al (1968) and others have indicated analytic techniques to calculate the elements of the magnetotelluric impedance matrix. This matrix relates the telluric and geomagnetic fields for two and three dimensional structures.

Magnetotelluric investigations from a variety of locations in North America, Europe, and Russia have been reported by Vozoff, Hasegawa, and Ellis (1963), Srivastava, Douglas and Ward (1963), Caner and Auld (1968), Whitham and Anderson (1966), Vozoff et al (1969), Berdichevsky (1966), and many others. A compilation of known apparent resistivity curves was assembled by Fournier (1963).

Some interpretation of magnetotelluric results from various arrays and profiles has been attempted. Swift (1967) studied an electrical conductivity anomaly in the south-west United States, and in 1968 Vozoff and Swift reported on studies of a salt basin in northern Germany.

1.3 The Geology and Structure of Southern Alberta

The region involved in this investigation lies in the sedimentary basin of western Canada. A cross section of sedimentary features in this area is shown in Figure 1.3a. This cross section begins at Nordegg in the Alberta foothills and passes through Leduc (see Figure 1.3b) making the cross section approximately perpendicular to the strike of the Rocky Mountain System. Since the vertical scale of Figure 1.3a has been expanded by a factor of 42 it is seen that the sedimentary layers are locally horizontal and uniform in thickness. This basin was thought to be horizontally iso-tropic electrically and, therefore, an ideal location for short period magnetotelluric analysis.

Burwash (1957) determined from wells that the depth to the Precambrian surface ranges from about 1.43 kilometers near the Saskatchewan border to about 3.6 kilometers at the base of the foothills.

Garland and Burwash (1959) have shown that the major part of the Bouguer gravity anomoly field over central Alberta must be attributed to lithological changes in the Precambrian basement. The lithological changes could lead to an anisotropy in electrical conductivity due to material anisotropy and/or other lateral structural inhomogenieties.

Richards and Walker (1959), Cumming and Kanasewich (1966), and others agree that there exists another major seismic discontinuity below the Precambrian surface known locally as the Riel discontinuity, which possibly corres-

Figure 1.3a: The Western Canada Sedimentary Basin

(after the Alberta Society of Petroleum Geologists).
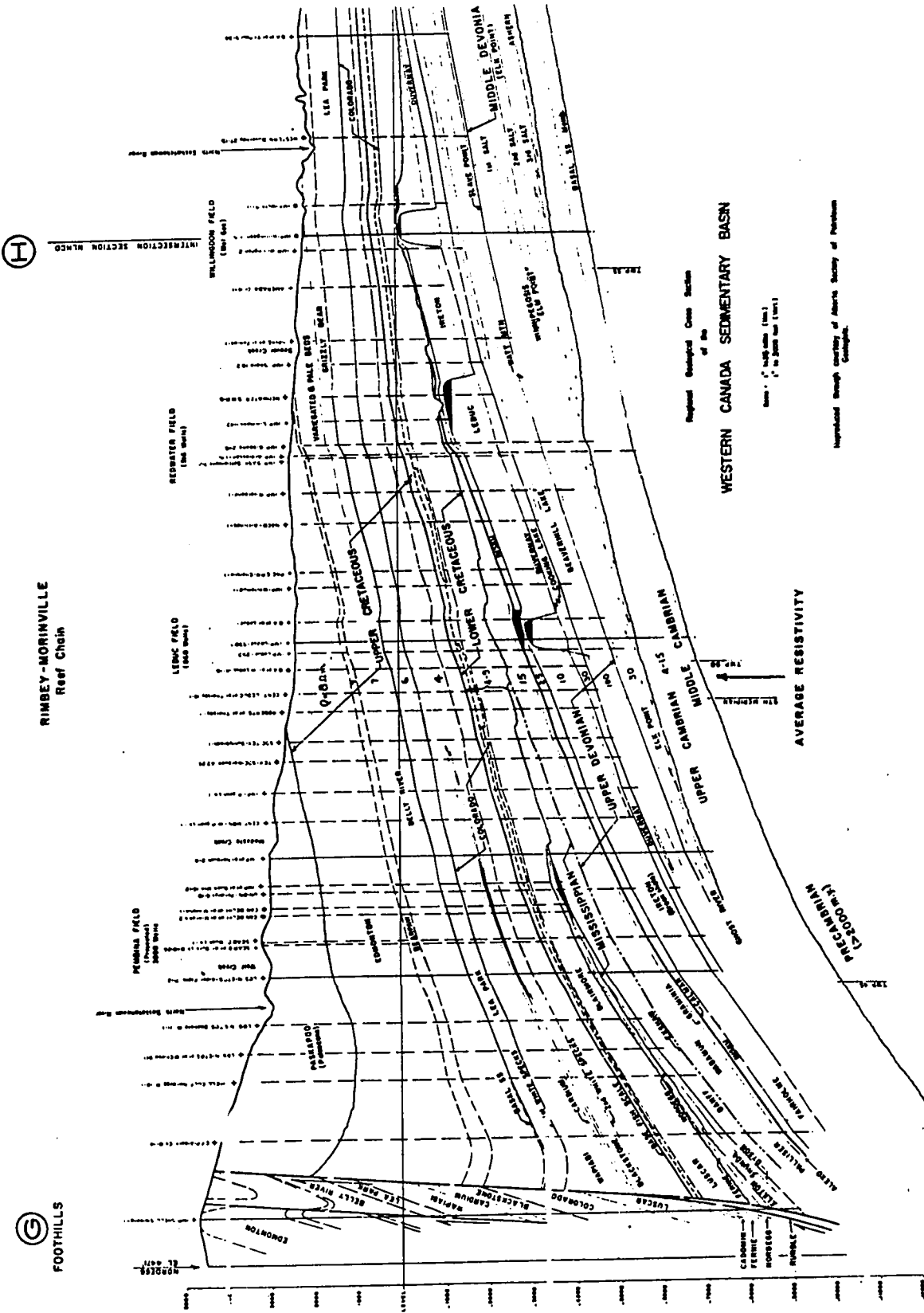
RIMBEY-MORINVILLE
Reef Chain

Regional Geological Cross Section
of the
WESTERN CANADA SEDIMENTARY BASIN

AVERAGE RESISTIVITY

Figure 1.3b: Locations of magnetotelluric field stations and other regions of interest.

Scale in Miles
0   50   100

ALBERTA

LEGEND
● TOWN
○ MT RECORDING SITE

120° 118° 114° 110° 60°

55°   55°

MEANOOK ○

EDMONTON ●
        ● LEDUC

NORDEGG ●   ○ RD

            ○ HT
CALGARY ●
                ○ L7
              ○   ○ L5
            KC ○
            CA ○   ○ TU

49°
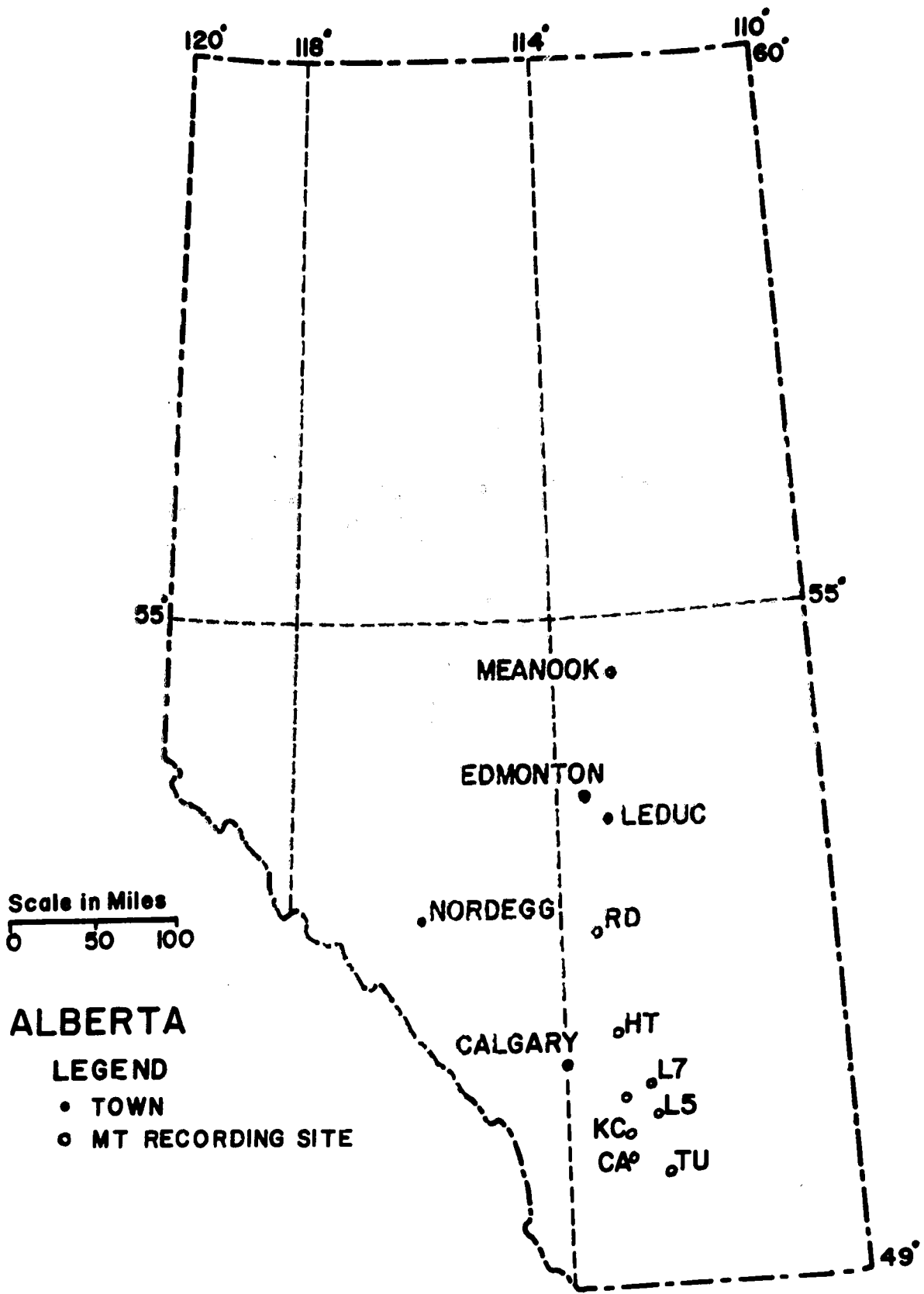
ponds to the European discontinuity known as the Conrad. The Riel appears to vary in depth from 26 to 37 kilometers. The next major seismic discontinuity is the Mohorovičić which varies in depth from 38 to 47 kilometers in Alberta.

Clowes, Kanasawich and Cumming (1968) have used deep crustal seismic reflections at near vertical incidence to detect an elongated precambrian graben-horst structure (rift valley) in southern Alberta (Figure 4.3c). This structure seems to coincide with a notable anomalous linear trend in gravity (Figure 4.3a) and magnetic surveys (Figure 4.3b) which extends across Alberta and into British Columbia.

1.4 Outline of the Thesis

Chapter two will present the theoretical development of the apparent resistivity function, assuming plane wave incidence for an isotropic, horizontally layered earth model. The basic magnetotelluric impedance tensor relationships for a two-dimensional structure are introduced and the properties of the impedance tensor presented. This is followed by a short discussion of the effects of lateral resistivity changes and the effect of finite source dimensions on magnetotelluric quantities.

Chapter three contains a brief description of the recording equipment and the digital processing technique used for this study followed by a basic description of the procedure used to calculate the power spectra of the magnetotelluric fields, and how the spectra were used to

calculate the magnetotelluric impedance tensor.

In chapter four, the basic analyses for eight locations in southern Alberta at which magnetotelluric results were obtained are presented and correlated with other geophysical measurements. An explanation is offered for the ambiguous results obtained by other workers in Alberta and for the anisotropic resistivity properties which are consistent over nearly the entire province.

Chapter five contains the conclusions of this work and suggestions for further work.

CHAPTER II

MAGNETOTELLURIC THEORY

2.1 Basic Magnetotelluric Theory

The basic theory of magnetotelluric fields is contained in a boundary value problem involving Maxwell's equations and the resultant electromagnetic wave equation. The relationship between orthogonal components of the electric and magnetic fields measured at the surface of the earth are a measure of the electrical properties of the earth.

The reference coordinate frame for the theoretical development which follows is a right-handed cartesian system with the positive x axis northward and z vertically downward. The earth is initially considered to consist of n - 1 horizontally stratified, isotropic, homogeneous conducting layers above a basal half space. The origin of the co-ordinate system lies on the upper surface of the first layer as shown in Figure 2.1. The rationalized MKS system will be used in the theoretical discussion.

The natural electromagnetic disturbance fields are thought to originate in the ionosphere or magnetosphere at altitudes of 100 kilometers and greater and these fields then propagate downward to the surface of the earth. The similarity of the magnetotelluric field over large regions at the earth's surface was noticed by Schlumberger and Kunetz (1946) and Kunetz (1953); thus Cagnaird (1953) made

Figure 2.1: The horizontally stratified earth model used in the theoretical development of the apparent resistivity function.

Earth's Surface $z = 0$

Layer 1 σ_1 ϵ_1 h_1

$z = z_1$

Layer 2 σ_2 ϵ_2 h_2

$z = z_2$

z

$z = z_i - 2$

Layer i − 1 σ_{i-1} ϵ_{i-1} h_{i-1}

$z = z_i - 1$

Layer i σ_i ϵ_i h_i

$z = z_i$

Layer i + 1 σ_{i+1} ϵ_{i+1} h_{i+1}

$z = z_i + 1$

$z = z_{n-1}$

Layer n − 1 σ_{n-1} ϵ_{n-1} h_{n-1}

$z = z_n$

Layer n σ_N ϵ_N

∞
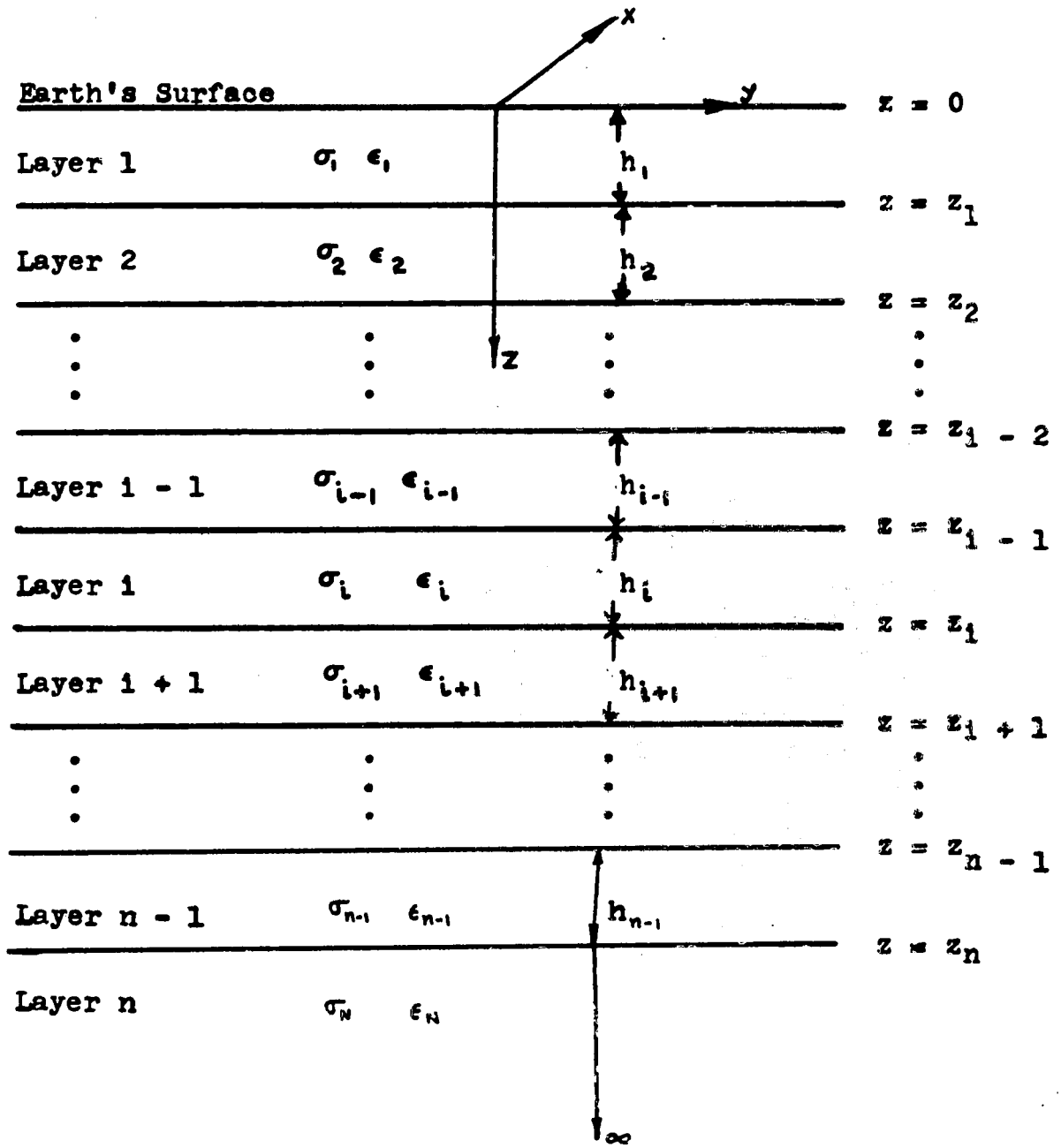
the *a priori* assumption that the natural electromagnetic disturbances could be treated as plane waves.

Since the layers of the model are assumed to contain no primary sources, Maxwell's equations in the ith layer are given by:

$$\nabla \times \vec{E} = - \frac{\partial \vec{B}}{\partial t} \qquad \text{2.1 - 1}$$

$$\nabla \times \vec{H} = \vec{J} + \frac{\partial \vec{D}}{\partial t} \qquad \text{2.1 - 2}$$

$$\nabla \cdot \vec{D} = \rho = 0 \qquad \text{2.1 - 3}$$

$$\nabla \cdot \vec{B} = 0 \qquad \text{2.1 - 4}$$

where $\vec{J} = \sigma\vec{E}$, $\vec{D} = \varepsilon\vec{E}$, and $\vec{B} = \mu\vec{H}$.

For a steady state sinusoidal time dependence of the form $e^{-j\omega t}$ for the electric and magnetic fields, equations 2.1 - 1 and 2.1 - 2 can be written:

$$\nabla \times \vec{E} = j\omega\mu\vec{H} \qquad \text{2.1 - 5}$$

$$\nabla \times \vec{H} = \sigma\vec{E} - j\omega\varepsilon\vec{E}. \qquad \text{2.1 - 6}$$

Taking the curl of equations 2.1 - 5 and 2.1 - 6 and assuming ε and σ are constant within each layer, we obtain two vector Helmholtz equations

$$\nabla^2 \begin{bmatrix} \vec{E} \\ \vec{H} \end{bmatrix} + k^2 \begin{bmatrix} \vec{E} \\ \vec{H} \end{bmatrix} = 0 \qquad \text{2.1 - 7}$$

where $k^2 = j\omega\sigma\mu + \varepsilon\mu\omega^2$. Solutions of the Helmholtz equations are given by:

$$\begin{bmatrix} \vec{E} \\ \vec{H} \end{bmatrix} = \begin{bmatrix} \vec{E}_O \\ \vec{H}_O \end{bmatrix} e^{j\vec{K}\cdot\vec{r} - j\omega t} \qquad \text{2.1 - 8}$$

where

$$\vec{K} = (k_x, \ k_y, \ k_z,)$$

$$\vec{r} = (x, \ y, \ z).$$

The frequencies considered in magnetotelluric methods are nearly always less than 10 Hz. Using normal parameters of conductivity, permittivity, and permeability appropriate to materials composing the earth, the displacement currents are negligible in comparison to conduction currents for the low frequencies considered herein

$$|j\omega\sigma\mu| >> |\epsilon\mu\omega^2|.$$

The Helmholtz equations then reduce to diffusion equations with a diffusion constant (skin depth) given by

$$\delta = \sqrt{\frac{2}{\mu\omega\sigma}}. \qquad\qquad 2.1 - 9$$

Since the wave number of the electromagnetic field in air is much less than in the earth,

$$k^2_{Air} = \epsilon_o\mu_o\omega^2 << |\ j\omega\mu\sigma\ | = k^2_{Earth},$$

at the air-earth interface the incident plane waves are refracted and propagate through the earth nearly parallel to the vertical axis for nearly all incident angles.

For the geometry and conditions stated above, $\vec{E}$ and $\vec{H}$ are independent of x and y and thus all derivatives of the field with respect to x and y vanish. Thus, in the ith layer a solution of equation 2.1 - 7 is given by

$$E^i_{x} = \left[A^i e^{jk_i z} + B^i e^{-jk_i z}\right] e^{-j\omega t} \qquad \qquad 2.1 - 10$$

and from equation 2.1 - 5

$$H^i_{y} = \frac{+k_i}{\omega\mu} \left[A^i e^{jk_i z} - B^i e^{-jk_i z}\right] e^{-j\omega t}. \qquad 2.1 - 11$$

For the simple case of a basal half space of uniform conductivity, the ratio of the electric field strength to the magnetic field strength can be defined as the characteristic plane wave impedance of the medium:

$$Z_c = \frac{E}{H} = \frac{\omega\mu}{k_1} \cdot \frac{A\,e^{jk_1 z} + B\,e^{-jk_1 z}}{A\,e^{jk_1 z} - B\,e^{-jk_1 z}}$$

$$= \frac{\omega\mu}{k_1} \coth\left[k_1 z + \ln\sqrt{\frac{A}{B}}\right]. \qquad 2.1 - 12$$

The reflection and transmission coefficients, A and B, are determined by the evaluation of the impedance at two different positions $z = z_1$, z_2 within the medium.

$$Z(z_1) = \frac{\omega\mu}{k_1} \coth\left[k_1 z_1 + \ln\sqrt{\frac{A}{B}}\right]$$

therefore:

$$\ln\sqrt{\frac{A}{B}} = \coth^{-1}\left[\frac{k_1}{\omega\mu} Z(z_1)\right] - k_1 z_1. \qquad 2.1 - 13$$

At the second position in the medium:

$$Z(z_2) = \frac{\omega\mu}{k_1} \coth\left[k_1(z_2 - z_1) + \coth^{-1}\left\{\frac{k_1}{\omega\mu} Z(z_1)\right\}\right].$$

Letting $z_2 = 0$ and $z_1 \to \infty$:

$$Z_o(\omega) = \frac{\omega\mu}{k_1} = -\left[j\omega\mu\rho\right]^{\frac{1}{2}} \qquad \qquad 2.1 - 14$$

and the resistivity of the medium is given by:

$$\rho(\omega) = \frac{1}{j\omega\mu} Z_o(\omega) = \frac{1}{j\omega\mu} \left| \frac{E_x}{H_y} \right|^2. \qquad 2.1 - 15$$

For an n - layer electrically isotropic earth, both the electric field, E_x, and the magnetic field H_y, must be continuous across the boundaries between layers and therefore the impedance at the top of layer i must be equal to the impedance at the bottom of the next upper layer, i - 1. The impedance measured at the surface of the earth can therefore be written as (Berdichevski - 1960):

$$Z^n_o(\omega) = \frac{-\omega\mu}{k_1} \coth \left[k_1 h_1 + \coth^{-1}\left\{\frac{k_1}{h_2} \coth (k_2 h_2 \right.\right.$$

$$\left. + \coth^{-1}\left\langle \frac{k_2}{k_3} \cdots \coth^{-1}\left(\frac{k_{n-2}}{k_{n-3}} \coth \right.\right.\right. ($$

$$\left.\left.\left. k_{n-1} h_{n-1} + \coth^{-1} \frac{k_n}{k_{n-1}} \right) \cdots \right\rangle\right\}\right] \qquad 2.1 - 16$$

and the apparent resistivity of the medium can now be defined as:

$$\rho_a(\omega) = \frac{1}{\omega\mu} \left| Z^n_o(\omega) \right|^2. \qquad 2.1 - 17$$

The apparent resistivity thus represents a weighted resistivity value for all layers and is the resistivity of an equivalent homogeneous half space at a particular frequency.

2.2 The Basic Magnetotelluric Relationships for an
     Electrically Anisotropic Earth

     The importance of considering anisotropic conductivity

in models has been emphasized by Cantwell (1960), Bostick
and Smith (1962), Ward and Morrison (1966) and others. Mann
(1965) gave an analytical description of the effect of a
plane wave incident on a basal half space with anisotropic
electrical properties. This work was extended by O'Brien
and Morrison (1967) to consider plane wave incidence on a
horizontally layered medium in which each layer was
electrically anisotropic and the principal resistivity axis
of each layer aligned in an arbitrary horizontal direction.

The works of both Mann and O'Brien and Morrison have
shown that if the wave impedance is defined as the scalar
ratio of the electric field strength to the orthogonal
magnetic field strength then the impedance is highly
dependent on changes in the polarization of the disturbance
fields.

When the conditions of model anisotropy and field
polarization changes are considered, the relationship
between the telluric and geomagnetic field can be expressed
as a tensor:

$$\begin{vmatrix} Ex \\ Ey \end{vmatrix} = \begin{vmatrix} z_{11} & z_{12} \\ z_{21} & z_{22} \end{vmatrix} \cdot \begin{vmatrix} Hx \\ Hy \end{vmatrix} \qquad\qquad 2.2 - 1$$

The mathematically equivalent admittance formulation
introduced by Cantwell in 1960 can also be used. In the
impedance formulation, the electric field is assumed to
depend on both the parallel and the perpendicular magnetic
fields. Changes in polarization of the source magnetic

field should have no effect on the tensor elements if the source field is a plane or quasi-plane wave.

The off diagonal elements $(z_{ij}; i \neq j)$ of the impedance tensor can now be used to interpret geological structure if the principal axes of a two dimensional conductivity structure are aligned with the coordinate measuring axes. If the measuring axes are not aligned in the directions of principal conductivity then the tensor elements can be rotated computationally as follows.

Consider a two dimensional Cartesian coordinate system (x, y). When the system is rotated clockwise through some angle, θ, to form a new orthogonal system (x', y'), the transformed field components are given by:

$$\vec{E}'(x', y') = \gamma\vec{E}(x, y)$$

$$\vec{H}'(x', y') = \gamma\vec{H}(x, y)$$

$$\text{2.2 - 2}$$

where the orthogonal transformation matrix, γ, is given by

$$\gamma = \begin{vmatrix} \cos \theta & \sin \theta \\ -\sin \theta & \cos \theta \end{vmatrix}.$$

$$\text{2.2 - 3}$$

The rotated impedance tensor, Z', is given by

$$Z' = \gamma Z \gamma^{T}.$$

$$\text{2.2 - 4}$$

For an isotropic and homogeneous earth

$$z'_{11} = z'_{22} = 0$$

and

$$\text{2.2 - 5}$$

$$z'_{21} = -z'_{12}$$

for all θ.

Analysis of anisotropic layered models in which plane wave incidence is assumed reveals the existence of two skin depths, and two modes of propagation for plane waves for any anisotropic layer of the model. These two modes are independent and propagate in the positive and negative z direction. Thus for a model with a single layer anisotropy, or a multi-layer anisotropy in which the principal directions of conductivity are aligned, there exists a rotation angle, θ, such that the rotated tensor elements exhibit the properties:

$$z'_{11} = z'_{22} = 0$$

$$z'_{12} \neq z'_{21}$$

2.2 - 6

and it is valid to treat the resistivities in the two principal directions of anisotropy of the model as two separate isotropic resistivity systems.

To determine whether a two dimensional resistivity interpretation is possible, consider equation 2.2 - 4. It is easily shown that the following expressions are invariant under an orthogonal transformation:

$$z'_{11} + z'_{22} = z_{11} + z_{22}$$

and

2.2 - 7

$$z'_{12} - z'_{21} = z_{12} - z_{21}.$$

Since $z_{11} + z_{22}$ should vanish for the ideal two dimensional geometry, the ratio

$$SKEW = \frac{z'_{11} + z'_{22}}{z'_{12} - z'_{21}}$$

measures the skewness of the impedance tensor and thus

provides a measurable two dimensionality coefficient.

2.3 The Effects of Lateral Inhomogeniety

The addition of lateral resistivity changes to models

representative of the earth, while being a better represen-

tation of some of the actual geophysical situations encoun-

tered, nevertheless leads to great mathematical difficulties.

For this reason the exact solution of even a highly idealized

model with laterally changing resistivity is of great

benefit.

D'Erceville and Kunetz (1962) have analytically solved

the problem of a vertical contact of infinite length sepa-

rating two formations of resistivities ρ_1 and ρ_2 as shown

in Figure 2.3a. Their solution considered the case where

the magnetic field, $\vec{H}$, is parallel to the fault and constant

at the air-earth interface (z = 0) of the model. The

mathematical details of their solution will not be reproduced

here as they are readily available in the literature.

Figure 2.3a shows the results of d'Erceville and

Kunetz's solution for various resistivity ratios $(\frac{\rho_2}{\rho_1} =$

4, 9, 39, 100) across the contact. As can be seen, only at

distances greater than one skin depth does the $|\frac{Ex}{H}|$ ratio

approach the value of the non-fault model. This implies

that for any location in which a large lateral resistivity

contrast of sufficient spatial extent occurs, the apparent

Figure 2.3a: Variations of the $\left|\frac{E}{H}\right|$ ratio for an infin-
itely deep vertical contact fault where the electric
polarization is normal to the strike of the fault.
(After d'Erceville and Kunetz - 1962)
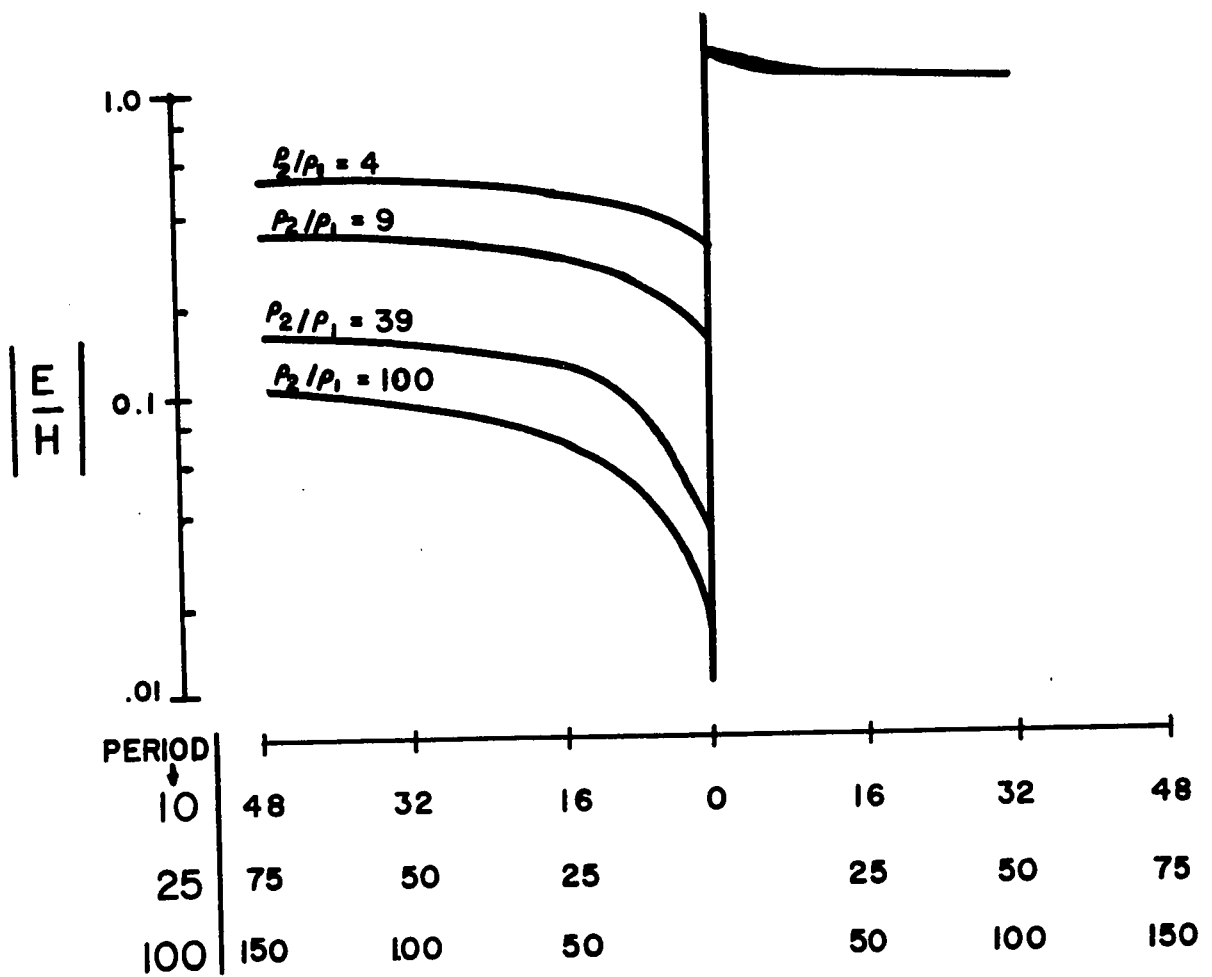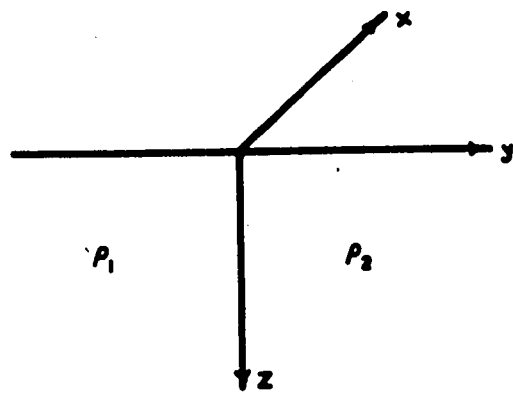
HORIZONTAL SCALE (KM) FOR VARIOUS PERIODS

$(\rho_1 = 400 \; \Omega M)$

resistivity function is biased by the fault structure and an accurate estimation of subsurface resistivities by the magnetotelluric method is doubtful unless a regional survey is made.

2.4 The Effect of Sources of Finite Size on Magnetotelluric Analysis

There exist no physical sources in nature which produce waves which are completely describable as mathematical plane waves. However valid the plane wave approximation may be for many cases of physical interest the effect of finite source dimensions on the magnetotelluric apparent resistivity function must be considered. This effect will be examined following the arguments of Wait (1954), Price (1962) and Morrison (1967).

Consider the two dimensional problem of a source above a horizontally layered earth model. The electric and magnetic fields produced by the source can be represented by an integral solution of the separated wave equation of the form:

$$\psi = \int_{-\infty}^{\infty} f(\lambda) \; e^{j\lambda x} \; e^{j\alpha z} \; d\lambda \qquad\qquad 2.4 - 1$$

(Morse and Feshback - 1953) where the λ's are associated with an effective propagation constant in the x direction and the effective horizontal spatial wavelength, λ_h, is given by:

$$\lambda_h = 2\pi/\lambda. \qquad\qquad 2.4 - 2$$

The horizontal gradient of the field, $\frac{\partial \psi}{\partial x}$, gives a measure of the horizontal spatial changes of the field and therefore a horizontal scaling length, δ_h, can also be defined.

$$\delta_h = 1/\lambda \qquad \qquad 2.4 - 3$$

where δ_h is the horizontal distance over which the field varies appreciably.

If the source had generated a plane wave which is incident upon the earth at an arbitrary angle θ, then λ would be associated with $k_o \sin \theta$. Since λ is a constant which characterizes the field in free space, let us denote λ as:

$$\lambda = k_o s \qquad \qquad 2.4 - 4$$

where k_o is the propagation constant in free space. The horizontal scaling length is then expressed as:

$$\delta_h = 1/k_o s. \qquad \qquad 2.4 - 5$$

Wait (1962) has shown that the surface impedance at the ith layer may be expressed in terms of the impedance of the $i - 1$ interface and the thickness and parameters of the layer as:

$$z_{i+1} = \eta_{i+1} \frac{z_i - \eta_{i+1} \tanh [j \, u_{i+1} \, h_{i+1}]}{\eta_{i+1} - z_i \tanh [j \, u_{i+1} \, h_{i+1}]} \qquad 2.4 - 6$$

where

$$u_i = \sqrt{k_i^2 - \lambda^2} = \sqrt{\sigma_i \mu_o \omega - \omega^2 \mu \epsilon s^2}$$

and

$$\eta_i = \frac{-j\, u_i}{\sigma_i}.$$

It is easily shown that the impedance value at the surface of a basal half space may be expressed as:

$$Z_o = \frac{E}{H} = -\sqrt{\frac{\omega \mu o}{j \sigma_1}} \left[1 + j\, \frac{\omega \epsilon}{\sigma_1}\, s^2 \right]^{\frac{1}{2}}. \qquad 2.4 - 7$$

For any conductivity and frequency parameters of this model, the maximum value of s can be calculated that will not radically alter the plane wave impedance value. From the above equation it can be seen that if $s < 0.1 \sqrt{\sigma/\omega \epsilon}$, the plane wave impedance is changed by less than 10% for a basal half space.

When the impedance value changes by 10% from the plane wave impedance, let s define the critical horizontal scale length:

$$L_c = 1/k_o s. \qquad 2.4 - 8$$

Morrison (1967) has used this technique to calculate the critical lengths (Figure 2.4a) for four models shown in Figure 2.4b.

As an example of a physically realizable source, consider a line current flowing in the y direction at a constant height, $z = -h$, above a layered earth. The field produced

Figure 2.4a: Critical length versus period for four

models described in figure 2.4b (after Morrison - 1967).
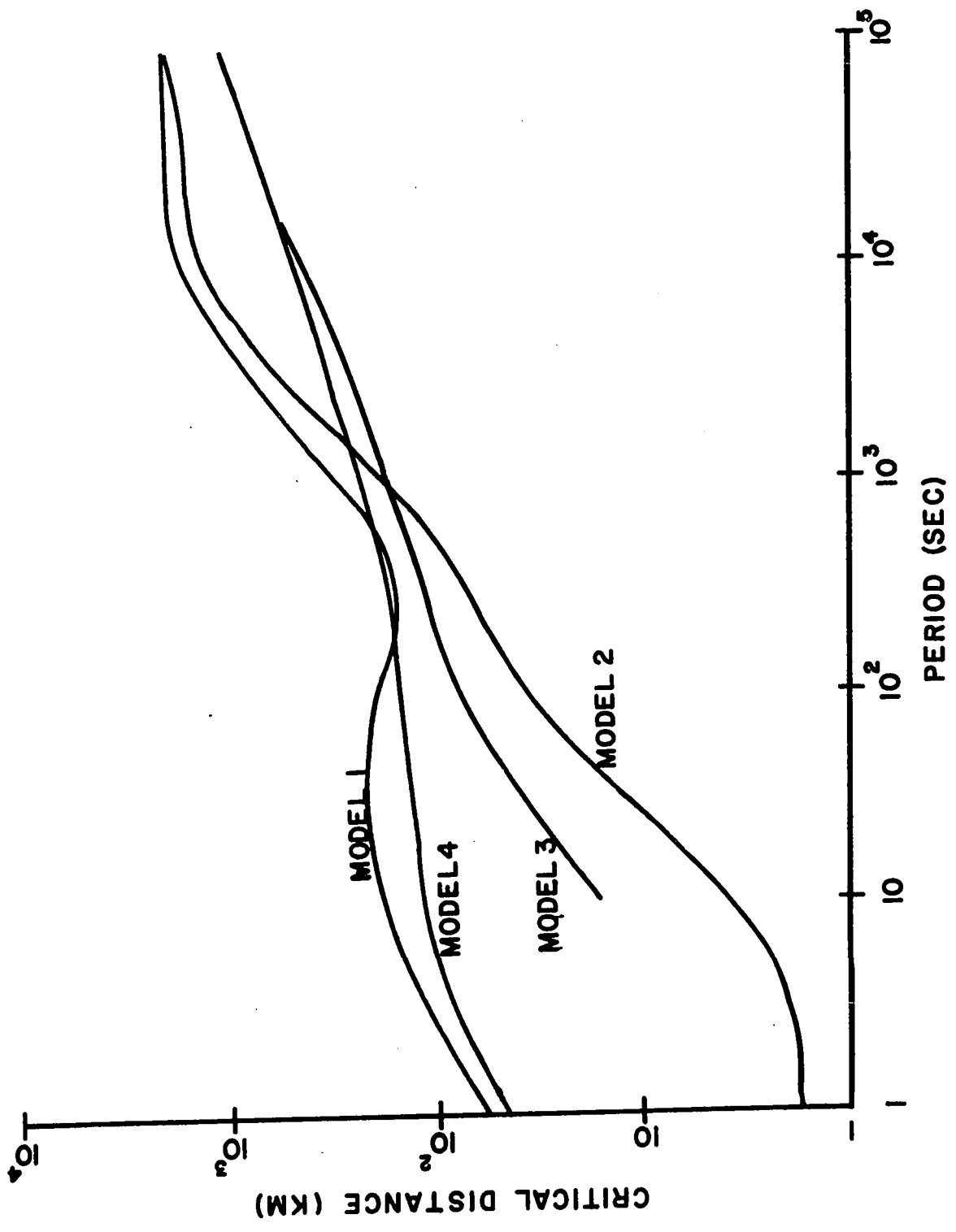
Figure 2.4b: Four resistivity models of the earth:

    Models 1 and 2: Fournier, Ward and Morrison
       Model (1963)

    Model 3: Modified Cantwell - McDonald Model
       (Madden and Nelson - 1964)

    Model 4: Cantwell - McDonald Model (Cantwell -
       1960, McDonald - 1957)

MODEL 1 ·—·—·
MODEL 2 ////
MODEL 3 ● ● ●
MODEL 4 ——
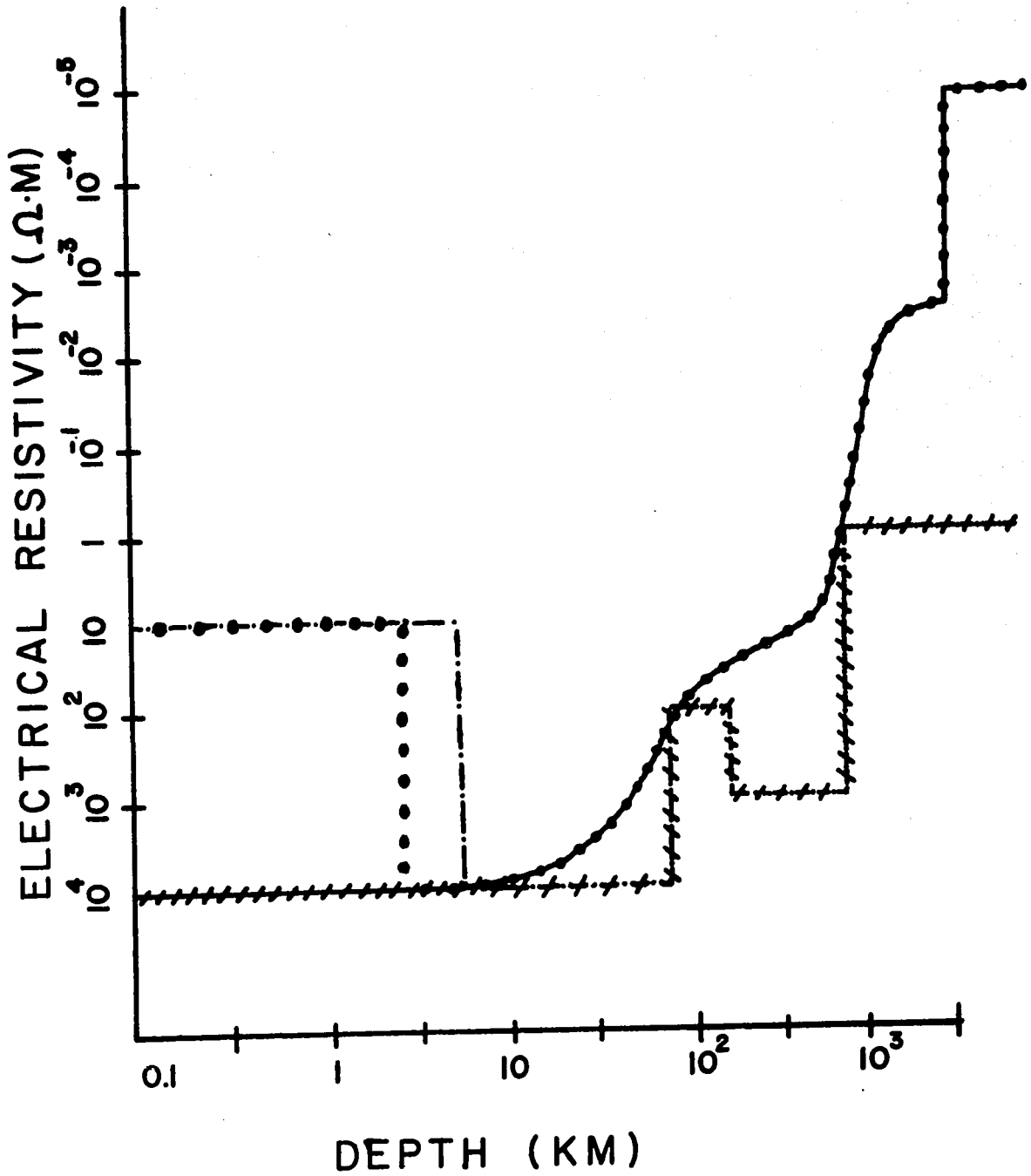
by the line source as measured at the surface of the earth
is given by:

$$E_y = A \int_\infty^\infty \frac{e^{-ju_o h} [1 + R(\lambda)]}{u_o} e^{-j\lambda x} d\lambda \qquad 2.4 - 9$$

(Wait - 1954) where $(1 + R(\lambda))$ accounts for the presence of
the medium at $z = 0$ and

$$R(\lambda) = \frac{u_o - u_1}{u_o + u_1}$$

$$u_i = \sqrt{k_i^2 - \lambda^2}.$$

Since the integrand of equation 2.3 - 9 decreases rapidly
for $\lambda > k_o$, then $u_o \approx j\lambda$ and $(e^{-ju_o h})/u_o \to e^{-\lambda h}/\lambda$, thus
the integrand becomes small for $\lambda > 1/h$, and the critical
length (equation 2.4 - 8) becomes:

$$L_c = 1/\lambda \approx h. \qquad 2.4 - 10$$

We may assume therefore that the critical length for a line
current source is approximately equal to the height of the
current system above the earth. If the line current is
located at an altitude of 100 - 200 kilometers, then from
Figure 2.4a we see that magnetotelluric analysis will only
be valid for periods less than 500 seconds if we are
studying a model with a highly conducting first layer
similar to the sedimentary basin of Alberta.

Although other source configurations may exist and
invalidate the above analysis, this formulation does show
the necessity for considering the effect of sources on
magnetotelluric quantities.

CHAPTER III

DETECTION AND ANALYSIS OF THE MAGNETOTELLURIC FIELD

3.1 Detection and Recording of the Magnetotelluric Signal

The telluric detection system consists of two inch
copper pipe used as electrodes with the electrode separation
approximately 600 feet (this separation distance varied
from location to location due to physical limitations
imposed by the area). The electrical potential difference
between electrodes was fed through a 100 µf capacitor to
block D.C. potentials due to polarization at the electrodes
and then into a filter/preamp/amp section.

The magnetic detection system consisted of two bobbins
each wound with 16,000 turns of #28 GA enameled copper wire
and then mounted on a 60 x 3/4 inch high permeability core.
The total inductance was 850 henrys at 0.1 Hertz with a
total impedance of 845 Ω. This unit was then sealed in a
waterproof plastic tube. The current generated by the
coil was fed to a galvanometer, and light beam coupled to
an amplifier section. The general form of the calibrated
responses of the telluric and magnetic systems (including
coils) are shown in Figure 3.1a.

The output of the two telluric detection systems
(Ex/ geographic north-south; Ey/ geographic east-west) and
the three magnetic detection systems (Hx/ geographic north-
south; Hy/ geographic east-west; and Hz/ vertical component)

Figure 3.1a: Calibrated phase and amplitude response for
the telluric and magnetic detection systems.

LAG

LEAD

MAGNETIC

ELECTRIC

PHASE (DEGREES)

0

60

120

180

240

10^3

10^2

10^1

PERIOD (SEC)
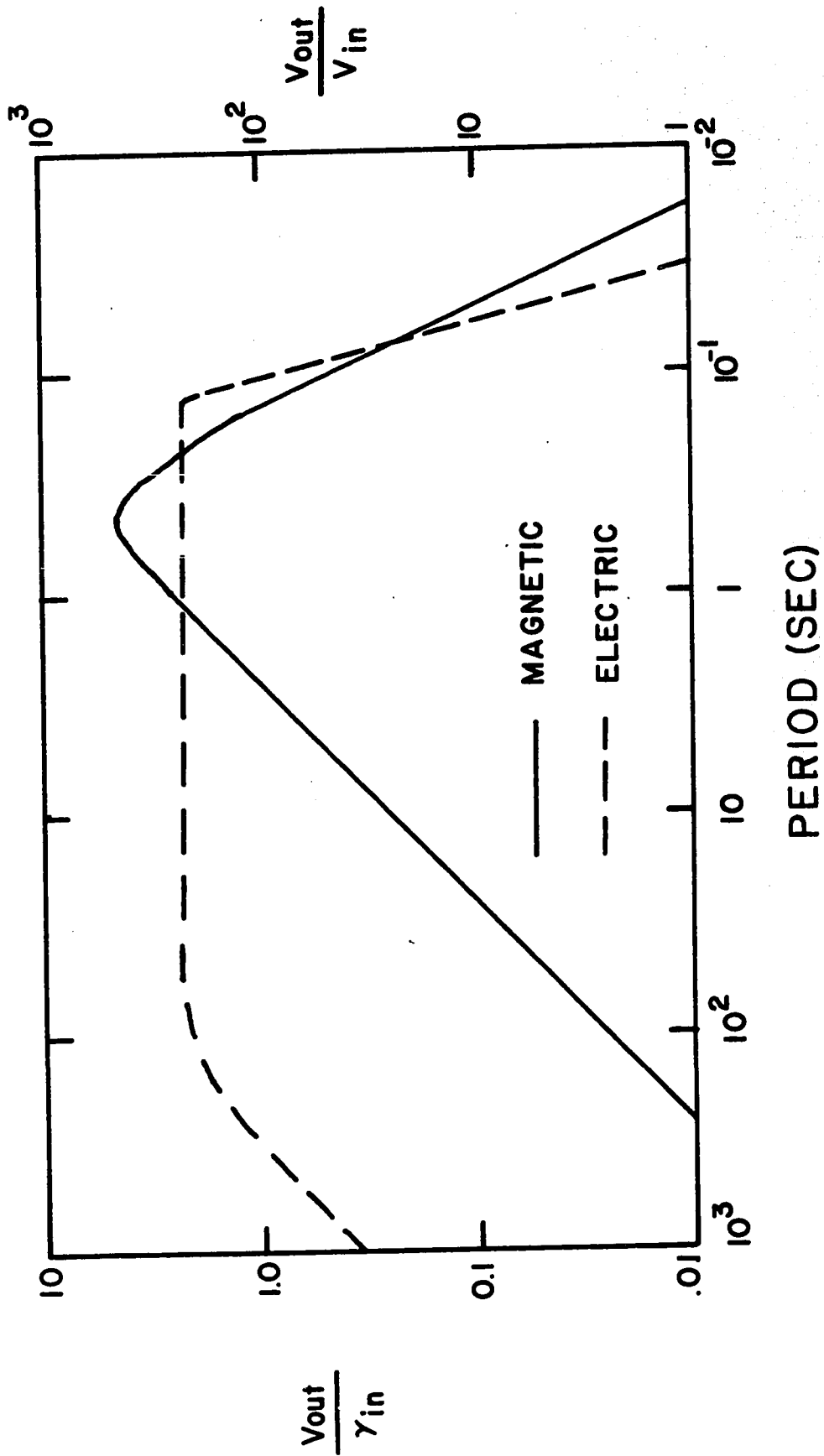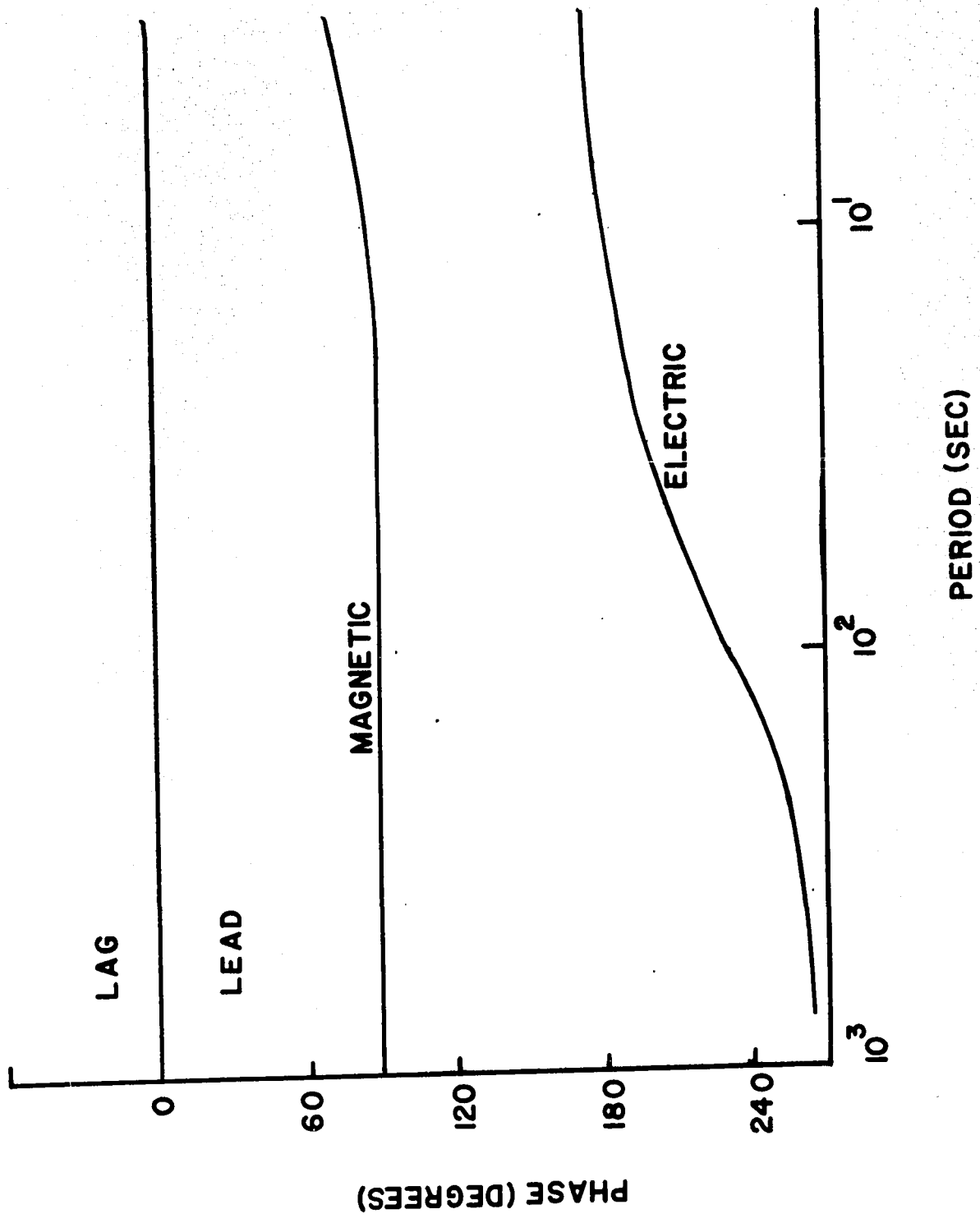
along with WWVB time signals were recorded in analogue form on seven channel FM magnetic tape at 15/16 i.p.s. using a Precision Instruments tape recorder. Simultaneously, a Brush paper recorder was used to monitor visually the signals and to provide an editing facility prior to the selection of records for digitization. A block diagram of the recording apparatus is shown in Figure 3.1b.

A series of calibration frequencies was fed through the system at the beginning and end of each twelve hour tape to provide a constant check on the phase and amplitude stability of the detection system.

3.2 Digital Processing of the Magnetotelluric Data

Records approximately 3.6 hours in length were selected for digitization from those analogue field tapes which were free of saturation (signal beyond the dynamic range of the FM recording system) and discontinuities (D.C. steps, etc.). The selection was based on the visual inspection of paper records obtained from replaying the FM tapes. The six channels of data (H_x, H_y, H_z, E_x, E_y, Time) in analogue form were then replayed at 30 i.p.s., alias filtered, and sampled by an electronic analog to digital converter at a rate of 15 samples per second per channel to give a digitizing interval of 2.13 seconds and a Nyquist frequency of .234$\cdots$ Hz.

Digital data in 12 bit binary form (with the least significant bit suppressed and used as a flag for channel identification) were recorded in blocks of 1200 two character

Figure 3.1b: A block diagram of the magnetotelluric

recording system.
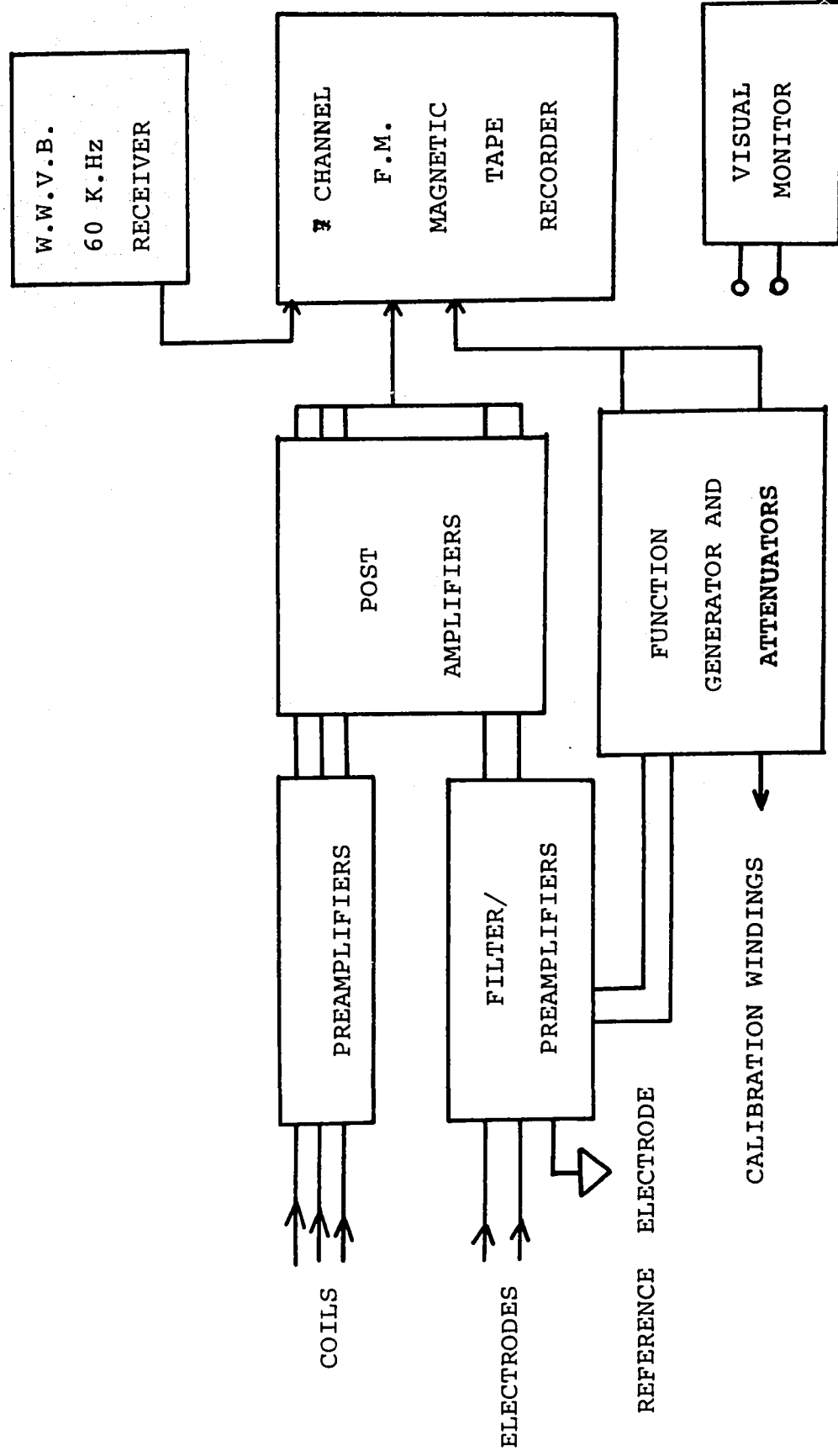
words on six channel asynchronous Kennedy seven track digital
tape recorders. Blocks were written alternately on digital
tapes by two Kennedy tape recorders to provide the necessary
I.R.G. (inter record gap) required for the tape reading
facilities of the I.B.M. 360/67 computer.

A block diagram of the above system is shown in Figure
3.2a.

The two Kennedy tapes were not FORTRAN compatible on
available computer facilities. Consequently a machine
language program was used to transfer the data to nine track
tapes with the proper computer word size (32 bits) for
analysis by the author's FORTRAN language programs.

3.3 Spectral Density Estimates of Magnetotelluric Fields

The magnetotelluric method consists of calculating the
Cagnaird or scalar apparent resistivity:

$$\rho_{a_{ij}}^{(s)}(\omega) = 0.2 \frac{2\pi}{\omega} \left| \frac{E_i(\omega)}{H_j(\omega)} \right|^2 \qquad \text{3.3 - 1}$$

$$i, j = 1, 2; \quad i \neq j$$

and/or the tensor apparent resistivity:

$$\rho_{a_{ij}}^{(Z)}(\omega) = 0.2 \frac{2\pi}{\omega} \left| Z_{ij} \right|^2 \qquad \text{3.3 - 2}$$

$$i, j = 1, 2: \quad i \neq j$$

for a measured magnetotelluric field and plotting the apparent
resistivity as a function of period (or frequency). The
curves are then matched with the apparent resistivity curves

Figure 3.2a: A block diagram of the analog to digital conversion system.

KENNEDY

D
I
G
I
T
A
L

TAPE
RECORDERS

TAPE
FORMAT
LOGIC

ANALOG
to
DIGITAL
CONVERTER

CLOCK

SYSTRON
FREQUENCY
MONITOR

SIX
CHANNEL
MULTIPLEXER

PAPER
MONITOR

SIX
ALIASING
FILTERS

PRECISION
INSTRUMENTS

TAPE
RECORDER

A
N
A
L
O
G
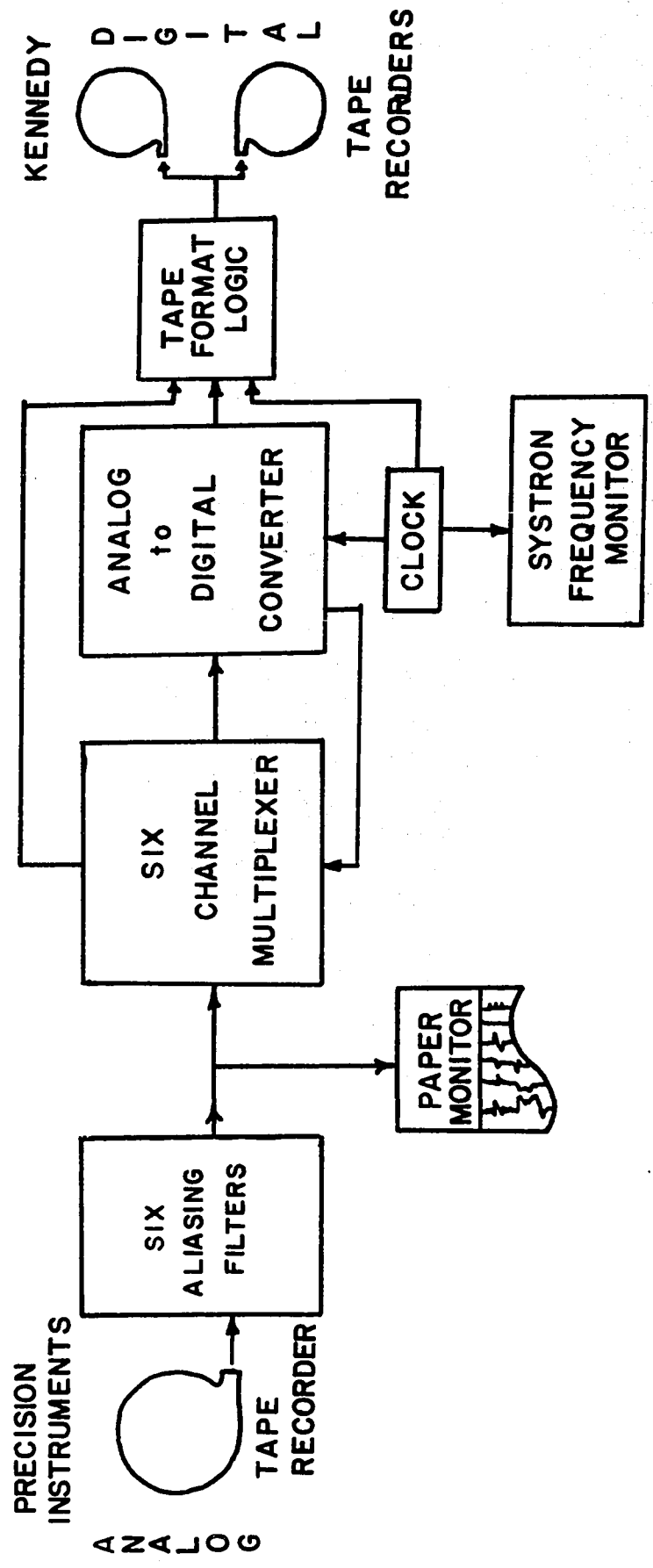
of various theoretical models until a reasonable fit to an appropriate model has been obtained.

The quantities $|E(\omega)|^2$ and $|H(\omega)|^2$ can be obtained by three general techniques:

1) Inspection of analogue records for sinusoidal events to obtain the amplitude values (Berdichevsky - 1960; Srivastava et al - 1963).

2) Filtering analogue or digital records for sinusoidal or quasi-sinusoidal events (Morrison - 1967).

3) Calculation of the digital power spectrum estimates by considering the records to be a sample from a stationary stochastic process (Cantwell - 1960; Vozoff, Hasagawa, and Ellis - 1964; Hopkins and Smith - 1966; and others).

The third method has been adopted for this study since the electronic processing of field data allows large quantities of information to be processed efficiently.

The power spectrum estimates were calculated using the techniques of Blackman and Tukey (1958) (calculating the auto-and-cross covariances) allied with the Fast Fourier Transform Algorithm (Cooley-Tukey - 1965). The covariance functions were obtained by convolution theorem techniques (Gentleman and Sande - 1965) rather than by summing the lagged products which is computationally expensive. Detailed mathematical proofs of the procedures which follow are readily available (e.g. Blackman and Tukey - 1958) and

will not be presented here.

For analysis, data sets $X_i (k*\Delta)$, $X_j (k*\Delta)$ $(1 < k < N;$ Δ = digitizing interval) were selected and zeros added to give the hyperseries:

$$X'_r (k*\Delta) = \begin{array}{ll} X_r (k*\Delta) & 1 < k < N; \quad r = i, j \\ 0 & N + 1 < k < N' \end{array}$$

where $(N' - N)$ is greater than the number of smoothed power spectrum estimates (M). The hyperseries were then discretely transformed to the frequency domain by an N' point Fourier transform. The resulting Fourier amplitudes, $F_i (\omega)$, $F_j (\omega)$ were squared to give unsmoothed periodogram estimates, $|F_{ij} (\omega)|^2$, which have a high variance.

Time series in general are characterized by random changes of frequencies, amplitudes and phases. Since a basic requirement of Fourier analysis involves the assumption of fixed frequencies, amplitudes, and phases, the Fourier results must be modified to take into account the random nature of the time series, that is, techniques are needed to reduce the variance of the spectral estimates. To achieve this reduction, the periodogram estimates were inverse Fourier transformed to the lag domain (Wiener - Kintchine theorem: Sande - 1965) by the Fast Fourier Transform and the auto- (or cross-) covariance function, $C_{ij} (\tau)$, was smoothed with a Parzen window (Parzen - 1961).

$$C'_{ij} (\tau) = W(\tau) \cdot C_{ij} (\tau)$$

where

$$
W(\tau) = \begin{cases}
1 - 6(\tau/M)^2 + 6(|\tau|/M)^3 & |\tau| < M/2 \\
2(1 - |\tau|/M)^3 & M/2 < |\tau| < M \\
0 & |\tau| > M
\end{cases}
$$

and M is the maximum lag number. The power spectrum estimates were then obtained by transforming the smoothed covariances to the frequency domain by a 2M point Fourier transform.

The Parzen lag window was chosen because it has a positive definite character, and achieves the smallest variance and greatest number of degrees of freedom of the windows tested. This was estimated to be of greater value than the negative effect of its relatively large bias seen in Figure 3.3a. The sample coherence function, $\gamma_{ij}(\omega)$, between data sets $X_i(k*\Delta)$, and $X_j(k*\Delta)$ was calculated by the usual definition

$$
\gamma_{ij}(\omega) = \frac{P_{ij}(\omega)}{\sqrt{P_{ii}(\omega) * P_{jj}(\omega)}}
$$

where $P_{ii}(\omega)$ and $P_{jj}(\omega)$ are auto power estimates and $P_{ij}(\omega)$ is the cross power estimate (in which the phase shift introduced by the digitizing process has been removed).

It was decided that the prewhitening technique would not be applied on the original data series as the instrument response (see Figure 3.1a) effectively prewhitens the spectra. To check this assumption, artificial time series were generated and various prewhitening windows were applied

Figure 3.3a: Common spectral windows.
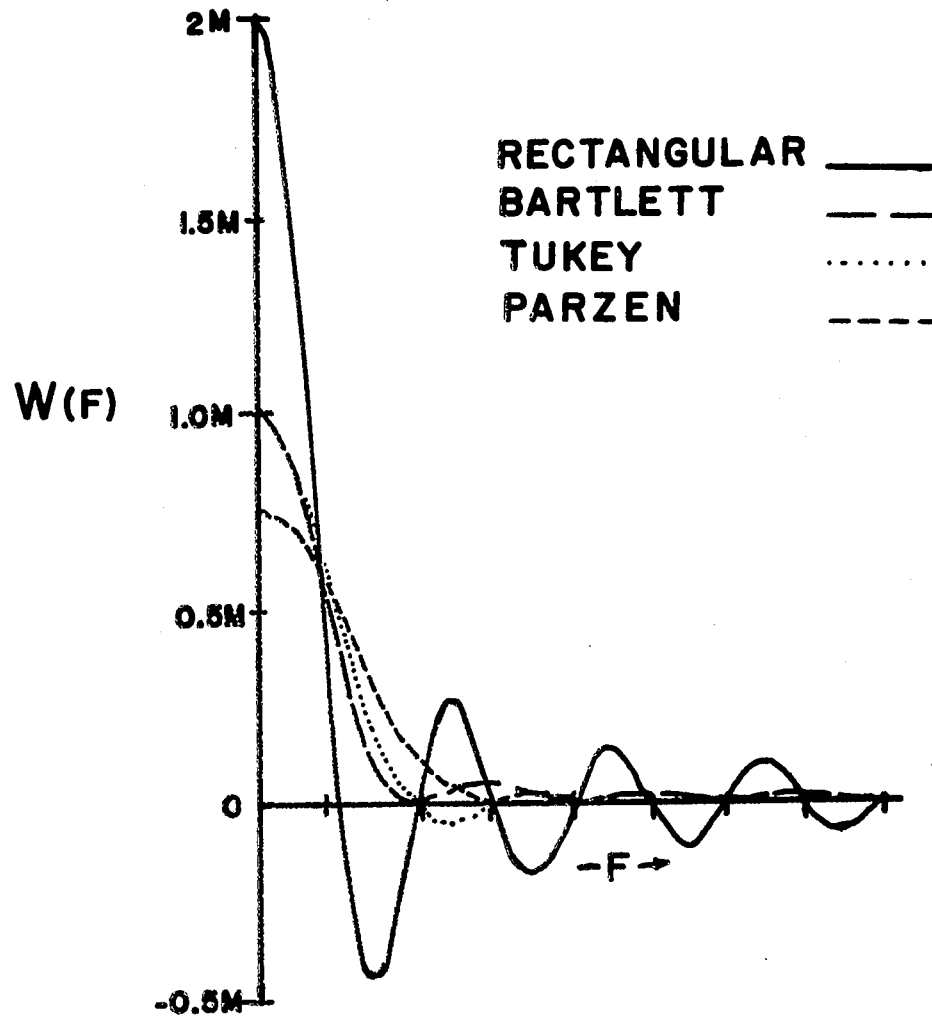
but the prewhitening technique did not sufficiently enhance the reliability of the power spectrum estimates.

Although the above technique of computing spectral estimates was rather involved, the high speed and large storage capabilities of modern computers makes this process acceptable. Also, the Fourier transformation of two series at a time "in place" (see Gentlemen and Sande - 1966) reduces computer time and storage requirements considerably. These techniques, although slightly slower than the direct calculation and modification of the Fourier amplitude spectra, allow the direct inspection of the covariance function.

After testing, it was decided to use a minimum value of 0.90 for the sample coherency function as the criterion for acceptance of spectral estimates used to calculate the Cagnaird apparent resistivity function. Although this choice produced a high rejection rate of estimates, the effect produced was a very high reliability of power spectrum estimates and small scatter of the apparent resistivity estimates. Furthermore the choice of N = 3,000, M = 256 gave each spectral density estimate 42 degrees of freedom (Jenkins and Watts - 1968) which increased the statistical confidence of the final results to _very_ acceptable levels.

3.4 The Estimation of the Impedance Tensor Elements

The basic impedance relationship can be written:

$$\begin{vmatrix} Ex \\ Ey \end{vmatrix} = \begin{vmatrix} z_{11} & z_{12} \\ z_{21} & z_{22} \end{vmatrix} \cdot \begin{vmatrix} Hx \\ Hy \end{vmatrix} \qquad 3.4 - 1$$

or

$$Ex(\omega) = z_{11} \, Hx(\omega) + z_{12} \, Hy(\omega)$$
$$Ey(\omega) = z_{21} \, Hx(\omega) + z_{22} \, Hy(\omega)$$

<div align="right">3.4 - 2</div>

Post-multiplying the above equations by $H^*x(\omega)$, $H^*y(\omega)$, $E^*x(\omega)$, $E^*y(\omega)$ (where * indicates complex conjugate) yields eight equations in four unknowns. Solving any two equations from this overdetermined system of equations simultaneously, six solutions for each impedance element can be obtained (see APPENDIX I). The techniques described in Section 3.3 were used to calculate the auto- and cross- power spectra required for the estimation of each magnetotelluric impedance element.

Since no completely satisfactory "coherency" function exists as a criterion for the validity of the various tensor element estimates, a quantitative technique was demanded for the rejection of estimates with an unsatisfactory signal to noise ratio. Swift (1967) used a coherency function based on the "predictability" of the E field, however a simpler method seems satisfactory. Assume that the magnetotelluric fields are unpolarized, that is, $<Ex \cdot E^*y>$, $<Hx \cdot H^*y>$, etc. are negligible (where $< >$ denotes a cross power spectral estimate), then only four of the six possible solutions are stable (see APPENDIX I). If the magnetotelluric field is polarized, one of the four "unpolarized" estimates is unstable.

If incoherent noise exists in the recorded magnetic and electric signals then two of the above stable unpolarized tensor estimates will have the form:

$$z'_{ij} = z_{ij} \left(1 + \frac{E \text{ noise power}}{E \text{ signal power}} \right) \qquad 3.4 - 3$$

where z'_{ij} is the computed estimate and z_{ij} is the actual tensor value. The remaining two stable unpolarized tensor estimates have the form:

$$z'_{ij} = z_{ij} / \left(1 + \frac{H \text{ noise power}}{H \text{ signal power}} \right). \qquad 3.4 - 4$$

Thus two unpolarized solutions are biased high due to electric noise while two unpolarized solutions are biased low due to magnetic noise. By averaging the four estimates of each impedance element the biasing effect of incoherent noise on the estimation of the tensor element can be reduced if the incoherent noise has the same power level in both the electric and magnetic data.

To eliminate further scatter, a minimum signal strength criterion was developed. The power level that six cycles of data (with an amplitude twenty times greater than the minimum increment of the digitizing apparatus) would produce for a given record length at each Fourier frequency was calculated. Rejection of those frequency bands in which the magnetic signal was less than the arbitrary minimum power level reduces the scatter of the tensor apparent resistivities by effectively increasing the signal to noise ratio to more acceptable limits.

3.5 Programming Considerations.

After a thorough study of spectral analysis and

statistical communication theory, FORTRAN language programs
were written to facilitate the analysis of magnetotelluric
data. Using the Fast Fourier Transform algorithm and the
techniques outlined in Section 3.3, calculations of the
power spectra, orthogonal scalar resistivities, phases, and
coherencies for the recorded magnetotelluric field data were
performed. All digitized magnetotelluric data was processed
in this manner, and displayed by means of a typewriter
plotter utilizing graphing programs developed by the
University of Alberta Computing Science Department. This
program was later expanded to calculate the rotated scalar
resistivities, coherencies and phases but the results of a
rotated scalar type of analysis were never satisfactory.

This led to the development of a FORTRAN language
program to calculate the impedance tensor elements of the
magnetotelluric data. Tensor estimates were calculated, and
the impedance tensor elements computationally rotated
(equation 2.2 - 4) and graphing routines were written to
display the tensor elements and resistivities on the line
printer. The four averaged tensor elements, rotated by 10°
increments from 0° - 90° and plotted as a function of period,
were then inspected visually to ascertain the rotation angle
producing the $\min|z_{11}(T, \theta)|$. The impedance tensor elements
were then recalculated, rotated into the principal directions
of resistivity computationally, and the tensor apparent
resistivity function was calculated (equation 3.3 - 2).
All data from one location was treated in this manner and

programs were written to display the maximum, minimum and average values of apparent resistivity using a CALCOMP plotter.

Another program was written to calculate and display the polarization characteristics (degree of polarization, polarization angle, and ellipicity) of the magnetic field using the techniques of Born and Wolf (1959) as outlined by Fowler et al (1967) and the results of the analysis were also displayed on the CALCOMP plotter (see APPENDIX II).

CHAPTER IV

A MAGNETOTELLURIC EXPERIMENT IN SOUTHERN ALBERTA

4.1 General Observations

During the summer of 1966 a magnetotelluric survey was
made along a north-south profile in southern Alberta. In
the summers of 1967-8, this profile was expanded and a
second, three station profile made to facilitate a corre-
lation of geologic structure between the two profiles. The
locations of the stations comprising the profiles are shown
in Figure 1.3b and this chapter will present the results of
this survey.

The analysis of all data was made using the tensor
techniques discussed in CHAPTER 3 and APPENDIX I and all
computed quantities were calculated for record sections
6400 seconds long. For periods between 10 and 100 seconds,
the time averaged impedance elements from various records
of sufficient power show very little scatter. However for
periods greater than 100 seconds the impedance elements are
characterized by rather large variances. For all data
presented in this chapter, the skew values of the magneto-
telluric impedance were less than 0.3. This indicates that
the sub-surface resistivity structure at all the stations
could be reasonably represented by two dimensional models.

Figure 4.1a (Campbell - 1966) shows a very general
diagram of field strength versus period for geomagnetic

*Figure 4.1a: Identification of the geomagnetic micro-
pulsation spectrum in the magnetotelluric frequency
range (after Campbell - 1966).*
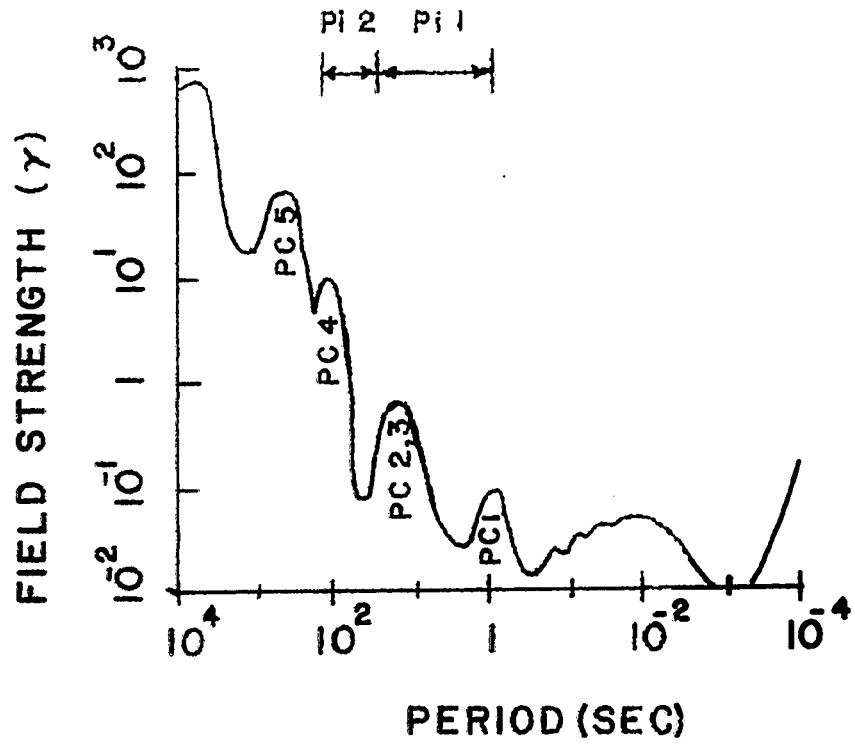
Pulsation	Period
Pc 1	0.2-5.0
Pc 2	5.0-10.0
Pc 3	10- 45
Pc 4	45-150
Pc 5	150-600
Pi 1	1 - 40
Pi 2	40-150

micropulsations. Sharp dips in the spectrum (e.g. between the Pc4 and Pc5 bands) can decrease the reliability of the spectral analysis estimates and distort the apparent resistivity estimates. It is most desirable to obtain recordings of the magnetotelluric field which produce a spectrum containing a slowly varying power level at all frequencies.

To obtain the principal directions of resistivity, the tensor impedance elements were rotated computationally (equation 2.2 - 4) and the principal directions were defined by the angles, θ, which produced a minima in the absolute value of the rotated diagonal elements of the magnetotelluric impedance tensor. Although all frequency estimates of the rotated impedance tensor were calculated and examined, only three or four representative estimates will be presented in a diagram for each station. Several general observations can be immediately made.

1) Only in a few cases was $\min|z_{11}(T, \theta)|$ actually zero. This is expected due to noise contamination in the signal, source effects, a non-two dimensional resistivity structure, or to the fact that if the power spectra have sharp peaks, spectral analysis techniques will produce an averaged value of power over the band-width of the particular spectral window used.

2) The angle, θ, defined by $\min|z_{11}(T, \theta)|$ does not appear to be time invariant and variations as large as 25° in the rotation angle have been observed for the

same period in different data sets recorded at the same location. This is probably due to the inability of the spectral analysis techniques to reliably process data with steep power spectra slopes, since the estimation of θ is consistent from record to record if the power spectra was of sufficient activity and slowly varying.

For periods greater than 100 seconds, the magnetic field tends on the average to exhibit strong elliptical and linear polarization with the major axis of the polarization ellipse oriented between north and east. Graphs of representative magnetic polarization parameters and instrument prewhitened magnetic spectra for all stations are presented in APPENDIX II.

The tensor analysis of magnetotelluric data from all locations studied in southern Alberta indicated that the minor axis of resistivity aligned between N 40°E and N 80°E. This alignment of the principal direction of resistivity and the magnetic polarization ellipse meant that a much lower signal to noise ratio existed for one tensor apparent resistivity estimate than the other. This resulted in a relatively large scatter of the $\rho_{a_{12}}^{z}$ estimates as compared to the $\rho_{a_{21}}^{z}$ scatter.

4.2 Analysis of Magnetotelluric Data

Over twenty magnetotelluric recording locations have been occupied in central and southern Alberta. The analysis of results from eight of these stations will now be presented.

i)   Red Deer Location (RD)   (52° 10' Latitude, 113° 27'

      longitude, elevation: +3100 feet)

This location was chosen to determine the apparent resistivity curves over the sedimentary basin of western Canada at a large distance from the seismically determined elongated horst-graben structure (rift valley) in southern Alberta.   Garland and Burwash (1959) indicate that the Precambrian rock at the basement surface is gneiss at the magnetotelluric recording location but within 25 miles to the south and west the basement character is chiefly granitic (see Figure 4.4b).

Preliminary scalar resistivity analysis (Figure 4.2a) would indicate that the subsurface resistivity properties were reasonably isotropic.   The scalar apparent resistivity curves displayed in Figure 4.2a are a composite of results from the analysis of seven data sets (each data set 6400 seconds long).   The averaged apparent resistivity is indicated by a symbol and the error bars indicate the maximum scatter in apparent resistivity for estimates with a coherency greater than 0.90.

Tensor analysis of the seven data sets indicated however that the location has anisotropic resistivity properties for periods greater than ten seconds.   The magnetotelluric impedance tensor indicated definite minima of the diagonal elements for the rotation angles $\theta_1 \approx$ N 40°E and $\theta_2 \approx$ N 40°W (as shown in Figure 4.2b) implying that the major and minor

directions of resistivity are approximately cartesianally orthogonal.

Skew values of the magnetotelluric impedance tensor were less than 0.3 for all estimates shown on the tensor apparent resistivity curves. For this reason, the subsurface resistivity structure cannot be three dimensional in character. The tensor apparent resistivity ρ_{21} curve has been modeled with a one dimensional isotropic layered model assuming plane wave incidence.

The basic surface features for the model of the $\rho_{21}(T, \theta)$ curves was derived from local well log data. This model does not appear to fit the Red Deer $\rho_{21}(T, \theta)$ curve nearly as well as it should if the resistivity structure were actually one dimensional. Figure 4.4b from Garland and Burwash (1959) indicates lateral inhomogenieties in the basement composition near this site and this may explain the deviation of the experimental curves from a one dimensional model curve. The effect of large scale distant structures will be discussed below.

Figure 4.2a: The scalar apparent resistivity curves from
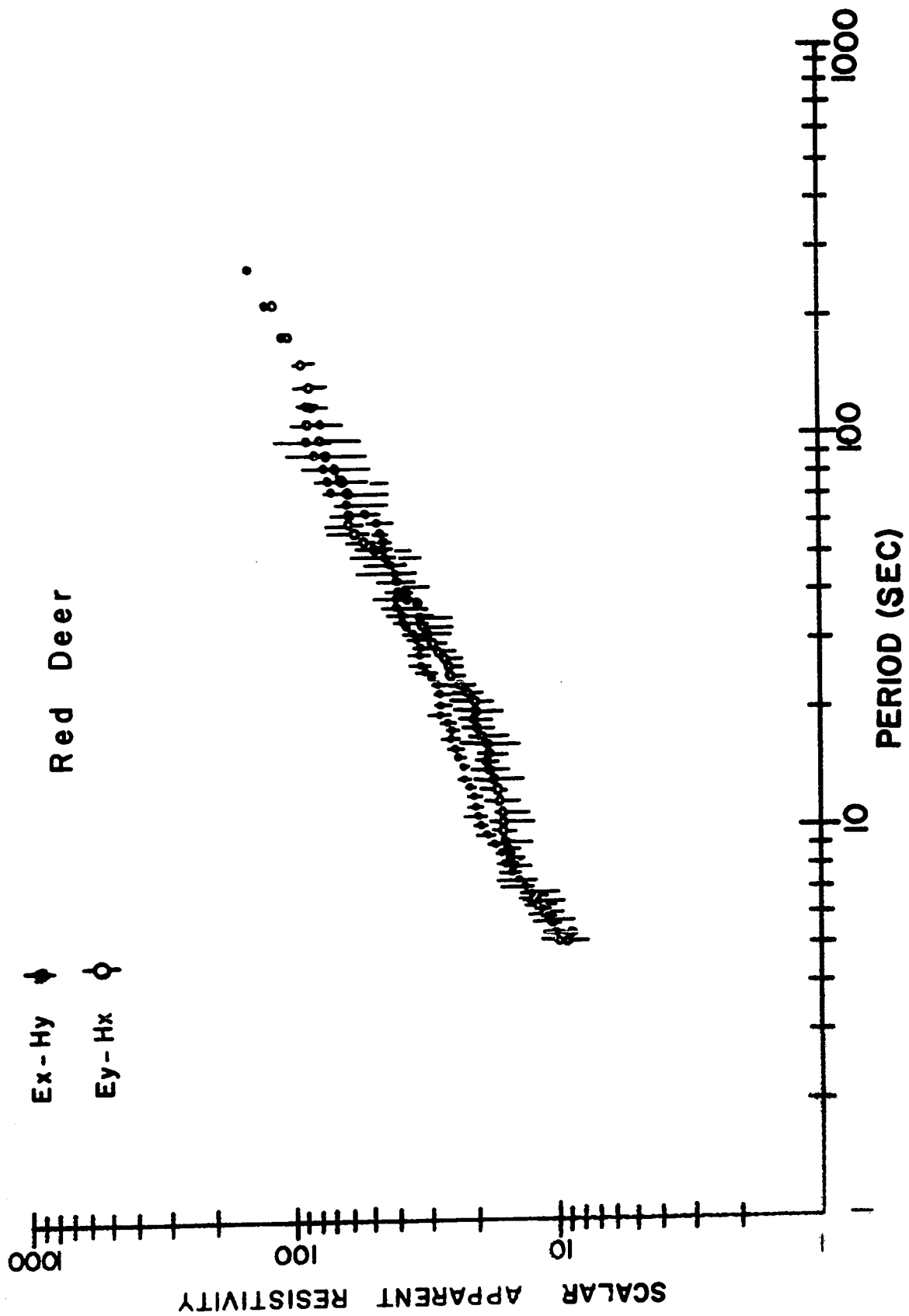the Red Deer location.

Red Deer

Ex – Hy ●
Ey – Hx ◇

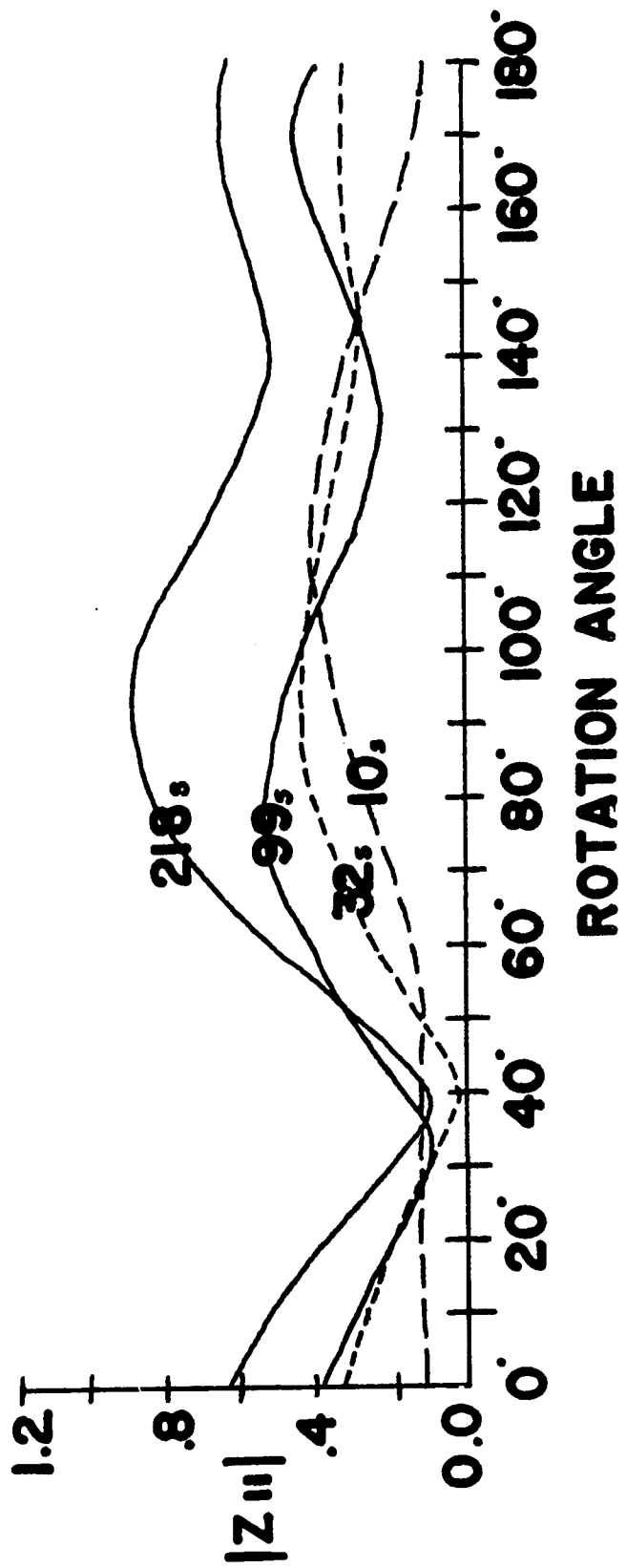PERIOD (SEC)

SCALAR APPARENT RESISTIVITY

Figure 4.2b: Rotated diagonal tensor element at selected periods for Red Deer location data.

RED DEER

Figure 4.2c: Tensor apparent resistivities for the Red Deer location.

TENSOR APPARENT RESISTIVITY

PERIOD (SEC)

RED DEER

Theoretical Model

$\rho_1 = 6\,\Omega M$ $h_1 = 1.0\,km.$
$\rho_2 = 10\,\Omega M$ $h_2 = 0.83\,km.$
$\rho_3 = 30\,\Omega M$ $h_3 = 1.47\,km.$
$\rho_4 = 400\,\Omega M$

△ ρ_{21}
○ ρ_{12}
$\theta = 50°$
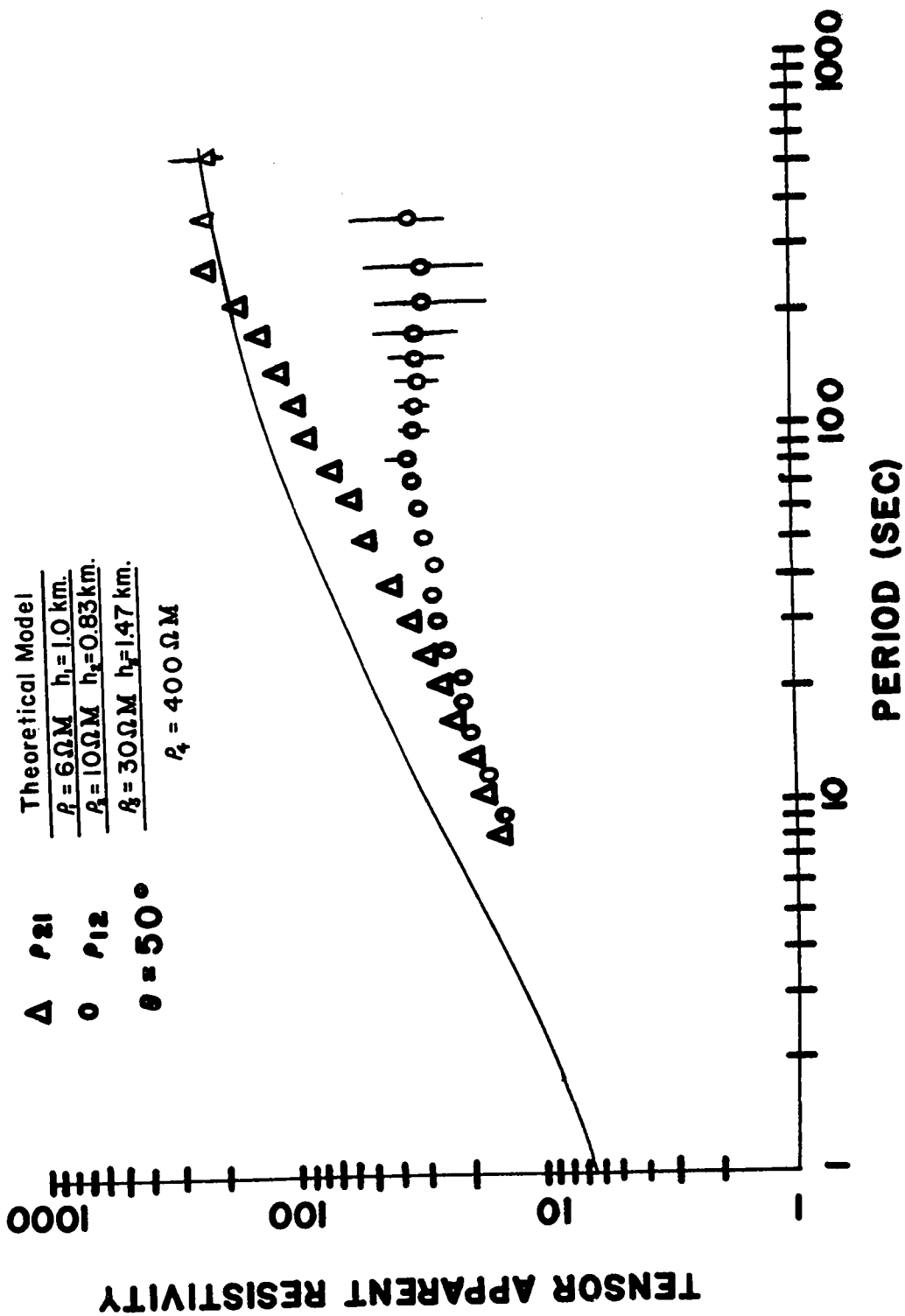
ii)   Horse Thief Canyon (HT) (51° 34' latitude, 112° 55'

longitude, elevation: +2300 feet)

This location was chosen to represent the north end of
both the expanded 1966 profile and the additional 1968
profile.   The recording apparatus was situated on the floor
of a canyon 400 feet below the regional surface level of the
plains.   The canyon forms a north-south trending rectangular
channel which is approximately 13,000 feet wide.   The Red
Deer River runs north-south along the canyon floor.

A plot of $|z_{11}|$ versus rotation angle indicates that
the principal directions of resistivity are defined by the
rotation angles $\theta_1 = 90° - 110°$, and $\theta_2 = 160° - 170°$, for
all periods investigated as shown in Figure 4.2d.   This
relatively high degree of noncartesian orthogonality (com-
pared to other locations investigated) for the principal
directions of resistivity is primarily due to topographical
features superimposing their effect on the true resistivity
features.   The electrodes at this station were only 600 feet
in length and therefore far less than ten times greater than
the major topographical variations.   Wescott and Hessler
(1962) have made a telluric current model study of a
rectangular channel and found that the measured electrical
potential per unit length was greater in a rectangular
channel than external to the channel region.   As the width
to height ratio of the rectangular channel increased the

ratio of

$$\frac{\text{potential per unit length in channel}}{\text{potential per unit length outside channel}}$$

decreases to approximately one. The canyon has a width to height ratio of 33:1. Since the telluric (and magnetic) measurements were made entirely within the canyon, the measured apparent resistivities were biased by the shape of the canyon. The model shown in Figure 4.2d was derived from local well log data and again is a poor fit. Figure 4.4b (basement lithology) indicates lateral inhomogenities in the basement composition within 25 miles to the west of this location. This also contributes to the inability of a one dimensional model to adequately explain the form of the apparent resistivity curve. In addition to the large scale structural effect of the more distant Rocky Mountains the local surface structure effects the high frequency end of the curves.

The relatively large scatter in the tensor ρ_{12} curve, Figure 4.2e, is caused by the magnetic signal being highly linearly polarized in the north-to-east direction with little power in the perpendicular direction.

Figure 4.2d: Rotated diagonal tensor element for Horse
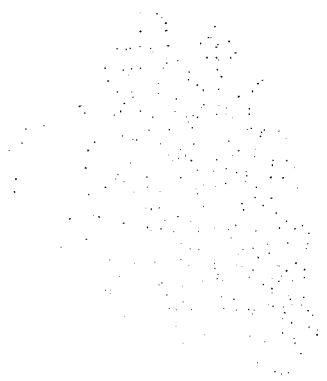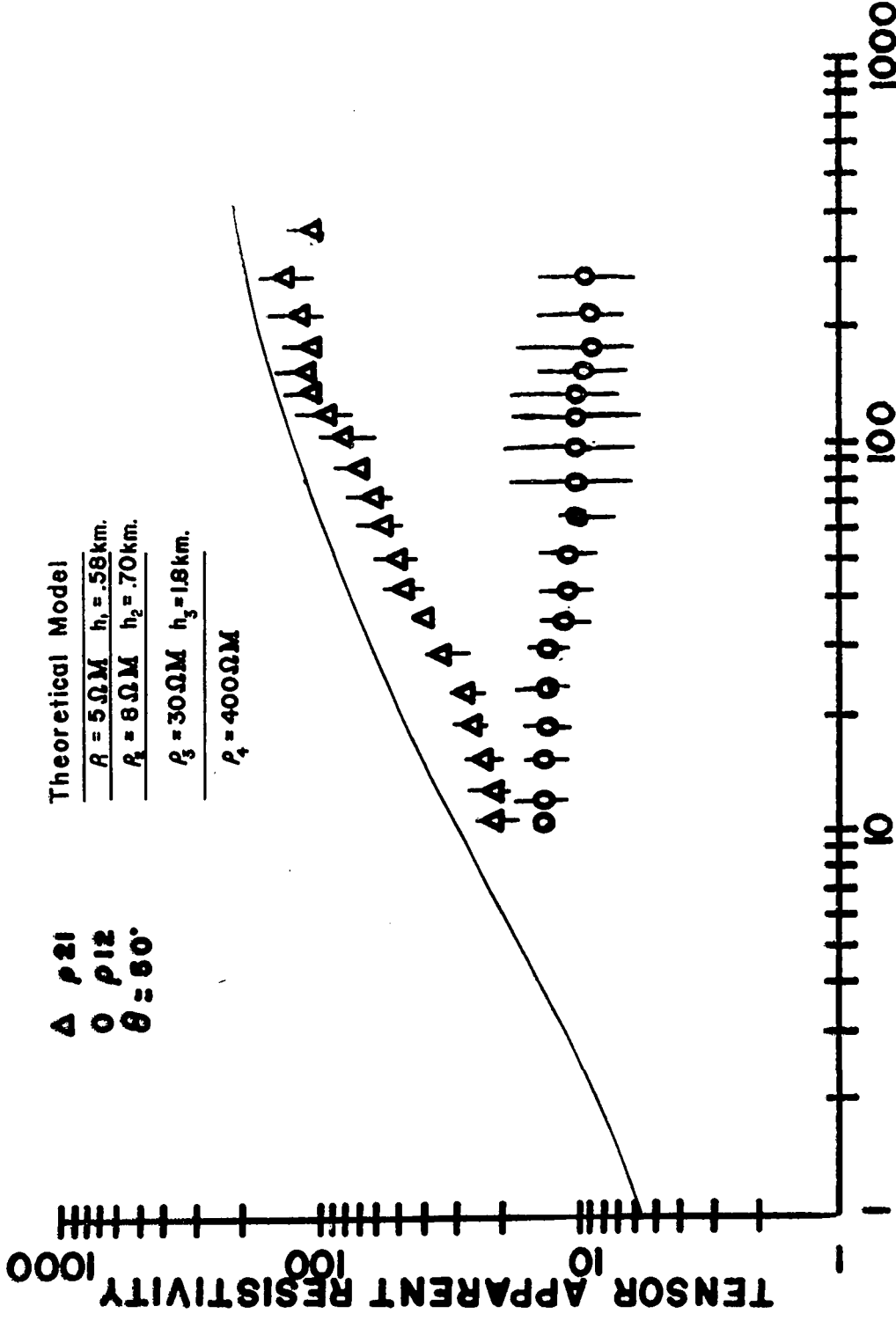*Thief Canyon location data at selected periods.*

HORSE THIEF CANYON
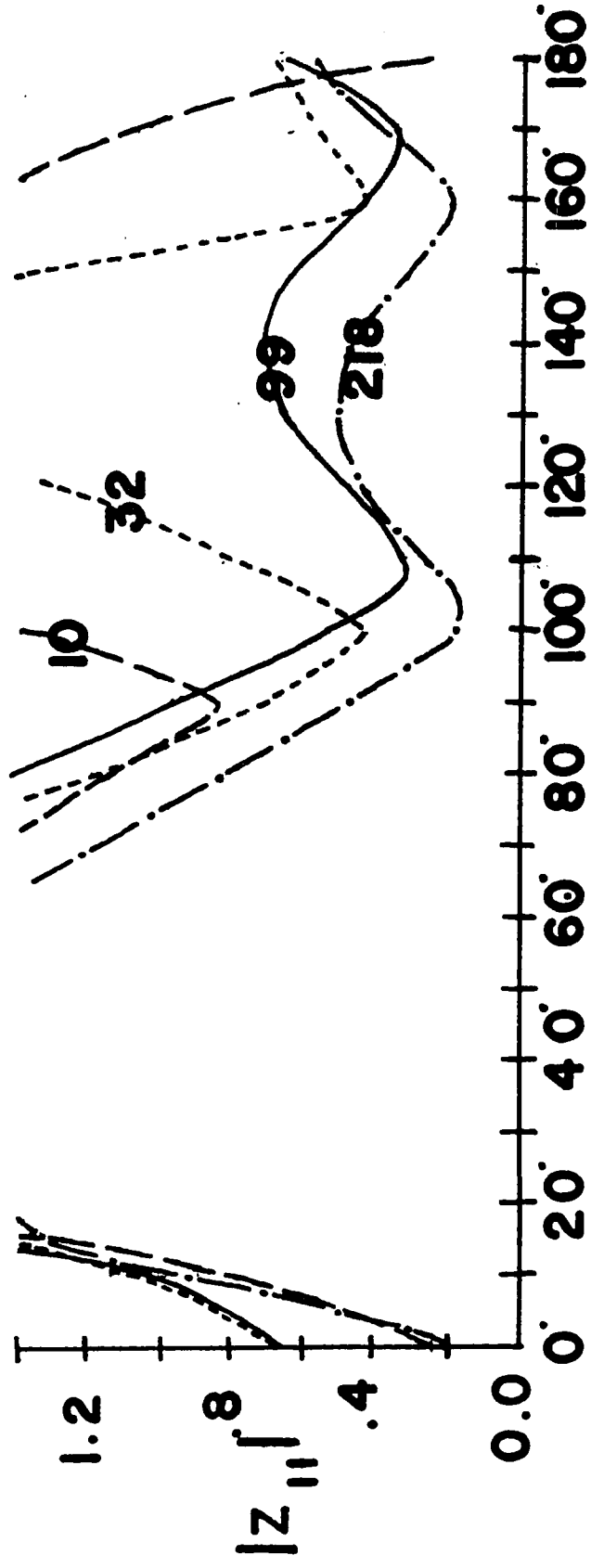
Figure 4.2e: Tensor apparent resistivities for the Horse
Thief Canyon location with a one dimensional model
based on local well log information.

TENSOR APPARENT RESISTIVITY

HORSE THIEF
CANYON

PERIOD(SEC)

Theoretical Model

$\rho_1 = 5 \Omega M$	$h_1 = .58$ km.
$\rho_2 = 8 \Omega M$	$h_2 = .70$ km.
$\rho_3 = 30 \Omega M$	$h_3 = 1.8$ km.
$\rho_4 = 400 \Omega M$	

△ $\rho 21$
O $\rho 12$
$\theta = 80°$

iii) Location 7 (L7) (50° 53' latitude, 112° 35' longitude,

elevation: +2800 feet)

Analysis of data recorded at Location 7 shows anisotropic resistivity properties as seen in Figure 4.2f. The principal directions of resistivity as defined by the rotation of the magnetotelluric impedance tensor as θ_1 = N 70°E and θ_2 = N 30°W (Figure 4.2g).

The topography around this location is essentially flat and no deviations in apparent resistivity are expected due to vertical variations in surface features. While no obvious features serve to explain the apparent anomalous splitting of the ρ_{12}, ρ_{21} curves it will be seen that both of these fit well on the profiles shown in Figure 4.4c.

Figure 4.2f: *Tensor apparent resistivities for Location 7.*
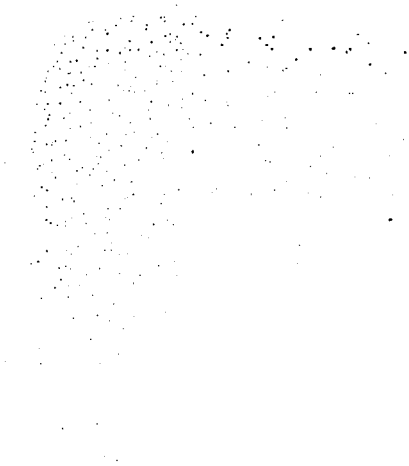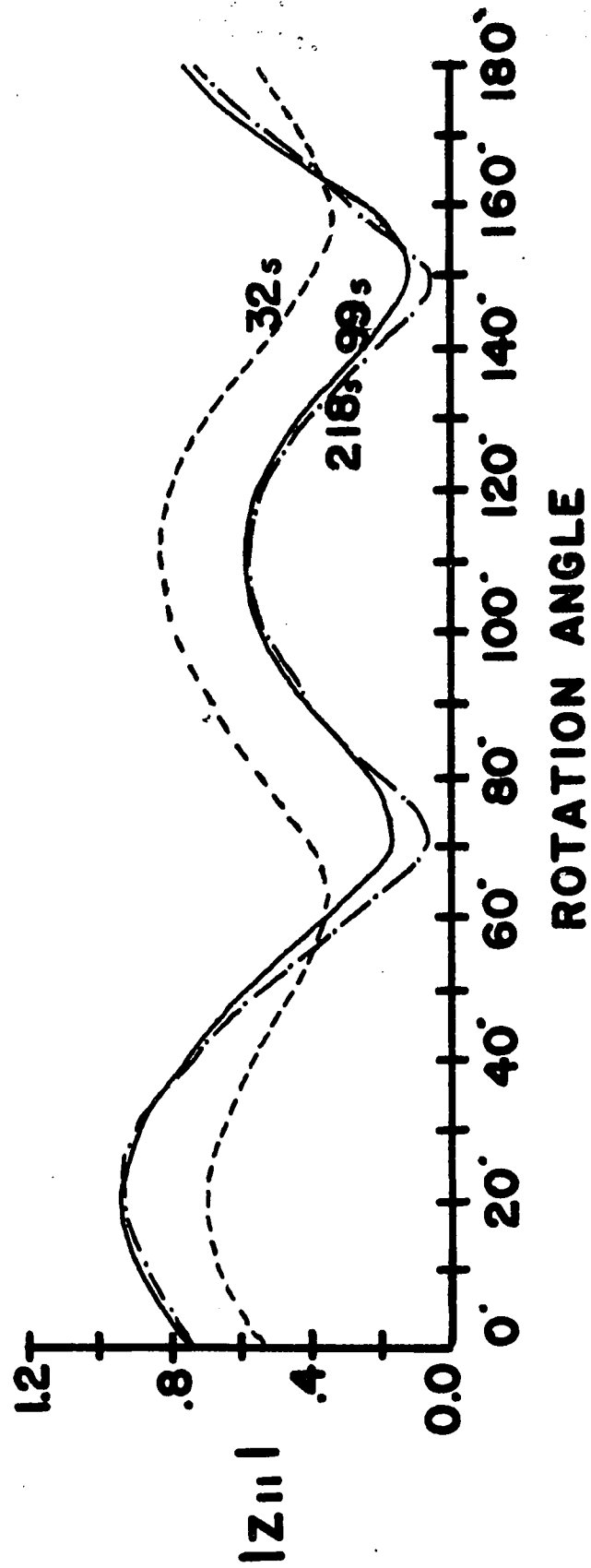
TENSOR APPARENT RESISTIVITY

PERIOD (SEC)

LOCN. 7

P_{21} ●

P_{12} ◇

$\theta = 70°$
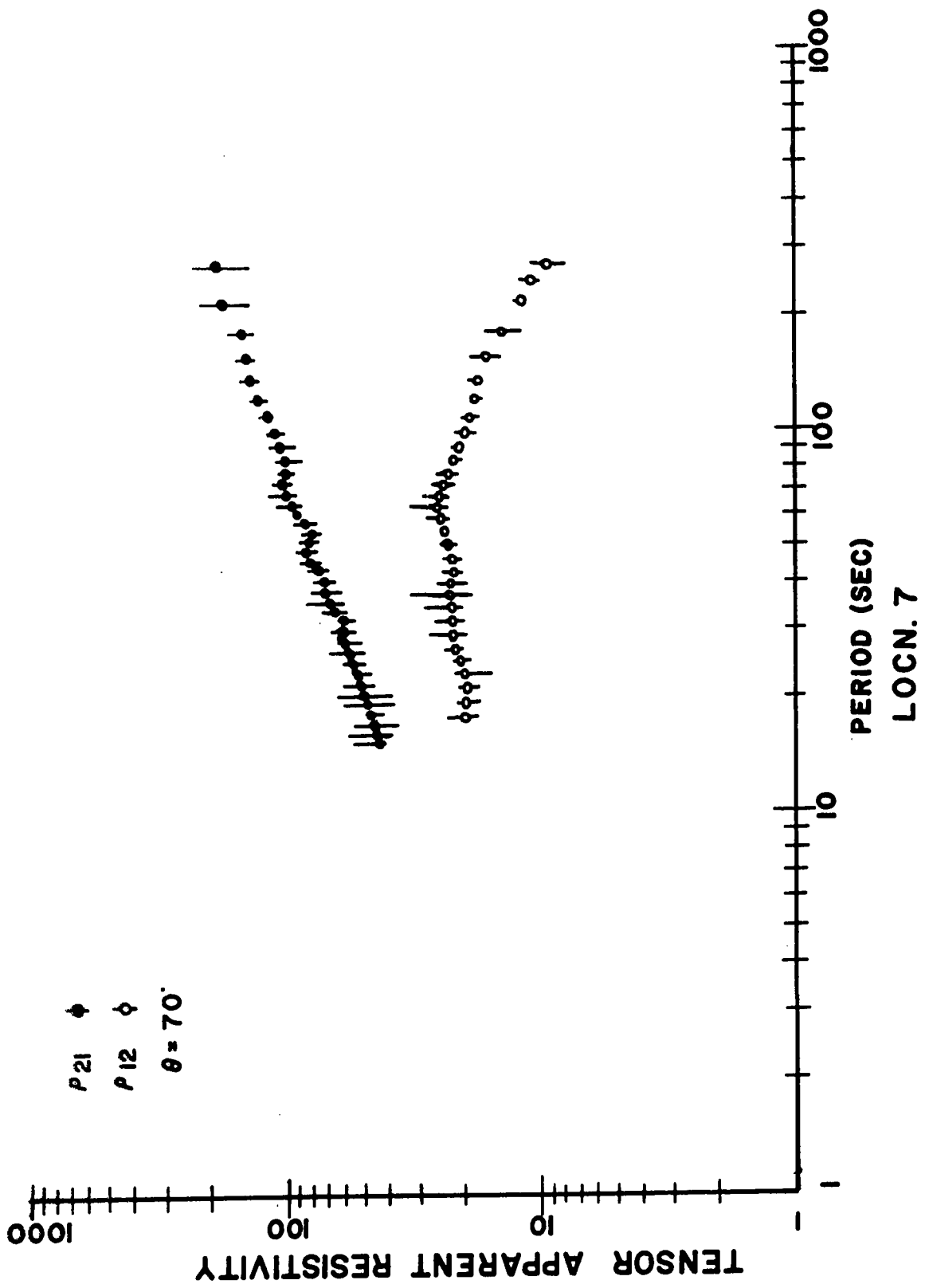
Figure 4.2g: *Rotated diagonal tensor element as selected periods for Location 7 data.*

ROTATION ANGLE

LOCN. 7

$|Z_{11}|$

32 s

218,99 s

iv) Location 5 (L5)(50° 34' latitude, 112° 30' longitude,

elevation: +3000 feet)

Location 5, like all other locations investigated in
this study, exhibits anisotropic resistivity features.
Regional surface relief in this area is virtually nil. Tensor
analysis indicated two approximately orthogonal directions for
the principal directions of resistivity given by θ_1 = N 70°E
and θ_2 = N 20° - 30°W (see Figure 4.2h). The rotated tensor
ρ_{21} resistivity of Location 5 (Figure 4.2i) is very similar
to the tensor ρ_{21} curve of Station 7. However the Location 5
ρ_{12} curve has appreciably greater values than ρ_{12} curve of
Station 7 at the same period.

Figure 4.2h: *Rotated diagonal tensor element at selected periods for Location 5 data.*
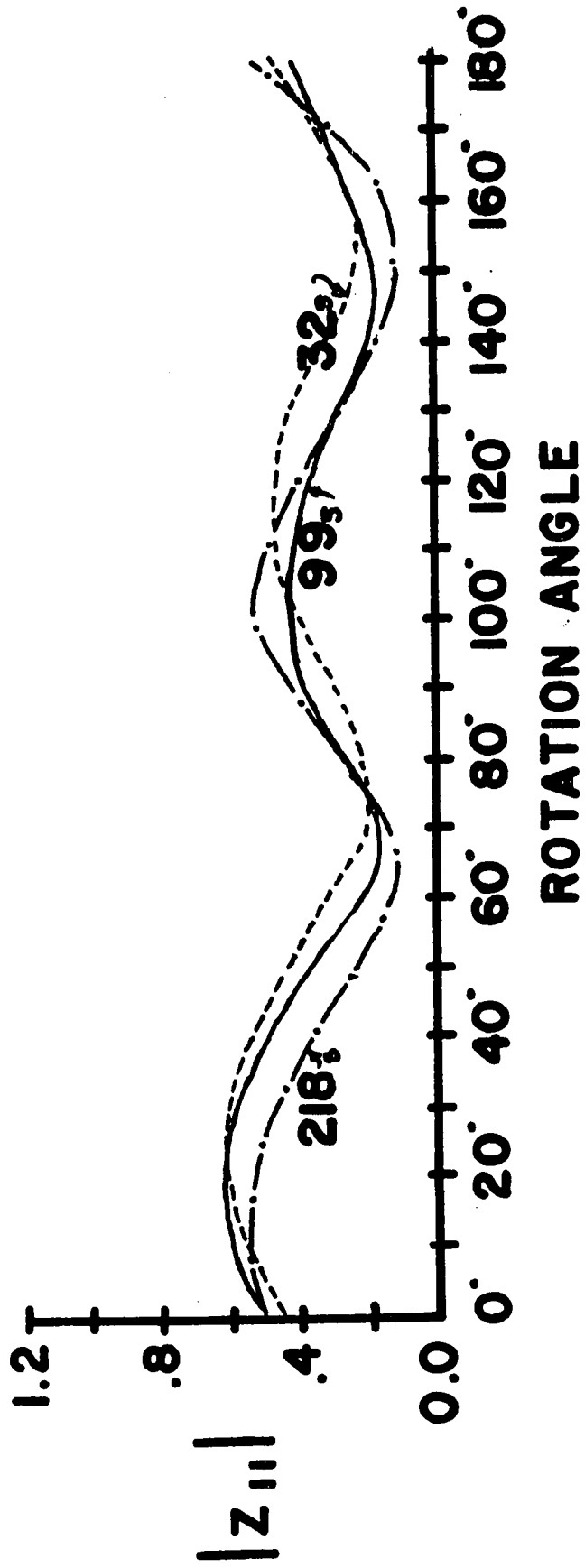
LOCN. 5

Figure 4.2i: Tensor apparent resistivities for Location 5.

PERIOD (SEC)

LOCN.5

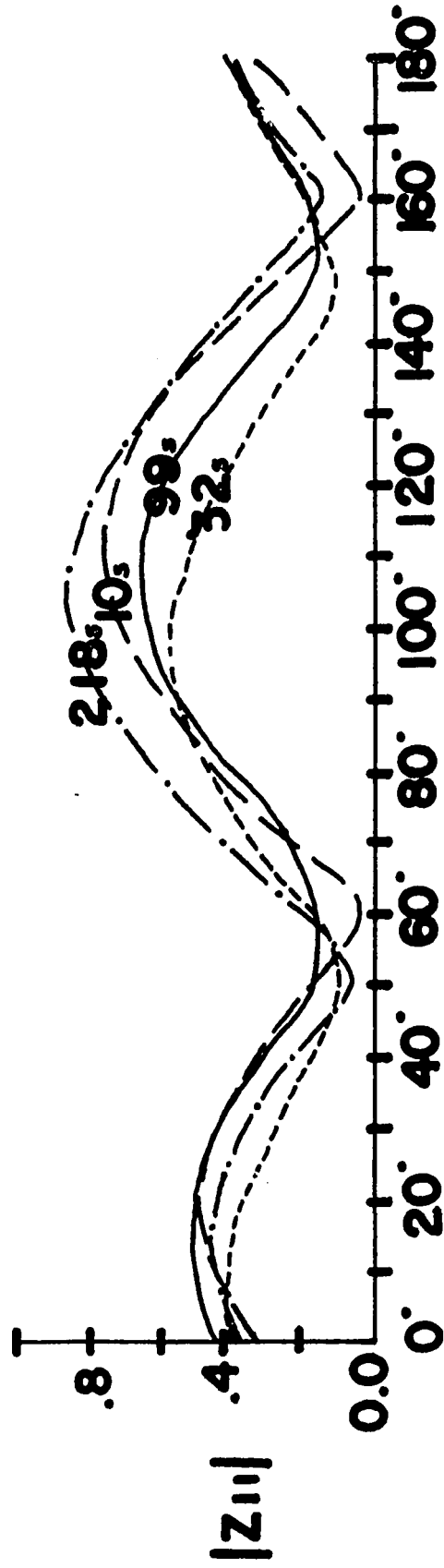TENSOR APPARENT RESISTIVITY

△ ρ21
○ ρ12
● ρ0
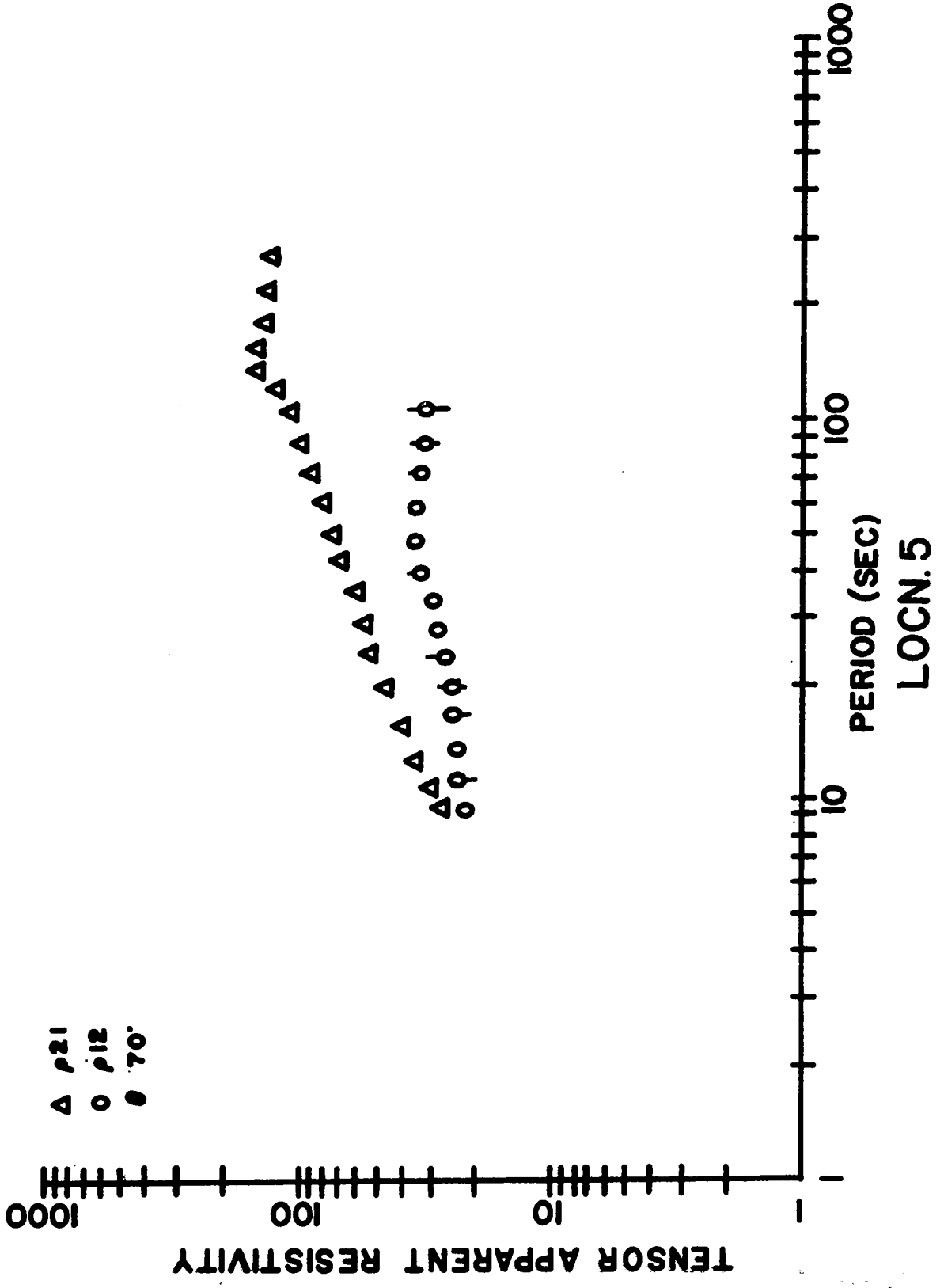
v)   Turin (TU) (50° 2' latutude, 112° 31' longitude,

elevation: +2700 feet)

This recording site is the southern most location which
will be presented for the "eastern" magnetotelluric profile.
Local surface features are reasonably flat and topographic
effects are assumed to have no major effect on the apparent
resistivities. Rotation of the diagonal tensor impedance
elements as shown in Figure 4.2j, define the directions given
by θ_1 = N 60°E and θ_2 = N 30°W as the approximate principal
directions of resistivity.

Figure 4.2k shows the averaged polarization character-
istics for two of the records used in the analysis. The high
degree of linear polarization of the magnetic signal for
periods T > 100 seconds explains the spread in sample ρ_{12}
resistivity values (Figure 4.21).

Superimposed on the ρ_{21}(T, θ) curve is a one dimensional
layered earth model interpretation of reasonably fit which
was deduced from well log data. The basement lithology map,
Figure 4.4b, indicates that this station lies in a region
where the basement composition is assumed to be reasonably
laterally homogeneous.

Figure 4.2j: Rotated diagonal tensor element at selected periods for Turin data.

TURIN

Figure 4.2k: Instrument prewhitened magnetic power
   spectra and polarization characteristics (averaged
   over 6400 seconds) for a sample record recorded
   at Turin.

SPECTRUM

PERIOD (SEC) TU-I

ELLIPTICITY

POLARIZATION ANGLE (+)

DEGREE OF POLARIZATION (⊙)

PERIOD (SEC) TU-I

161.
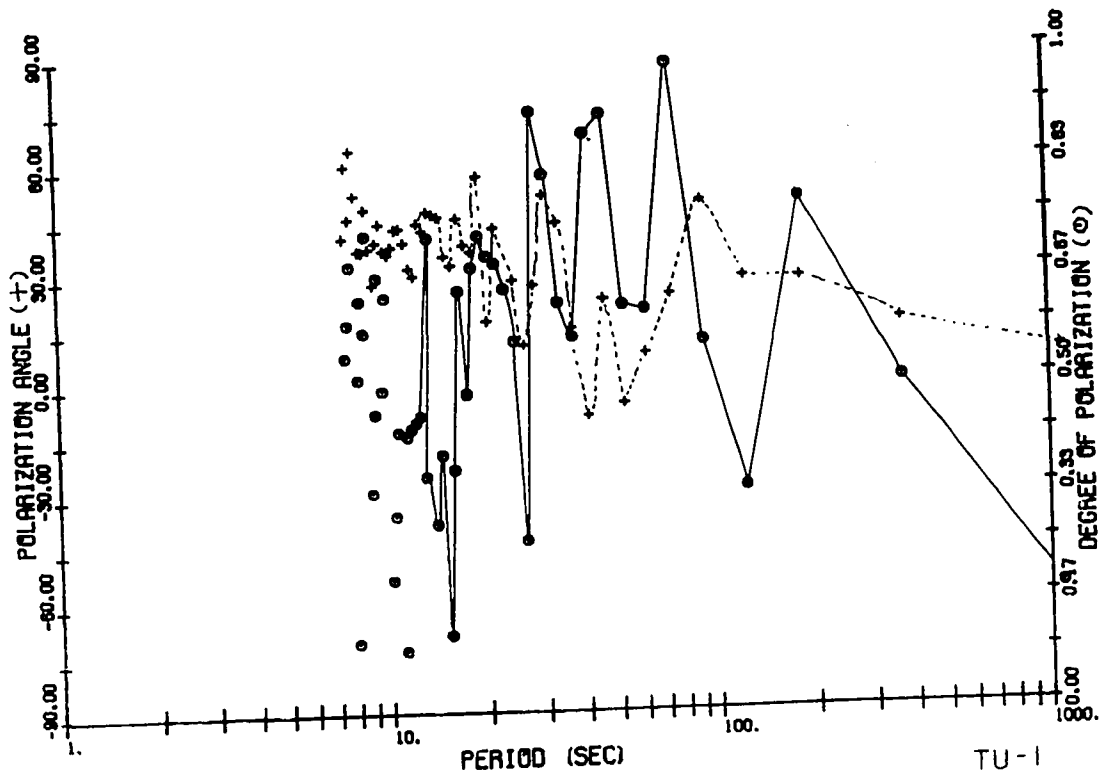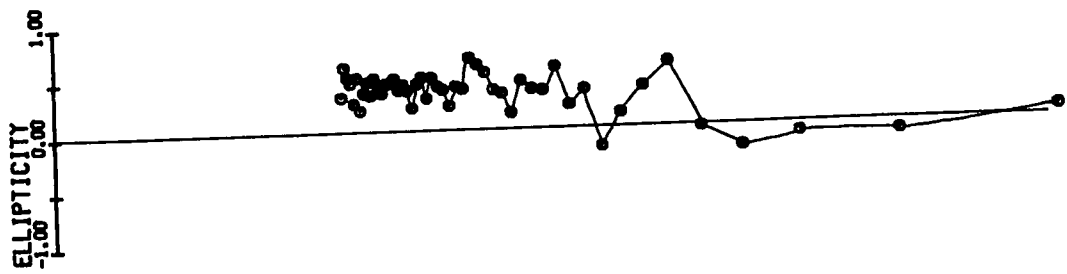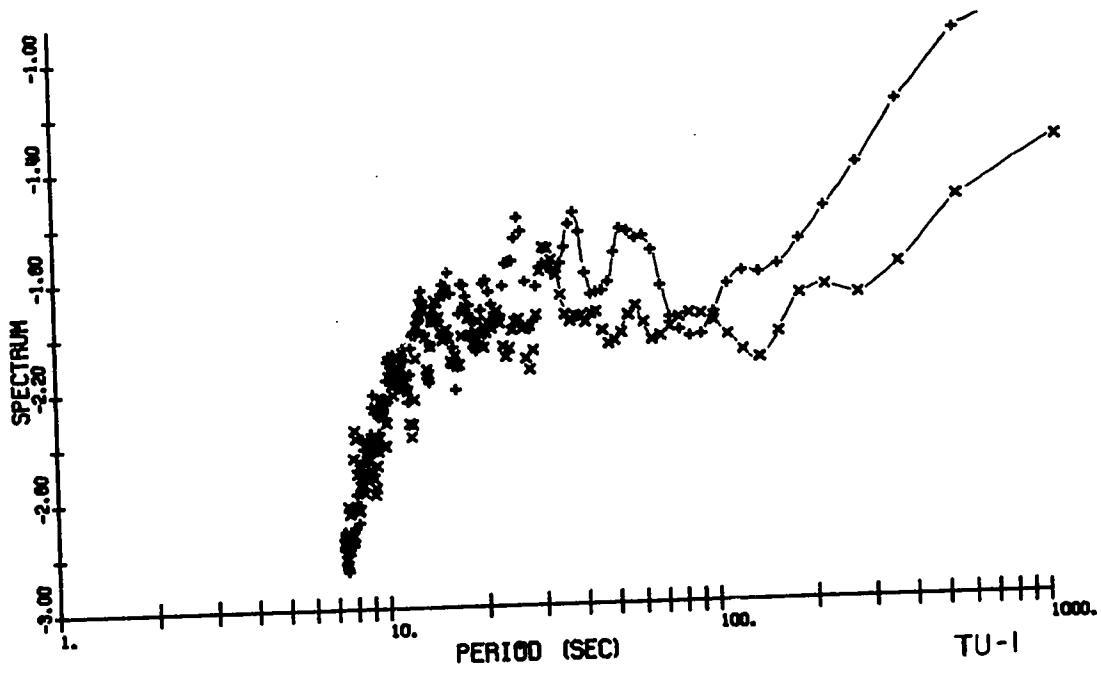
Figure 4.21:   Tensor apparent resistivities for Turin location.

Theoretical Model

$\rho_1 = 7\,\Omega M$	$h_1 = 0.37$ km.
$\rho_2 = 15\,\Omega M$	$h_2 = 0.43$ km.
$\rho_3 = 8\,\Omega M$	$h_3 = 0.24$ km.
$\rho_4 = 30\,\Omega M$	$h_4 = 2.15$ km.

$\rho_5 = 400\,\Omega M$

$\triangle$ ρ_{21}
$\circ$ ρ_{12}
$\bullet$ $= 60°$

TENSOR APPARENT RESISTIVITY

1000
100
10
1

PERIOD (SEC)

TURIN

1   10   100   100(
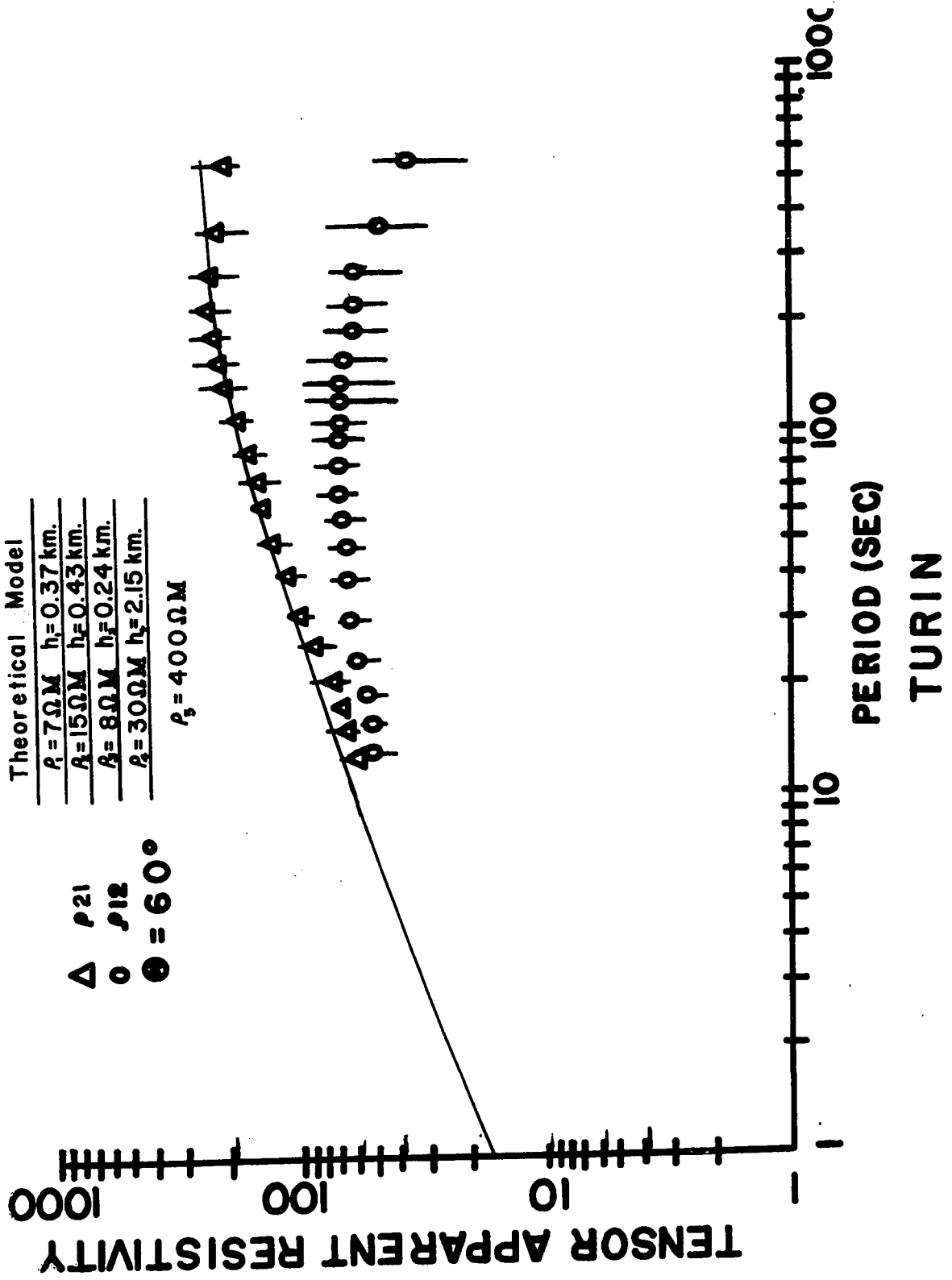
vi) Mossleigh (MO) (50° 48' latitude, 113° 18' longitude,

elevation: +3100 feet)

This recording site lies at the northern end of the "western" magnetotelluric profile. The location exhibits the same general characteristic anisotropy as all other stations presented in this work.

Figure 4.2m shows the results of rotating the impedance matrix. The minima of the diagonal tensor elements are shown to occur for rotation angles θ_1 = N 60°E and θ_2 = N 30°W. The anisotropy in apparent resistivity, shown in Figure 4.2n, occurs for periods of ten seconds and greater. As seen in Figure 4.4b, at this recording site the basement composition is reasonably homogeneous. Superimposed on the tensor $\rho_{21}(T, \theta)$ curve is a model derived from local well log data, and is a reasonable match to the experimental curve.

Figure 4.2m: Rotated diagonal tensor element at selected periods for Mossleigh data.

MOSSLEIGH

ROTATION ANGLE

$|Z_{11}|$
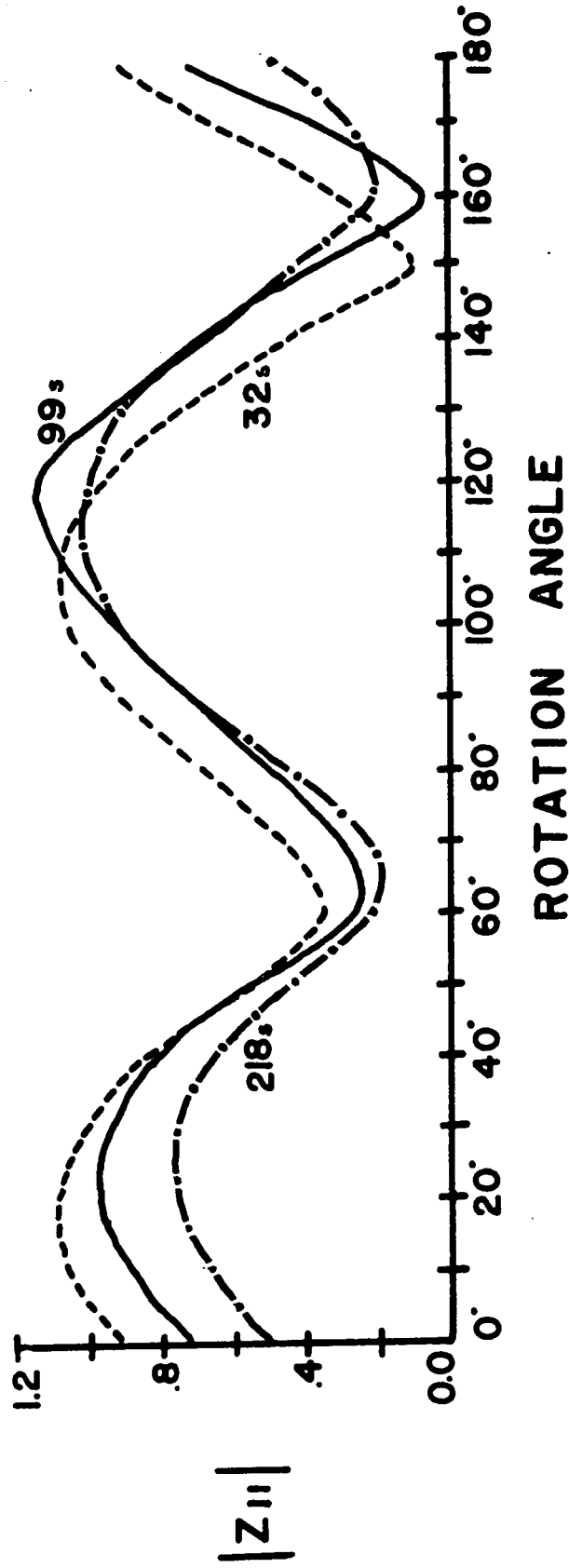
Figure 4.2n: Tensor apparent resistivities for Mossleigh data.

Theoretical Model

$\rho_1 = 6\,\Omega M$	$h_1 = .85\,km.$
$\rho_2 = 15\,\Omega M$	$h_2 = .80\,km.$
$\rho_3 = 30\,\Omega M$	$h_3 = 1.55\,km.$
$\rho_4 = 400\,\Omega M$	

$\triangle$ $\rho 21$
O $\rho 12$
θ $60°$

TENSOR APPARENT RESISTIVITY

PERIOD (SEC)

MOSSLEIGH
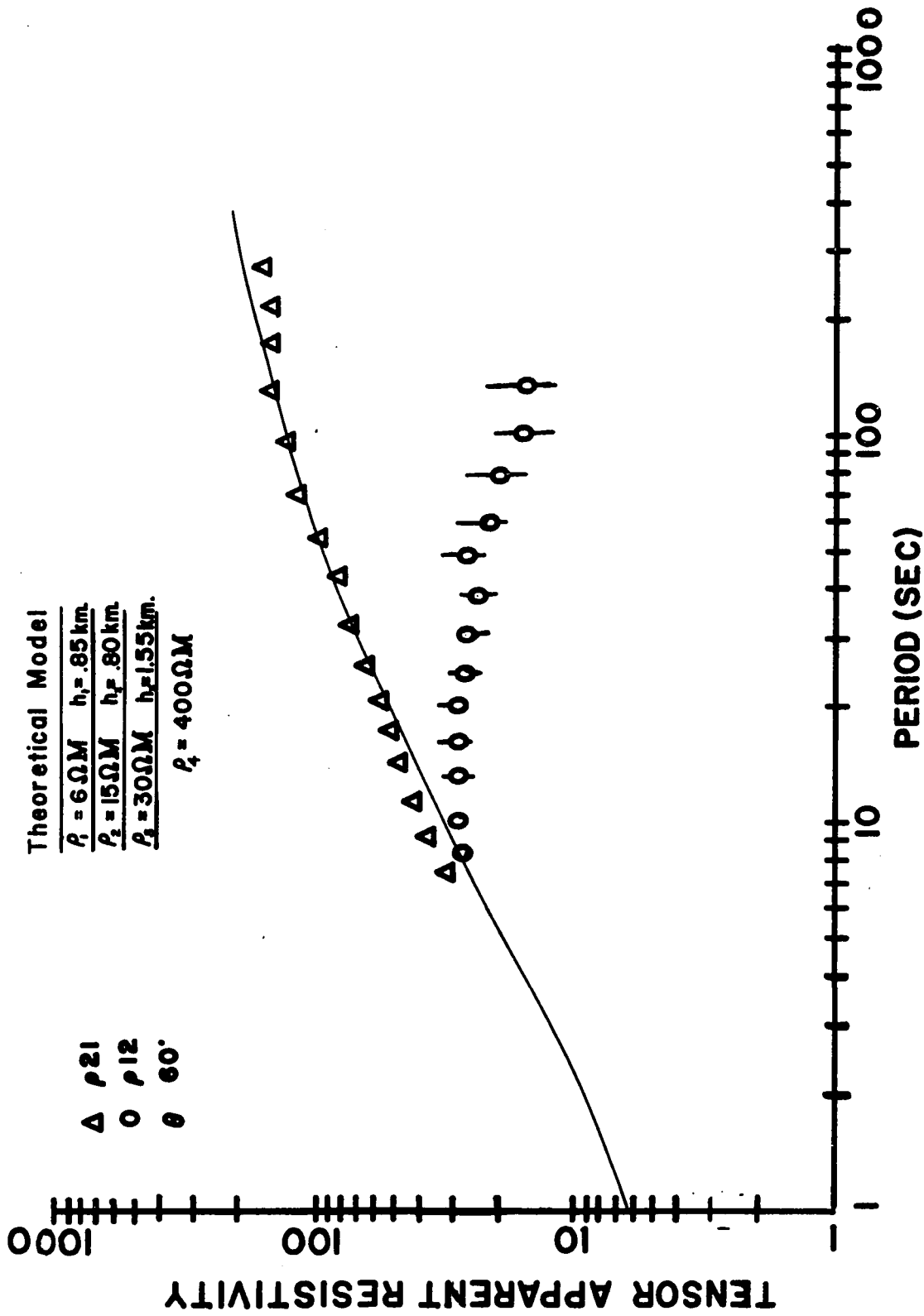
vii) Kilcardy (KC) (50° 17' latitude, 113° 15' longitude,

elevation: +3250 feet)

The Kilcardy and Carmangay locations are within 30 kilometers of the base of the foothill region in southern Alberta. Both of these stations exhibit a consistent anisotropy for all periods studied.

The principal directions of resistivity, as defined by $\min|z_{11}(T, \theta)|$, are defined by the rotation angles $\theta_1 \approx$ N 70°E and $\theta_2 \approx$ N 20°W (Figure 4.2o). A one dimensional model derived from local well log data appears to be a very reasonable fit to measured apparent resistivities for this station as seen in Figure 4.2p.

Figure 4.2o: Rotated diagonal tensor element at selected periods for the Kilcardy data.
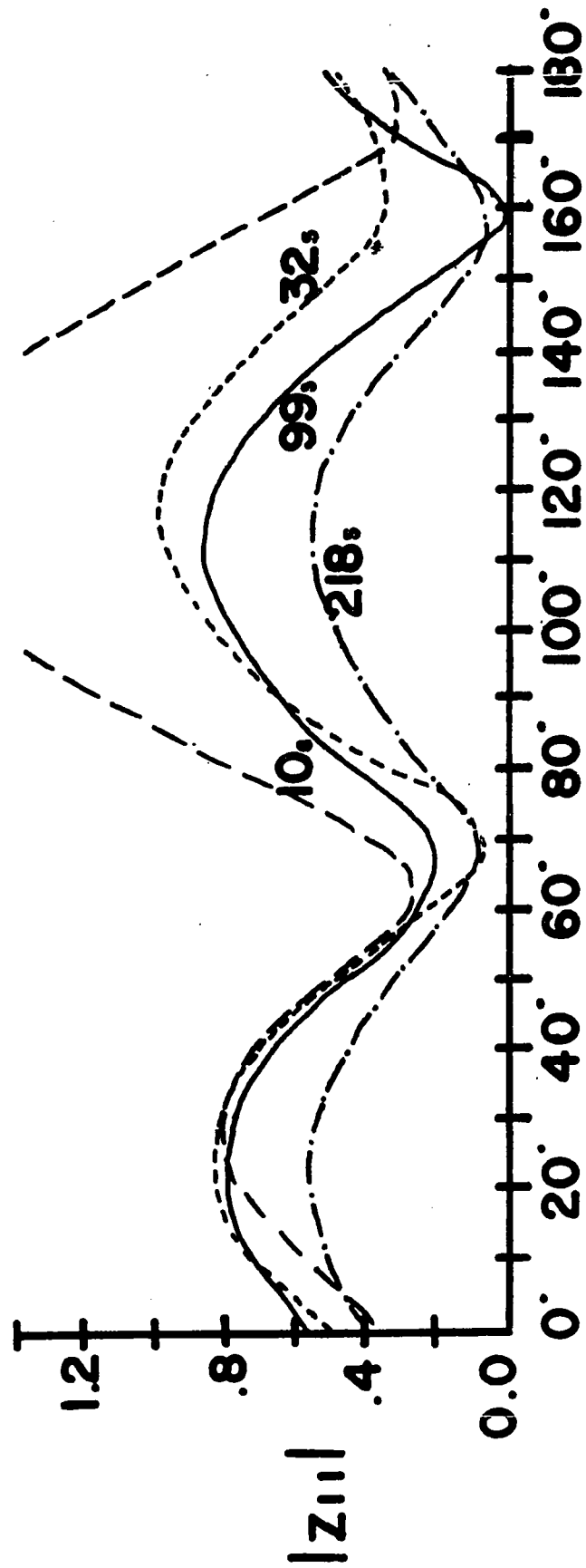
KILCARDY

Figure 4.2p: Tensor apparent resistivities for Kilcardy location.

TENSOR APPARENT RESISTIVITY

PERIOD (SEC)

KILCARDY

1000
100
10
1

1000
100
10

Theoretical Model
$\rho_1 = 10\,\Omega M$ $h_1 = 1.0$km.
$\rho_2 = 25\,\Omega M$ $h_2 = 1.0$km.
$\rho_3 = 30\,\Omega M$ $h_3 = 1.2$km.
$\rho_4 = 400\,\Omega M$

△ $\rho 21$
○ $\rho 12$
● $70'$

viii) Carmangay (CA) (50° 5' latitude, 113° 18' longitude, elevation: +3250 feet)

This station is the southern most location of the western profile. Tensor analysis indicate two orthogonal directions of principal resistivity defined by the rotation angles θ_1 = N 70°E and θ_2 = N 20°W (Figure 4.2q). Agreement between scalar and tensor analysis was quite good. The low degree of scatter of the scalar resistivities indicated only very small changes in the polarization parameters. Figure 4.2r shows the tensor apparent resistivities obtained from data at this location. The dip observable on the $\rho_{21}(T, \theta)$ curve for periods greater than 100 seconds appears to be due primarily to the fall off in magnetic activity and the inability of spectral analysis techniques to reliably handle the steep slopes of the power spectra.

The theoretical one dimensional model was derived from local well log data and represents a good fit for shorter periods. This location is in an area where the basement composition is reasonably laterally homogeneous.

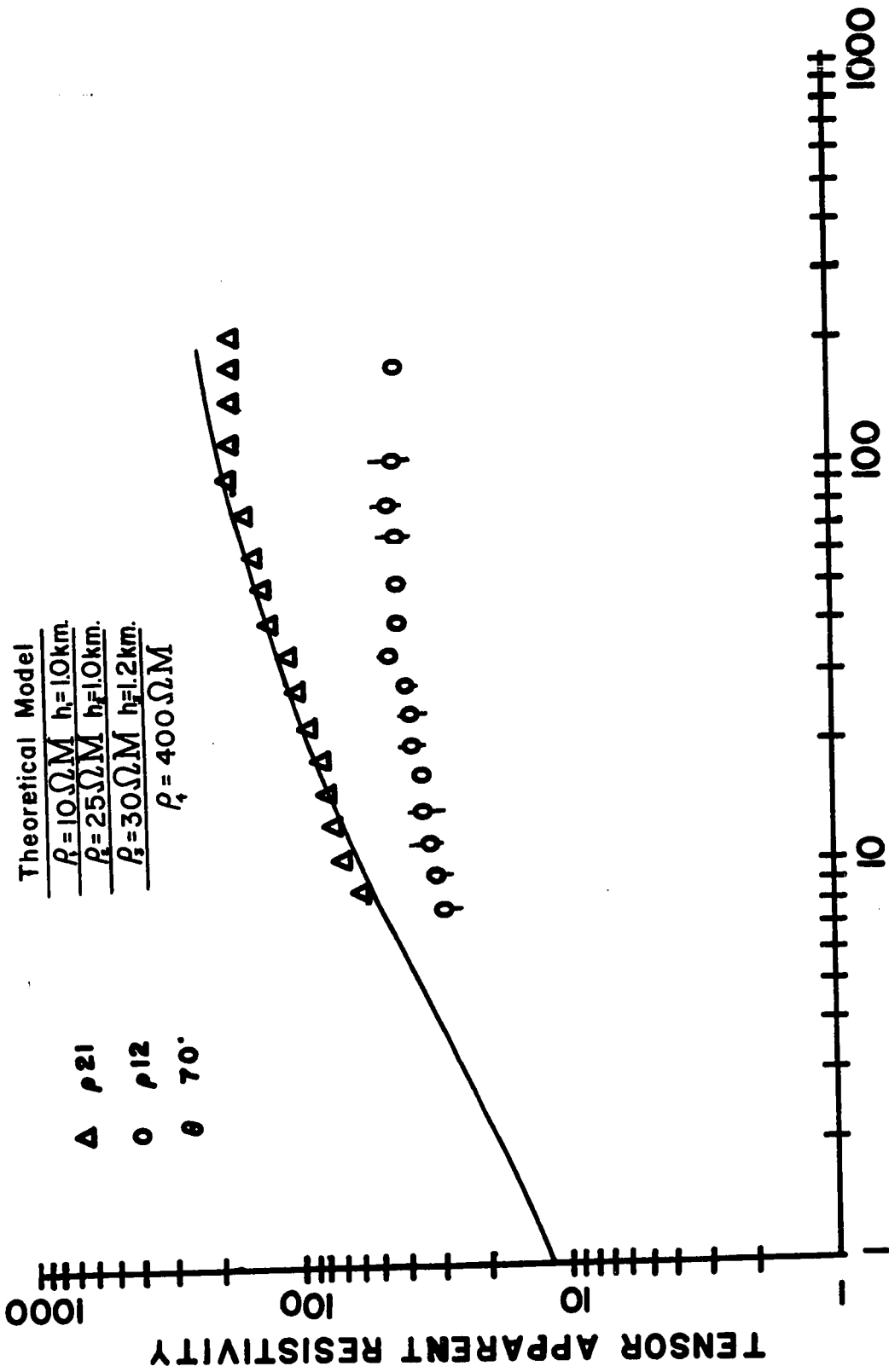*Figure 4.2q: Rotated diagonal tensor element at selected periods for Carmangay data.*
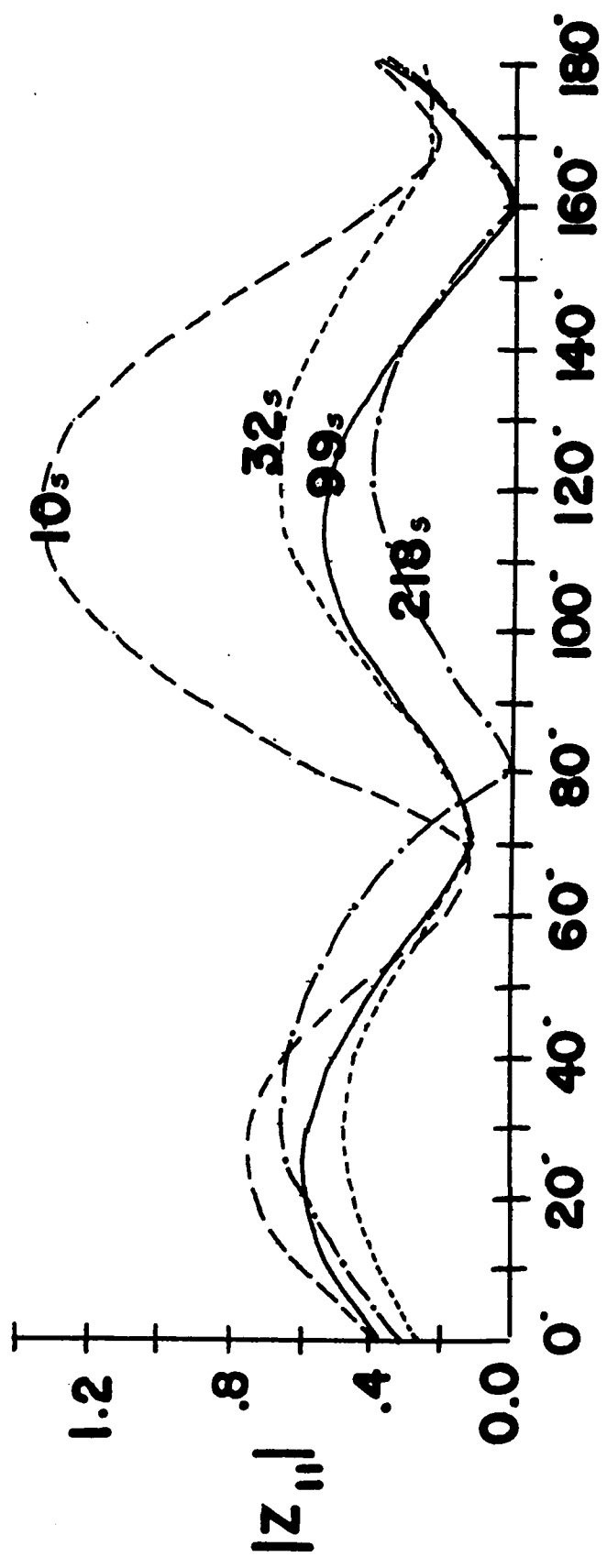
CARMANGAY

Figure 4.2r: *Tensor apparent resistivities for Carmangay location.*

CARMANGAY (68)

PERIOD (SEC)

TENSOR APPARENT RESISTIVITY

Theoretical Model

$\rho_1 = 15\Omega M$ $h_1 = .55km.$
$\rho_2 = 8\Omega M$ $h_2 = .67km.$
$\rho_3 = 20\Omega M$ $h_3 = 2.0km.$
$\rho_4 = 400\Omega M$

△ ρ 21
○ ρ 12
$\theta = 80°$
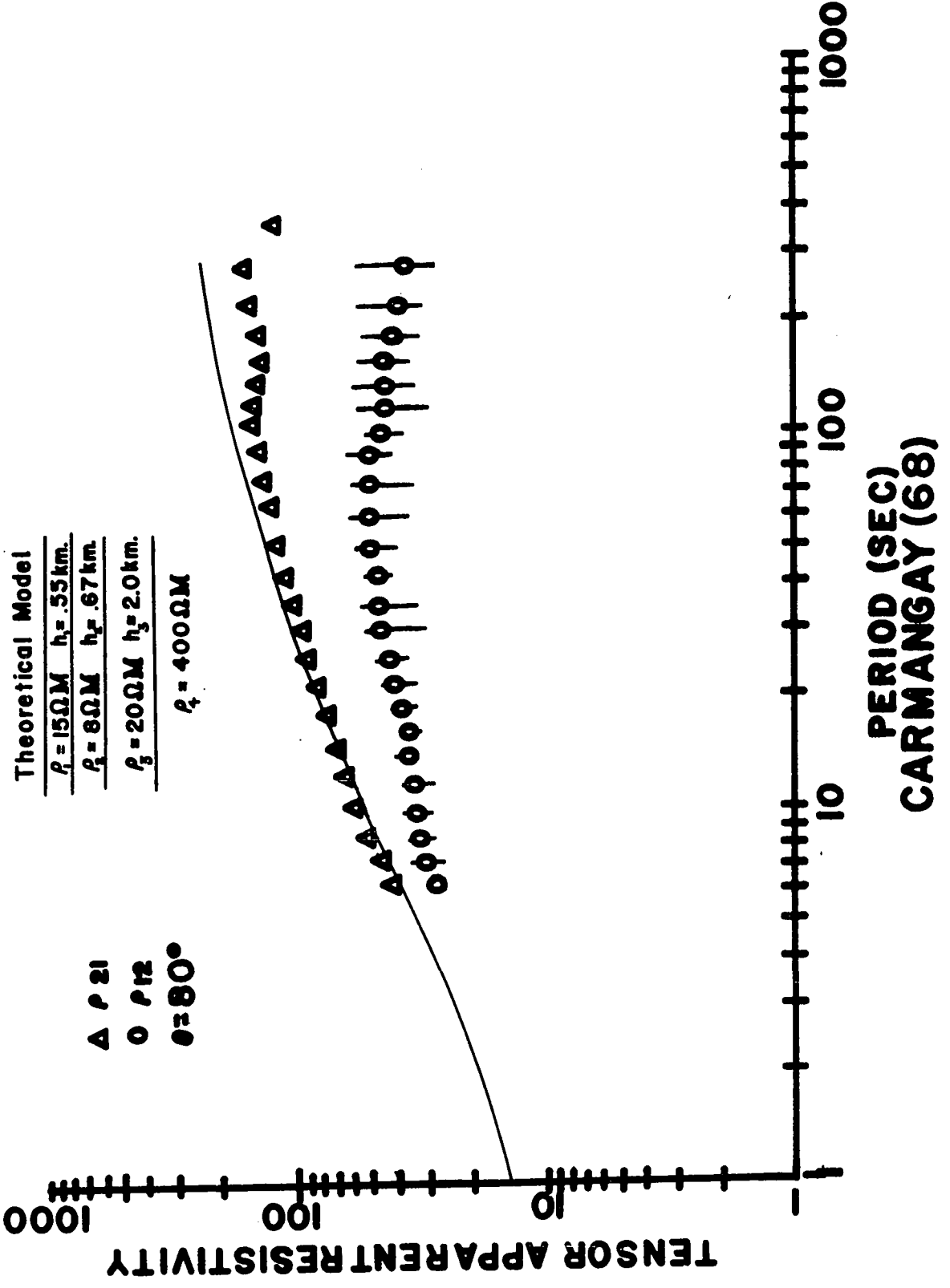
## 4.3 Other Geophysical Studies in Southern Alberta

a)   Gravity:

A gravity survey in southern Alberta has been carried out by the seismic members of the geophysics group at the University of Alberta using a Worden Model XPO gravimeter. The gravity readings were reduced to Bouguer gravity anomalies and combined with data provided by the Gravity Division of the Dominion Observatory of Canada, Gulf Canada Limited, and Chevron Standard Limited. A total of 1800 gravity readings was reduced and the complete Bouguer gravity anomaly map is shown in Figure 4.3a (Kanasewich et al - 1969). The pronounced east-west trending Bouguer gravity low extends across most of southern Alberta except for a positive anomaly northeast of Brooks called the Princess high and the north-south trend over the Rocky Mountain System.

Superimposed on the Bouguer gravity anomaly map are the locations at which magnetotelluric recording stations were placed. The principal directions of resistivity, obtained by minimizing the diagonal elements of the magnetotelluric impedance tensor, are also shown for seven recording stations.

The overall correlation of Bouguer gravity anomaly contours and principal resistivity directions is very good, implying that at least to some degree the subsurface geophysical features are being detected and trends are being outlined by the magnetotelluric technique.

Figure 4.3a: Bouguer gravity anomalies in southern Alberta (after Kanasewich et al - 1969) and the principal directions of resistivity for seven magnetotelluric recording locations. The larger apparent resistivities are indicated as the axis of increased length.
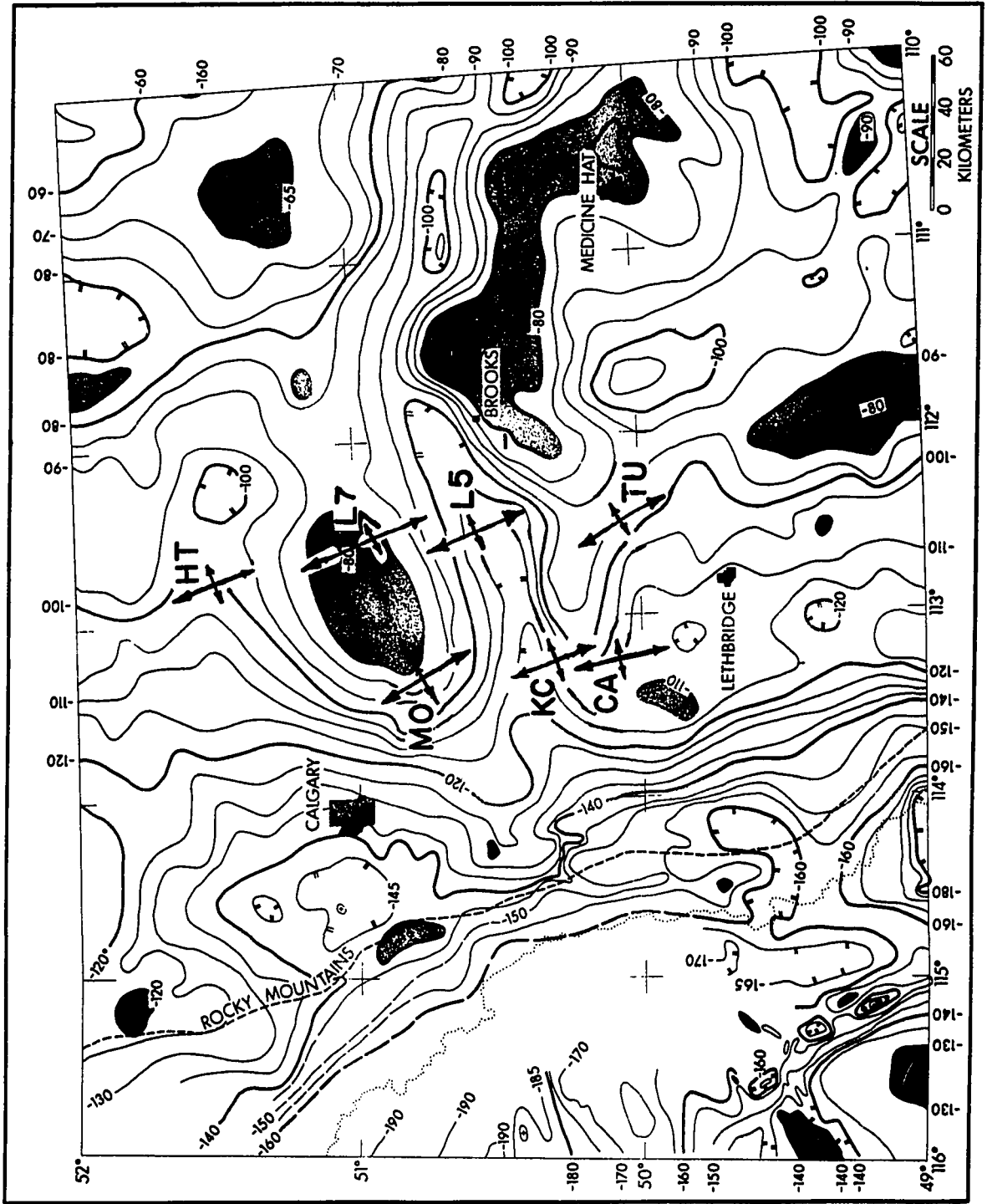
b)   Magnetometer Survey:

A ground magnetometer survey in the southern Alberta area was also compiled by the seismic members of the geophysics group at the University of Alberta using a Barringer Model GM - 102A nuclear precession magnetometer with an accuracy of 10 gammas. The residual total magnetic field intensity map, Figure 4.3b, (after Kanasewich - 1968) was computed by subtracting the first seven harmonics of the regional magnetic field from the observed magnetic values. The 100 gamma contours on the residual magnetic intensity map displays a strong east-west trend in the region of the magnetotelluric recording stations. Superimposed on the residual map contours are the principal directions of resistivity obtained by the magnetotelluric tensor analysis of data from each magnetotelluric recording station.

c)   Seismic:

On the basis of reflection seismology in this region and the gravity and magnetic survey previously mentioned, Clowes et al (1968) have produced the generalized crustal cross section shown in Figure 4.3c. The fault shown in the central part of the section has been confirmed seismically, but the postulated fault on the southern end of the profile is based on ambiguous reflection data. The gravity calculations show that the fault is required to produce the steep gravity gradient. (Clowes - 1969).

Figure 4.3b: A residual total magnetic field intensity map
for southern Alberta (after Kanasewich - 1968) with
the principal directions of resistivity for seven
magnetotelluric recording locations. The larger
apparent resistivities are indicated as the axis of
increased length.

RESIDUAL TOTAL

MAGNETIC FIELD INTENSITY

SCALE

0   20   40   60
KILOMETERS

Contour Interval: 100 Gammas

MEDICINE HAT

LETHBRIDGE

CALGARY

ROCKY MOUNTAINS

KIMBERLEY

ALBERTA

BRITISH COLUMBIA
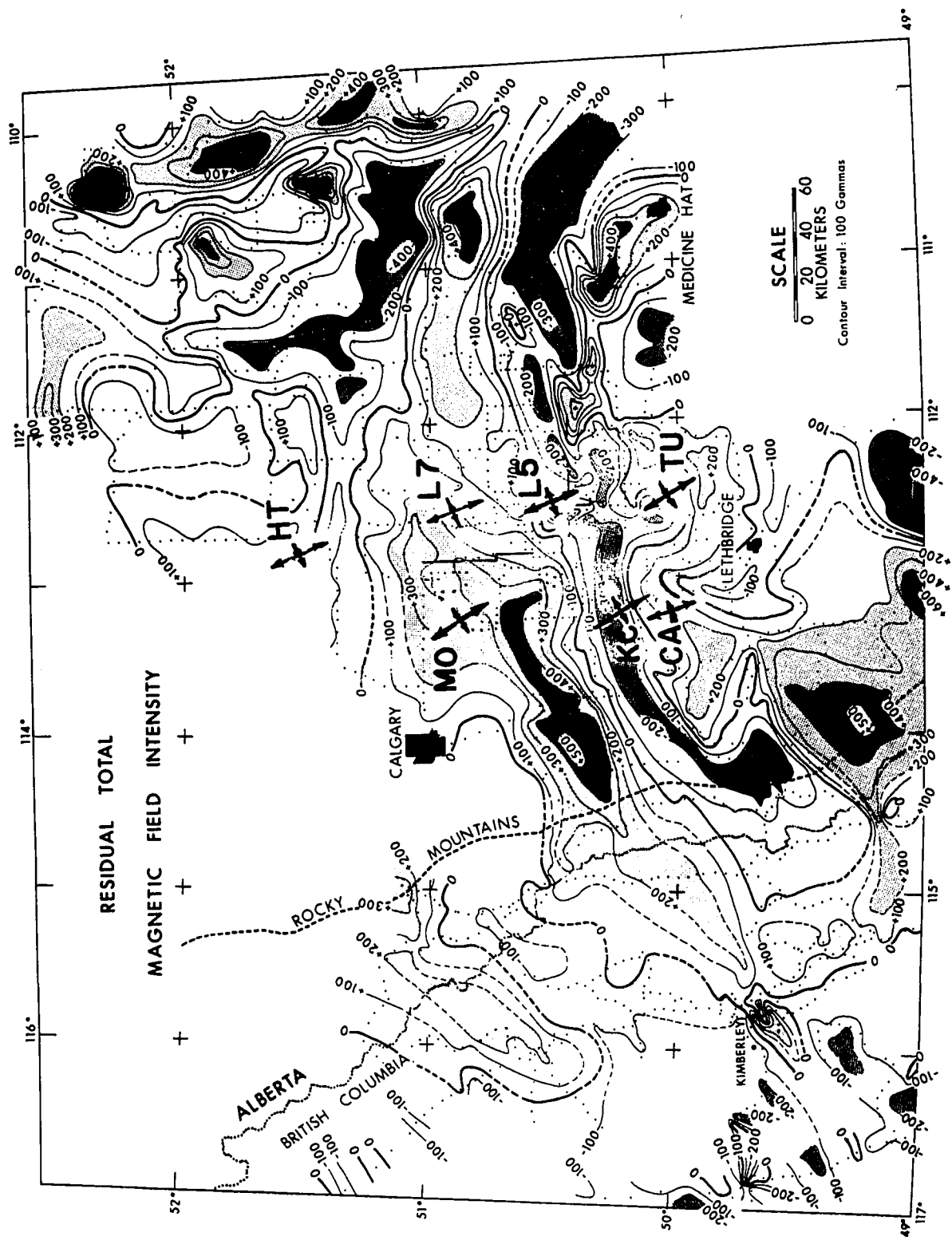
HT

MO

L7

L5

KC

CA

TU

Figure 4.3c: Generalized north-south cross section of
     residual total magnetic field intensity, Bouguer
     gravity, and generalized seismic cross section for
     southern Alberta.

BOUGUER GRAVITY (milligals)

DEPTH (kilometers)

DISTANCE (kilometers)

Residual Total Magnetic Field Intensity (gammas)

TURIN   LOCN I   LOCN 5   LOCN.7   Huxxar   Rosebud
Enchant Lomond   Crowfoot
         Jumping Buffalo

Mesozoic
Paleozoic
Precambrian

2.80   6.5   2.67   2.3   3.2   5.8

3.45 gm/cc   8.2 km/s

R   M
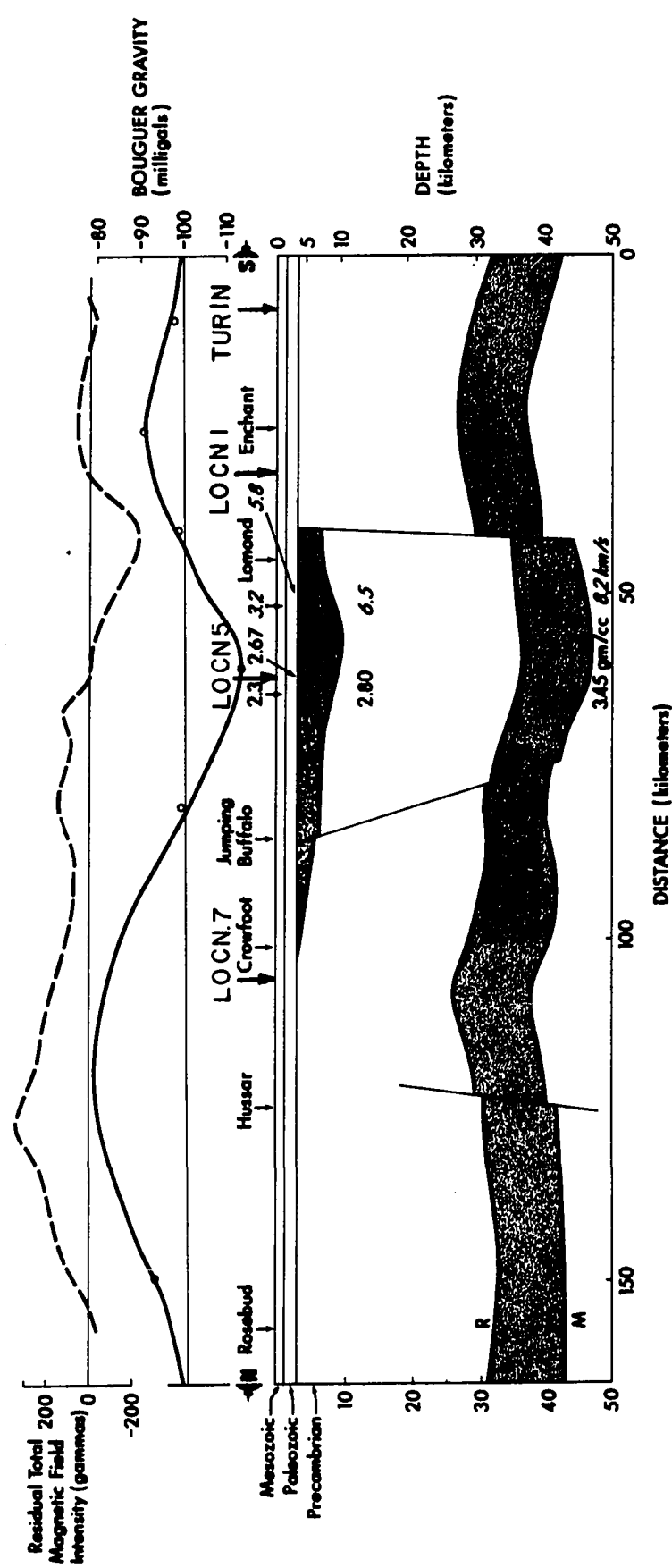
4.4 Interpretation of Magnetotelluric Results.

The ρ_{21} tensor apparent resistivity curves shown in section 4.2 generally agree with the work done by others in the Alberta plains (Srivastava and Jacobs - 1963; Vozoff, Hasegawa, and Ellis - 1963; Srivastava, Douglass, and Ward - 1963; Ellis - 1964; Vozoff and Ellis - 1966). However there is only a slight resemblance of the ρ_{12} apparent resistivity curves with those published by the above mentioned workers. This is partially due to the fact that previously only scalar resistivities have been calculated and this work represents the first regional magnetotelluric survey in Alberta using tensor analysis and rotation into the principal resistivity directions. I. K. Reddy (private communication) has found that data from other magnetotelluric recording sites in the Alberta plains which have been analysed using tensor techniques also show similar anisotropic behavior.

To interpret accurately the resistivity curves at this time would certainly be desirable but not enough information is presently available. The lack of high resolution data in the 100 - 1000 second range is a great drawback. Several workers (Niblett and Sayn-Wittenstein - 1960; Srivastava et al - 1963; Vozoff et al - 1963; Vozoff and Ellis - 1966) have presented magnetotelluric results from Alberta which reportedly indicate a high conductivity zone between 60 - 150 kilometers. If this zone does exist then the apparent resistivity curves presented here will not give a clear indication of deep crustal resistivities (which could be of

the order of 10^3 - 10^4 ΩM.) due to limited bandwidth of the recording apparatus. If the high conducting zone does not exist then the deep crustal resistivities must be approximately 300 - 400 ΩM. which does agree with values from well log data which penetrate the Precambrian surface in Alberta.

Caner and Auld (1968) have presented scalar resistivity curves taken at Victoria, B.C. These curves show apparent resistivities of 5000 ΩM. for T = 3 seconds which decrease to 2000 ΩM. for T = 80 seconds. This indicates the Rocky Mountain/Sedimentary Basin System, to a first order approximation, might be treated as a vertical fault with high resistivity values to one side and low resistivity values on the opposite side of the fault.

The case of a vertical contact fault with an infinitely deep basement has been treated analytically by d'Erceville and Kunetz (1962; see section 2.3). In this model the electric field is normal to the fault strike. Figure 2.3a (after d'Erceville and Kunetz) shows the behavior of the $|\frac{E}{H}|$ ratio as the fault is approached for various resistivity contrasts. As the fault is approached from the low resistivity side, the $|\frac{E}{H}|$ ratio drops rapidly in value. The ratio is discontinuous at the fault boundary, and then assumes a large value which converges to the value of $|\frac{E}{H}|$ for the non-fault case as x → ∞. Swift (1968) has used a network solution approximation to calculate theoretical apparent resistivities for a vertical contact fault (ρ_1 = 10 ΩM., ρ_2 = 100 ΩM., period = 10^3 seconds) for the electric

Figure 4.4a: Theoretical field relationships over an

infinite vertical contact fault (after Swift - 1967).

RESISTIVITY MODEL

$\rho_1 = 10 \, \Omega \, M$

$\rho_2 = 100 \, \Omega \, M$

○ E PARALLEL

● E PERPENDICULAR

ρ_a

DISTANCE FROM FAULT (KM)
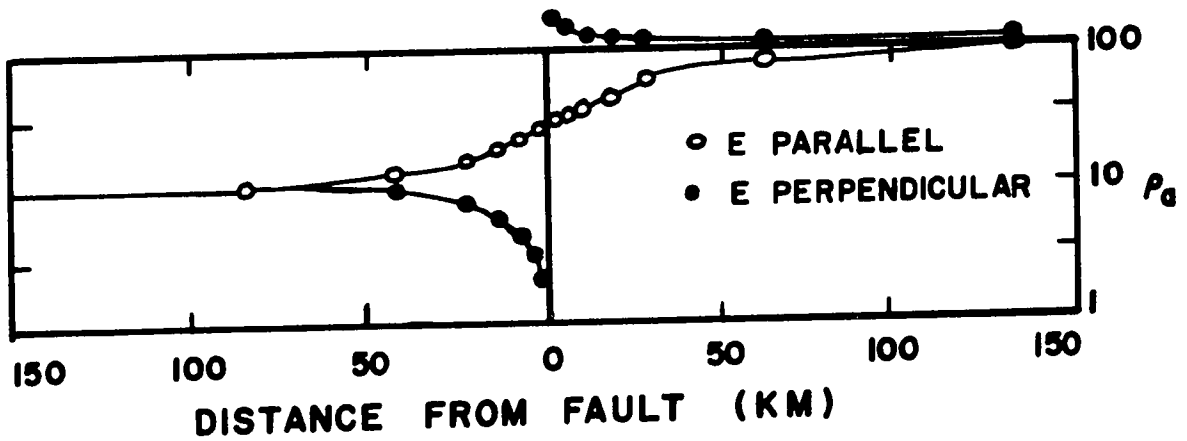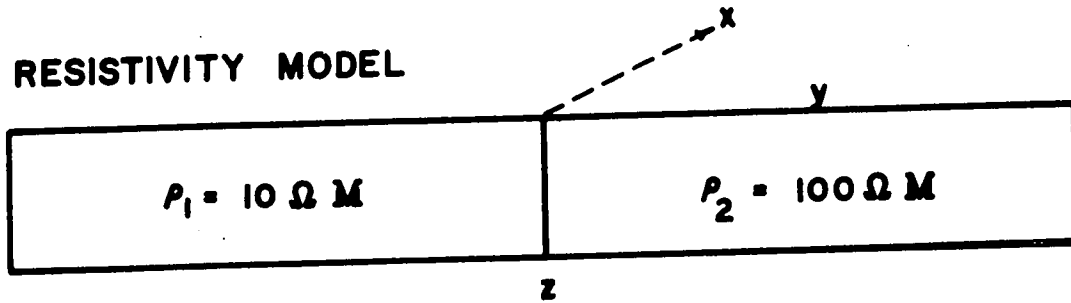
PERIOD = 10^3 SEC.

polarization parallel and normal to the vertical contact (see

Figure 4.4a).

This situation appears to model the results obtained in

the sedimentary basin in Alberta (the low resistivity side)

in this work. The $\rho_{12}(T, \theta)$ curves (corresponding to the $E_\perp$

case) have much lower values than the $\rho_{21}(T, \theta)$ values (cor-

responding to the $E_\parallel$ case). Since there are still signifi-

cant deviations of theoretical apparent resistivity curves

for the $E_\perp$ case with 10:1 resistivity ratio at 100 kilometers

from the fault (and since all magnetotelluric locations

presented here are within 100 kilometers of the base of the

foothills of the Rocky Mountain System) it is doubtful

whether the ρ_{21} curves give a true assessment of subsurface

resistivities. It is highly probable that the apparent

resistivities presented here are lower than the true values

of crustal resistivities.

A second interpretation possibility also exists.

Garland and Burwash (1959) have stated that the Bouguer

anomaly field over central Alberta must be due to lithologi-

cal changes in the basement which trend to the northeast in

the sedimentary basin. The lithology of the Precambrian

basement as inferred from well samples and gravity anomalies

is shown in Figure 4.4b. Their rough calculations indicate

that the changes in lithology begin somewhere near the

Precambrian surface and could extend as deep as nine kilo-

meters into the basement. Rankin and Reddy (1969) have

attempted to interpret scalar resistivity curves from the

Figure 4.4b: Lithology of the Precambrian basement as
inferred from well samples and gravity anomalies
(after Garland and Burwash - 1959).

Edmonton

RD

HT

Banff Calgary

L7

MO L5
KC
CA TU
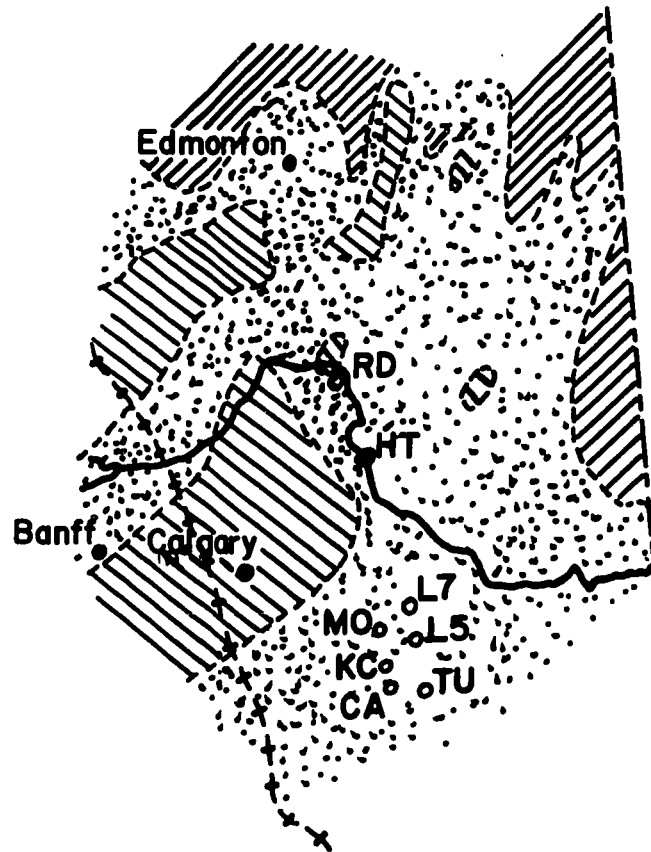
MT RECORDING LOCATION   o
FOOTHILLS FRONT (SURFACE) ┼

BASEMENT LITHOLOGY

Chiefly Gneiss
Granitic
Basic Phases

University of Alberta Geophysical Observatory, Edmonton, Alberta, in terms of the subsurface features. Their model indicates an anisotropic layer of 10:1 resistivity contrast from 5.5 kilometers to 14.5 kilometers in depth.

It should be noticed also that the closer the magneto- telluric recording location was to the base of the foot- hills, the shorter the period at which the anisotropy in apparent resistivity begins. Thus the Red Deer apparent resistivity curves, roughly 80 kilometers from the base of the foothills exhibit a divergence beginning at 20 seconds, while the closest stations to the foothills, Carmangay and Kilcardy, exhibit anisotropies which occur at periods con- siderably less than ten seconds. For these reasons, it is felt that lateral inhomogenieties must induce the major part of the anisotropy.

Despite the overall anisotropic character of apparent resistivity which appears to be consistent over a large area, it still appears possible to garner some general information about local subsurface structure by magnetotelluric methods. Figure 4.4c shows the apparent resistivity from the "eastern" north-south magnetotelluric profile plotted for four periods (25, 50, 75, and 100 seconds). The approximate location of the southern seismic fault is also shown. If the apparent resistivities do indicate a vertical fault it would appear to lie between stations Turin and Location 1. Figure 4.4d shows the same type of diagram for the "western" profile,

which while consistent with the eastern profile does not have enough coverage to be interpreted at present.

*Figure 4.4c: Rotated tensor apparent resistivity values
for selected periods along the "eastern" north-south
magnetotelluric profile in southern Alberta.*
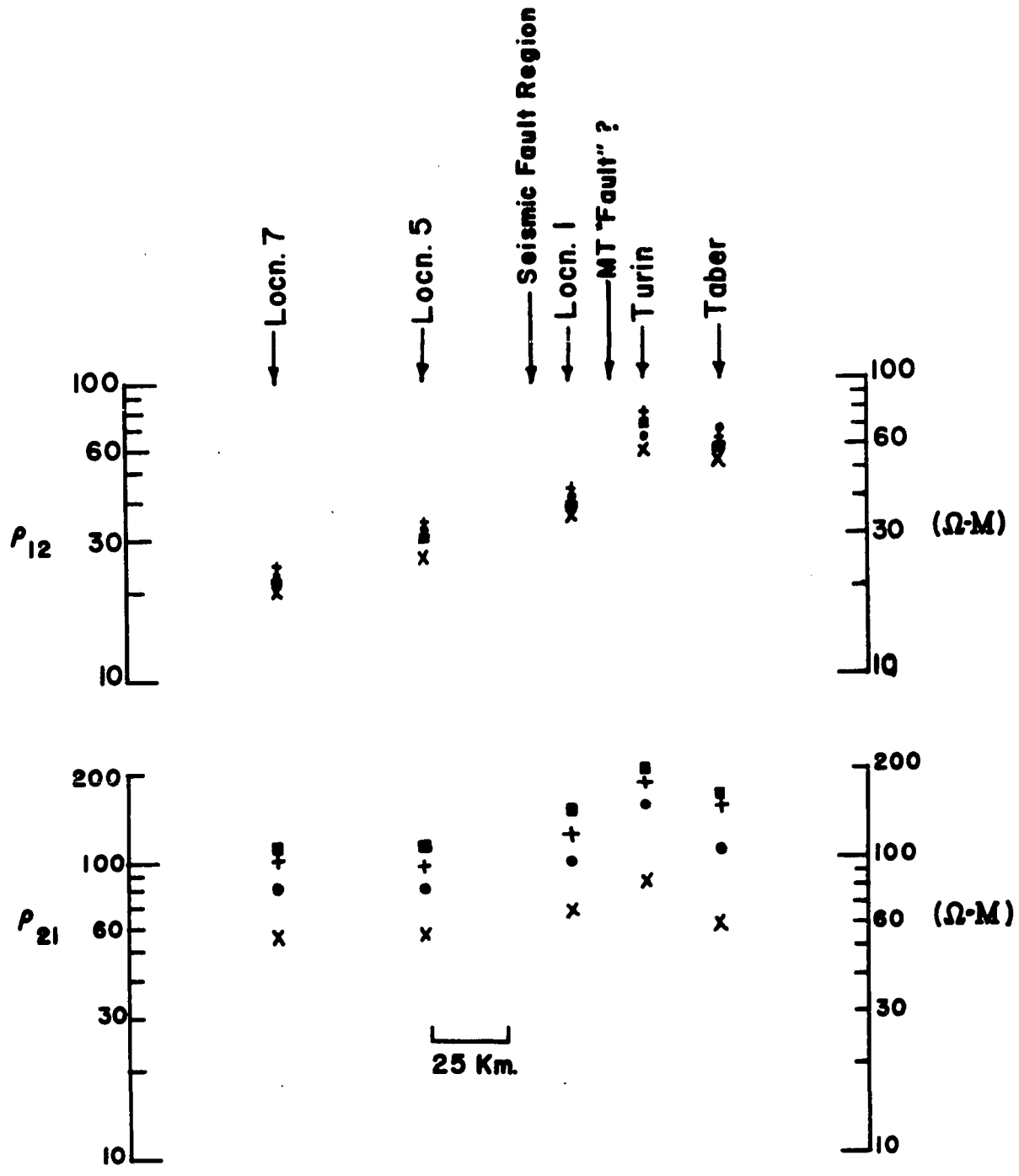
Figure 4.4d: *Rotated tensor apparent resistivity values for selected periods along the "western" north-south magnetotelluric profile in southern Alberta.*
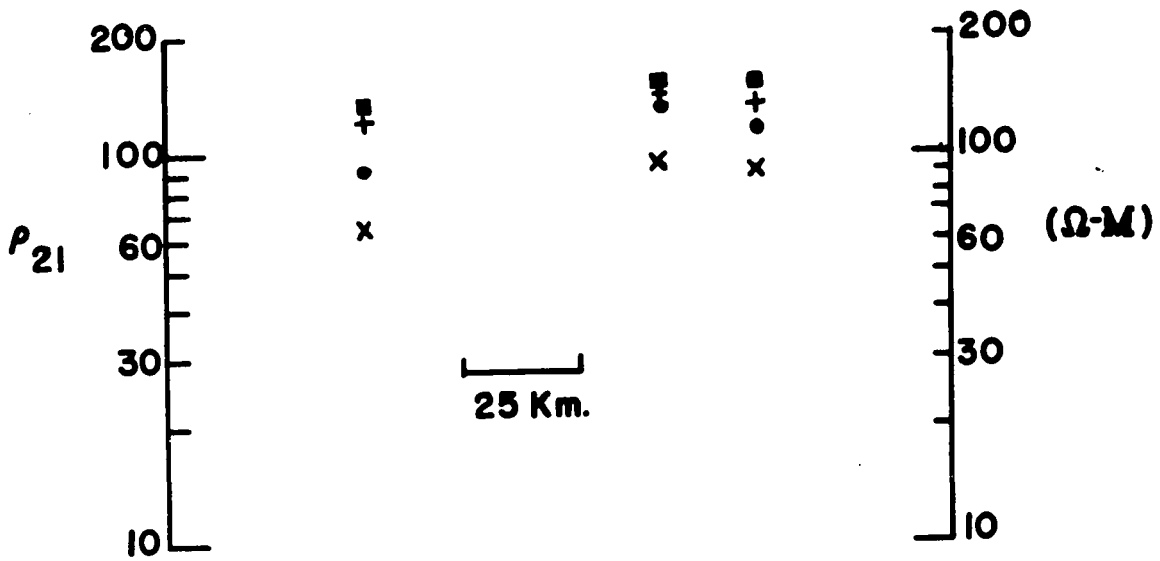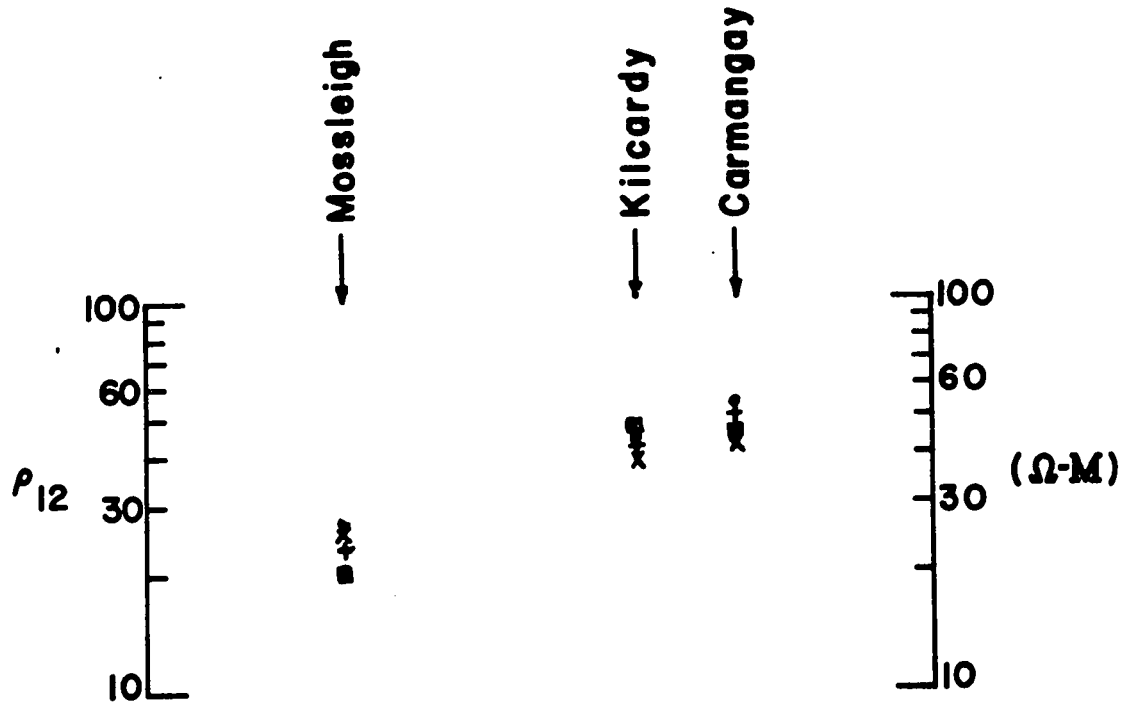
CHAPTER V

CONCLUSIONS

5.1 Conclusions

Techniques of analysis have been presented which produce consistent apparent resistivity estimates for periods of 10 to several hundred seconds. It has been indicated that some of the scatter in apparent resistivity curves previously presented by other workers using techniques of spectral analysis is due to steep slopes in the power spectra of the magnetotelluric fields and the inability of spectral techniques to reliably handle this situation.

Tensor analysis of magnetotelluric data has been shown to indicate a consistent and marked anisotropy for all magnetotelluric recording locations presented in central and southern Alberta. It has also been shown that the principal directions of tensor apparent resistivity show a correlation with both Bouguer gravity anomaly and residual total magnetic field trends. An argument has been presented to indicate that the Rocky Mountain System represents a lateral resistivity inhomogeniety which would appear as an anisotropy in apparent resistivity throughout the sedimentary basin. Modeling the Rocky Mountain/Sedimentary Basin as a vertical fault of 10:1 resistivity contrast offers tentative explanation for the observed anisotropies in apparent resistivity. This very crude model is greatly over simplified but

consistutes a major step towards understanding the true resistivity structure in Alberta.

Subsurface structure in central and southern Alberta generally trends in the northeast direction and these structures may induce a portion of the anisotropy. An accurate evaluation however of the relative magnitude of this effect is not possible with the present level of knowledge and degree of sophistication of interpretational techniques.

It has also been shown that magnetotelluric profiling the region of seismically located precambrian rift valley faults produced evidence which can be interpreted as a vertical contact resistivity fault and can be used to interpret local structural effects.

5.2 Suggestions for Future Work

The results obtained in this work indicate that an extensive program of magneto-telluric profiling would be justified in order to study the deep crustal structure in this sedimentary basin. Interpretational models capable of handling lateral inhomogenieties must be developed in order to understand fully the resistivity structure in this and other similar areas.

Before interpretation of upper mantle conductivities is attempted a thorough investigation must be made of source characteristics as they pertain to Alberta. Until this step has been accomplished, further magnetotelluric results for deep lying resistivities must be regarded as ambiguous.

Although data analysis techniques are presently well in advance of interpretational possibilities, some degree of further sophistication is still thought necessary. An extremely useful development would be techniques of pre-whitening in which the filter is individually tailored to each spectra. This would circumvent a major problem in the accurate estimation of spectra not only in magnetotelluric studies but many other disciplines which currently make use of spectral analysis techniques. Similarly, techniques should also be developed to use the polarization properties of magnetotelluric signals to enhance the signal to noise ratio in the same manner as seismic REMODE filters are used.

The spectral bandwidth of the recording instruments must be extended to expand the interpretational possibilities. The technical development of sensors and the conversion of recording systems to digital format will assist in this improvement.

Airy, G. B., 1868. Comparison of magnetic disturbances
    recorded by the self-registering magnetometers at the
    Royal Observatory, Greenwich, with magnetic disturbances
    deduced from the corresponding terrestrial galvanic
    currents recorded by the self-registering galvanometers
    of the Royal Observatory. *Phil. Trans. Roy. Soc.*,
    v. 158, p. 465.

Anderssen, R. S., 1968. Note on conductivity models for the
    earth. *J. Geophys. Res.*, v. 73, p. 6535 - 6543.

Berdichevsky, M.N., 1960. Electrical prospecting with the
    telluric current method. *Gostoptekhizdot*, Moscow.
    (English translation by G. V. Keller, 1965. *Quarterly
    of the Colorado School of Mines*, v. 60, p.1.)

Blackman, R. B., and J. W. Tukey, 1958. *The Measurement of
    Power Spectra*. Dover Publication, New York.

Born, M., and E. Wolf, 1959. *Principles of Optics*. Pergamon
    Press, New York.

Bostick, F. X., Jr., and H. W. Smith, 1962. Investigation of
    large-scale inhomogeneities in the earth by the magneto-
    telluric method. *Proc. IRE*, v. 50, p. 2339 - 2346.

Burwash, R. A., 1957. Reconnaissance of subsurface precam-
    brian of Alberta. *Bull. Am. Assoc. Pet. Geol.*, v. 41,
    p. 70 - 103.

Cagniard, L., 1953. Basic theory of the magnetotelluric
    method of geophysical prospecting. *Geophysics*, v. 18,
    p. 605 - 635.

Campbell, W. H., 1966. A review of the equatorial studies of
    rapid fluctuations in the earth's magnetic field. *Ann.
    Geophys.*, v. 22, p. 492 - 501.

Campbell, W. H., and S. Matsushita, 1962. Auroral zone
    geomagnetic micropulsations with periods of five to 30
    seconds. *J. Geophys. Res.*, v. 67, p. 555 - 573.

Caner, B. and D. R. Auld, 1968. Magneto-telluric determin-
    ation of upper mantle conductivity structure at Victoria,
    British Columbia. *Can. Journ. Earth Sci.*, v. 5,
    p. 1209 - 1220.

Cantwell, T., 1960. *Detection and analysis of low frequency
    magnetotelluric signals*. Ph.D. thesis, Department of
    Geology and Geophysics, Massachusetts Institute of
    Technology.

Cantwell, T., and T. R. Madden, 1960. Preliminary report on crustal magnetotelluric measurements. *J. Geophys. Res.*, v. 65, p. 4202 - 4205.

Clement, K. T., 1860. *Das Grosse Nordlicht in der Nacht zum 29. Aug. 1859 und die Telegraphenverwirrung in Nord-Amerika and Europa.* Hamburg.

Clowes, R. M., E. R. Kanasewich, and G. Cumming, 1968. Deep crustal seismic reflections at near - vertical incidence. *Geophysics*, v. 28, p. 441 - 451.

Clowes, R. M., 1969. *Seismic reflection investigations of crustal structure in southern Alberta.* Ph.D. thesis, Edmonton: University of Alberta, Department of Physics.

Cooley, J. W., and J. W. Tukey, 1965. An algorithm for the machine calculation. of complex Fourier series. *Mathematics of Computation*, v. 19, p. 297 - 307.

Cumming, G. L. and E. R. Kanasewich, 1966. *Crustal structure in western Canada.* Project Vela-Uniform, Final Report AFCRL-66-519, Bedford, Mass.

d'Erceville, I., and G. Kunetz, 1962. The effect of a fault on the earth's natural electromagnetic field. *Geophysics*, v. 27, p. 651 - 655.

Eckhardt, Donald H., 1968. Theory and interpretation of the electromagnetic impedance of the earth. *J. Geophys. Res.*, v. 73, p. 5317 - 5326.

Ellis, R. 1964. *Analysis of natural ultra low frequency electromagnetic fields.* Ph.D. thesis, Edmonton: University of Alberta, Department of Physics.

Foster, M. R., and N. J. Guinzy, 1967. The coefficient of coherence: its estimation and use in geophysical data processing. *Geophysics*, v. 32, p. 602 - 616.

Fournier, H. G., 1963. Some remarks a propos of presently known magneto-telluric investigation and sounding curves. *Acta Technica*, Scientarum Hungaricae, v. 43, p. 453 - 466. (English translation by S. H. Ward and H. Fournier, 1963. A.N.R. Contract NONR 222 (89), Series No. 4, Issue No. 79.)

Fowler, R. A., B. J. Kotick, and R. D. Elliott, 1967. Polarization analysis of natural and artificially induced geomagnetic micropulsations. *J. Geophys. Res.*, v. 72, p. 2871 - 2883.

Garland, G. D., and R. A. Burwash, 1959. Geophysical and
    petrological study of precambrian of central Alberta.
    Bull. Am. Assoc. Petrol. Geologists, v. 43, p. 790 - 806.

Gentleman, W. M., and G. Sande, 1966. Fast Fourier transform
    for fun and profit. *AFIPS Proc.*, Fall Joint Computer
    conf., v. 29, p. 563 - 578.

Green, A. W., Jr., and B. H. List, 1963. The use of a total-
    field magnetometer in the magnetotelluric method of
    vertical resistivity profiling. *J. Geophy. Res.*, v. 68,
    p. 869 - 875.

Hatakayama, H., 1938. On the bay disturbance and the pulsation
    of the earth current. *Geophys. Mag.*, v. 12, p. 189 - 210.

Hirayama, M. 1934. On the relations between the variations
    of earth potential gradient and terrestrial magnetism.
    Journ. Met. Soc. Japan, v. 12, p. 16 - 22.

Hopkins, A. H. and H. W. Smith, 1966. *An investigation of
    magnetotelluric method for determining subsurface
    resistivities*. Report No. 140, EERL, University of
    Texas.

Jenkins, G. M., and D. G. Watts, 1968. *Spectral analysis and
    its applications*. Holden - Day, Inc., San Francisco,
    California.

Kanasewich, E. R., 1968. Precambrian rift: genesis of
    stratabound ore deposits. *Science*, v. 161, p. 1002 -
    1005.

Kanasewich, E. R., R. M. Clowes, and C. H. McCloughan, 1969.
    A buried precambrian rift in western Canada. (in press)

Kunetz, G., 1953. Correlation et recurrence des variations
    des courants tellureques et du champ magnetique. *Actes
    du Congres de Lux*, 72 eme Seo. de l'Association pour
    l'Advancement des Sciences.

Madden, T. and P. Nelson, 1964. *A defense of Cagnaird's
    magnetotelluric method*. Project NR-371-401, Geophysics
    Laboratory, Massachusetts Institute of Technology.

Mann, J. E., Jr., 1965. The importance of anisotropic
    conductivity in magnetotelluric interpretation.
    J. Geophys. Res., v. 70, p. 2940 - 2942.

McDonald, K. L., 1957. Penetration of the geomagnetic field
    through the mantle. *J. Geophys. Res.*, v. 62, p.117 - 141.

Morrison, H. F., 1967. *A magnetotelluric profile across the state of California.* Ph.D. thesis, Berkeley: Univ. of Calif.

Morrison, H. F., E. Wombwell, and S. H. Ward, 1968. Analysis of earth impedances using magnetotelluric fields. *J. Geophys. Res.*, v. 73, p. 2769 - 2778.

Morse, Phillip and H. Feshbach, 1953. *Methods of Theoretical Physics.* McGraw - Hill Book Co., Inc., New York.

Neves, A. S., 1957. *The magnetotelluric method in two-dimensional structures.* Ph.D. Thesis, Department of Geology and Geophysics, Massachusetts Institute of Technology.

Niblett, E. R., and C. Sayn-Wittgenstein, 1960. Variations of electric conductivity with depth by the magneto-telluric method. *Geophysics*, v. 25, p. 998 - 1008.

O'Brien, B. P., and H. F. Morrison, 1967. Electromagnetic fields in an n-layer anisotropic half-space. *Geophysics*, v. 32, p. 668 - 677.

Orange, A. S. and F. X. Bostick, 1965. Magnetotelluric micropulsations at widely separated stations. *J. Geophys. Res.*, v. 70, p. 1407 - 1413.

Parzen, E., 1961. Mathematical considerations in the estimation of spectra. *Technometrics*, v. 3, p. 167 - 189.

Price, A. T., 1962. The theory of the magnetotelluric method when the source field is considered. *J. Geophys. Res.*, v. 67, p. 1907 - 1918.

Rankin, D., 1962. The magnetotelluric effect on a dyke. *Geophysics*, v. 27, p. 666 - 676.

Rankin, D. and I. K. Reddy, 1969. A magnetotelluric study of resistivity anisotropy. *Geophysics*, v. 34, p. 438 - 449.

Richards, T. C. and D. J. Walker, 1959. Measurements of the earth's crustal thickness in Alberta. *Geophysics*, v. 24, p. 262 - 284.

Sande, G., 1965. *On an alternative method of calculating covariance functions.* Unpublished manuscript of Princeton University.

Schlumberger, M., and G. Kunetz, 1946. Variations rapides simultanus de champ tellurique en France et a Madagascar. *C. R. Acad. Sci. Paris*, v. 223, p. 551 - 553.

Shanks, John L., 1967. Recursion filters for digital processing. *Geophysics*, v. 32, p. 33 - 51.

Sims, W. E., and R. X. Bostick, Jr., 1969. *Methods of magnetotelluric analysis*. Technical Report No. 58, EGRL, University of Texas at Austin.

Srivastava, S. P., J. L. Douglass, and S. H. Ward, 1963. The application of magnetotelluric and telluric methods in central Alberta. *Geophysics*, v. 28, p. 998 - 1008.

Srivastava, S. P., 1963. Application of the magnetotelluric method to anisotropic and inhomogeneous bodies. *J. Geophys. Res.*, v. 68, p. 5857 - 5868.

Swift, C. M., Jr., 1967. *A magnetotelluric investigation of an electrical conductivity anomaly in the south-western United States*. Ph.D. thesis, Cambridge, Mass.: Massachusetts Institute of Technology.

Terada, T., 1917. On rapid periodic variations of terrestrial magnetism. *Journ. Col. Sci.*, Tokyo Imp. Univ., v. 37, p. 56 - 84.

Tichonov, A. N., 1950. Determination of the electrical characteristics of the deep strata of the earth's crust. *Doklady Akad. Nauk.*, U.S.S.R., v. 73, p. 295 - 297.

Vozoff, K., and R. M. Ellis, 1966. Magnetotelluric measurements in southern Alberta. *Geophysics*, v. 31, p. 1153 - 1157.

Vozoff, K., H. Hasegawa, and R. M. Ellis, 1963. Results and limitations of magnetotelluric surveys in simple geologic situations. *Geophysics*, v. 28, p. 778 - 792.

Vozoff, K. and C. M. Swift, Jr., 1968. Magneto-telluric measurements in the North German Basin. *Geophys. Prosp.*, v. 16, p. 454 - 473.

Vozoff, K., A. Orange, and H. S. Lahman, 1969. *Magneto-telluric deep earth resistivity at eight U.S. "Type - Locations."* Project NR 081-251/3-23-65, Geoscience Incorporated, Cambridge, Massachusetts.

Wait, J. R., 1954. On the relation between telluric currents and the earth's magnetic field. *Geophysics*, v. 19, p. 281 - 289.

Wait, J. R., 1962. *Electromagnetic waves in stratified media*. Pergamon Press, Inc., New York.

Wait, J. R., 1962. Theory of magneto-telluric fields. *Journ. Res. Nat. Bur. Standards, D,* v. 66D, p. 509 - 541.

Ward, S. H. and H. F. Morrison, 1966. Discussion of the preceding paper. *J. Geophys. Res.,* v. 71, p. 4053 - 4054.

Wescott, E. M. and V. P. Hessler, 1962. The effect of topography and geology on telluric currents. *J. Geophys. Res.,* v. 67, p. 4813 - 4831.

Whitham, K. and F. Anderson, 1966. Magnetotelluric experiments in Northern Ellesmere Island. *Geophys. Journ. Roy. Ast. Soc.,* v. 10, p. 317 - 345.

APPENDICES

Appendix I: Tensor Element Calculations

Section A-I-1: Calculation of Impedance Estimates.

The basic impedance relationship is given by:

$$\vec{E} = Z \vec{H}$$

or:

$$E_x(\omega) = z_{11} H_x(\omega) + z_{12} H_y(\omega)$$

$$E_y(\omega) = z_{21} H_x(\omega) + z_{22} H_y(\omega).$$

<div align="right">2.5 - 2</div>

Post-multiplying each of the above equations successively by $E_x^*(\omega)$, $E_y^*(\omega)$, $H_x^*(\omega)$, $H_y^*(\omega)$ (where $*$ denotes the complex conjugate) we have two sets of four equations each:

$$\left\langle \begin{Bmatrix} E_x^* \\ E_y^* \\ H_x^* \\ H_y^* \end{Bmatrix} E_x \right\rangle = z_{11} \left\langle \begin{Bmatrix} E_x^* \\ E_y^* \\ H_x^* \\ H_y^* \end{Bmatrix} H_x \right\rangle + z_{12} \left\langle \begin{Bmatrix} E_x^* \\ E_y^* \\ H_x^* \\ H_y^* \end{Bmatrix} H_y \right\rangle$$

<div align="right">A-1a, b, c, d</div>

$$\left\langle \begin{Bmatrix} E_x^* \\ E_y^* \\ H_x^* \\ H_y^* \end{Bmatrix} E_y \right\rangle = z_{21} \left\langle \begin{Bmatrix} E_x^* \\ E_y^* \\ H_x^* \\ H_y^* \end{Bmatrix} H_x \right\rangle + z_{22} \left\langle \begin{Bmatrix} E_x^* \\ E_y^* \\ H_x^* \\ H_y^* \end{Bmatrix} H_y \right\rangle$$

<div align="right">A-2a, b, c, d</div>

where $\langle \ \rangle$ denotes a cross or auto power spectral density.

Solving the A-1 set of equations we find solutions are of the form:

From A-1a and A-1b

$$(1) \quad z_{11} = \frac{\langle E_x^* H_y\rangle \langle E_y^* E_x\rangle - \langle E_x^* E_x\rangle \langle E_y^* H_y\rangle}{\langle E_x^* H_y\rangle \langle E_y^* H_x\rangle - \langle H_x^* H_x\rangle \langle E_y^* H_y\rangle}$$

$$(1) \quad z_{12} = \frac{\langle E_x^* E_x\rangle \langle E_y^* H_x\rangle - \langle E_x^* H_x\rangle \langle E_y^* E_x\rangle}{\langle E_x^* H_y\rangle \langle E_y^* H_x\rangle - \langle E_x^* H_x\rangle \langle E_y^* H_y\rangle}$$

From A-1a and A-1c

$$(2) \quad z_{11} = \frac{\langle E_x^* H_y\rangle \langle H_x^* E_x\rangle - \langle E_x^* E_x\rangle \langle H_x^* H_y\rangle}{\langle E_x^* H_y\rangle \langle H_x^* H_x\rangle - \langle E_x^* H_x\rangle \langle H_x^* H_y\rangle}$$

$$(2) \quad z_{12} = \frac{\langle E_x^* E_x\rangle \langle H_x^* H_x\rangle - \langle E_x^* H_x\rangle \langle H_x^* E_x\rangle}{\langle E_x^* H_y\rangle \langle H_x^* H_x\rangle - \langle E_x^* H_x\rangle \langle H_x^* H_y\rangle}$$

From A-1a and A-1d

$$(3) \quad z_{11} = \frac{\langle E_x^* H_y\rangle \langle H_y^* E_x\rangle - \langle E_x^* E_x\rangle \langle H_y^* H_y\rangle}{\langle E_x^* H_y\rangle \langle H_y^* H_x\rangle - \langle E_x^* H_x\rangle \langle H_y^* H_y\rangle}$$

$$(3) \quad z_{12} = \frac{\langle E_x^* E_x\rangle \langle H_y^* H_x\rangle - \langle E_x^* H_x\rangle \langle H_y^* E_x\rangle}{\langle E_x^* H_y\rangle \langle H_y^* H_x\rangle - \langle E_x^* H_x\rangle \langle H_y^* H_y\rangle}$$

From A-1b and A-1c

$$(4) \quad z_{11} = \frac{\langle E_y^* H_y\rangle \langle H_x^* E_x\rangle - \langle E_y^* E_x\rangle \langle H_x^* H_y\rangle}{\langle E_y^* H_y\rangle \langle H_x^* H_x\rangle - \langle E_y^* H_x\rangle \langle H_x^* H_y\rangle}$$

$$(4) \quad z_{12} = \frac{\langle E_y^* E_x\rangle \langle H_x^* H_x\rangle - \langle E_y^* H_x\rangle \langle H_x^* E_x\rangle}{\langle E_y^* H_y\rangle \langle H_x^* H_x\rangle - \langle E_y^* H_x\rangle \langle H_x^* H_y\rangle}$$

From A-1b and A-1d

$$(5)_{z_{11}} = \frac{\langle E_y^* H_y \rangle \langle H_y^* E_x \rangle - \langle E_y^* E_x \rangle \langle H_y^* H_y \rangle}{\langle E_y^* H_y \rangle \langle H_y^* H_x \rangle - \langle E_y^* H_x \rangle \langle H_y^* H_y \rangle}$$

$$(5)_{z_{12}} = \frac{\langle E_y^* E_x \rangle \langle H_y^* H_x \rangle - \langle E_y^* H_x \rangle \langle H_y^* E_x \rangle}{\langle E_y^* H_y \rangle \langle H_y^* H_x \rangle - \langle E_y^* H_x \rangle \langle H_y^* H_y \rangle}$$

Finally, from A-1c and A-1d

$$(6)_{z_{11}} = \frac{\langle H_x^* H_y \rangle \langle H_y^* E_x \rangle - \langle H_x^* E_x \rangle \langle H_y^* H_y \rangle}{\langle H_x^* H_y \rangle \langle H_y^* H_x \rangle - \langle H_x^* H_x \rangle \langle H_y^* H_y \rangle}$$

$$(6)_{z} = \frac{\langle H_x^* E_x \rangle \langle H_y^* H_x \rangle - \langle H_x^* H_x \rangle \langle H_y^* E_x \rangle}{\langle H_x^* H_y \rangle \langle H_y^* H_x \rangle - \langle H_x^* H_x \rangle \langle H_y^* H_y \rangle}$$

Similarly, solutions can be obtained for z_{21} and z_{22}.

Section A-I-2: Polarized and Unpolarized Impedance Estimates.

The effect of an unpolarized magnetotelluric field on the impedance estimates calculated in Section A-I-1 will now be considered.

If the magnetotelluric fields are unpolarized then $<H_x^* H_y>$, $<E_x^* E_y>$, $<E_x^* H_x>$, and $<E_y^* H_y>$ should tend to zero. The z_{11} and z_{12} impedance estimates will then have the form:

$$(1) \quad z_{11} \approx \frac{E_x}{H_x}$$

$$(1) \quad z_{12} \approx \frac{<E_x^* E_x>}{<E_x^* H_y>} = \frac{E_x}{H_y}$$

$$(2) \quad z_{11} \approx \frac{E_x}{H_x}$$

$$(2) \quad z_{12} \approx \frac{<E_x^* E_x>}{<E_x^* H_y>} = \frac{E_x}{H_y}$$

$$(3) \quad z_{11} - \text{indeterminate}$$

$$(3) \quad z_{12} - \text{indeterminate}$$

$$(4) \quad z_{11} - \text{indeterminate}$$

$$(4) \quad z_{12} - \text{indeterminate}$$

$$(5) \quad z_{11} \approx \frac{E_x}{H_x}$$

$$(5) \quad z_{12} \approx \frac{\langle H_y^* E_x \rangle}{\langle H_y^* H_y \rangle} = \frac{E_x}{H_y}$$

$$(6) \quad z_{11} \approx \frac{E_x}{H_x}$$

$$(6) \quad z_{12} \approx \frac{\langle H_y^* E_x \rangle}{\langle H_y^* H_y \rangle} = \frac{E_x}{H_y}$$

and similar expressions exist for z_{21} and z_{22}. Thus two of the estimates are unstable $(^{(3)}z, \; ^{(4)}z)$ and the four remaining estimates are stable and predict

$$z_{ij} = \frac{E_i}{H_j}.$$

Section A-I-3: The Effect of Noise on the Tensor Elements estimates.

The effect of incoherent recorded noise on the stable unpolarized impedance element estimates can be seen as follows:

Let: $E = E^{SIGNAL} + E^{NOISE} = E^S + E^n$

$H = H^{SIGNAL} + H^{NOISE} = H^S + H^n$

$\langle E^* E \rangle = \langle (E^S + E^n)^* (E^S + E^n) \rangle$

$= \langle E^{S*} E^S \rangle + \langle E^{S*} E^n \rangle + \langle E^{n*} E^S \rangle + \langle E^{n*} E^n \rangle$

and if the noise is truly incoherent,

$\langle E^* E \rangle = \langle E^{S*} E^S \rangle + \langle E^{n*} E^n \rangle.$

Similarly

$\langle H^* H \rangle = \langle H^{S*} H^S \rangle + \langle H^{n*} H^n \rangle.$

Also

$\langle E^* H \rangle = \langle (E^S + E^n)^* (H^S + H^n) \rangle$

$= \langle E^{S*} H^S \rangle + \langle E^{S*} H^n \rangle + \langle E^{n*} H^S \rangle + \langle E^{n*} H^n \rangle$

$= \langle E^{S*} H^S \rangle$

Therefore

$$^{1,2}Z_{12}, \quad \frac{\langle E_x^* E_x \rangle}{\langle E_x^* H_y \rangle} = \frac{\langle E_x^{S*} E_x^S \rangle + \langle E_x^{n*} E_x^n \rangle}{\langle E_x^{S*} H_y^S \rangle}$$

and

$$^{5,6}Z_{12}, \quad \frac{\langle H_y^* E_x \rangle}{\langle H_y^* H_y \rangle} = \frac{\langle H_y^{S*} E_x^S \rangle}{\langle H_y^{S*} H_y^S \rangle + \langle H_y^{n*} H_y^n \rangle}$$

since

$$z_{12} = \frac{E_x}{H_y} \text{ represents the true impedance element in an}$$

unpolarized field, then:

$$^{1,2}z_{12}' = z_{12}\left\{ 1 + \frac{\langle E_x^{n*} E_x^{n} \rangle}{\langle E_x^{s*} E_x^{s} \rangle} \right\}$$
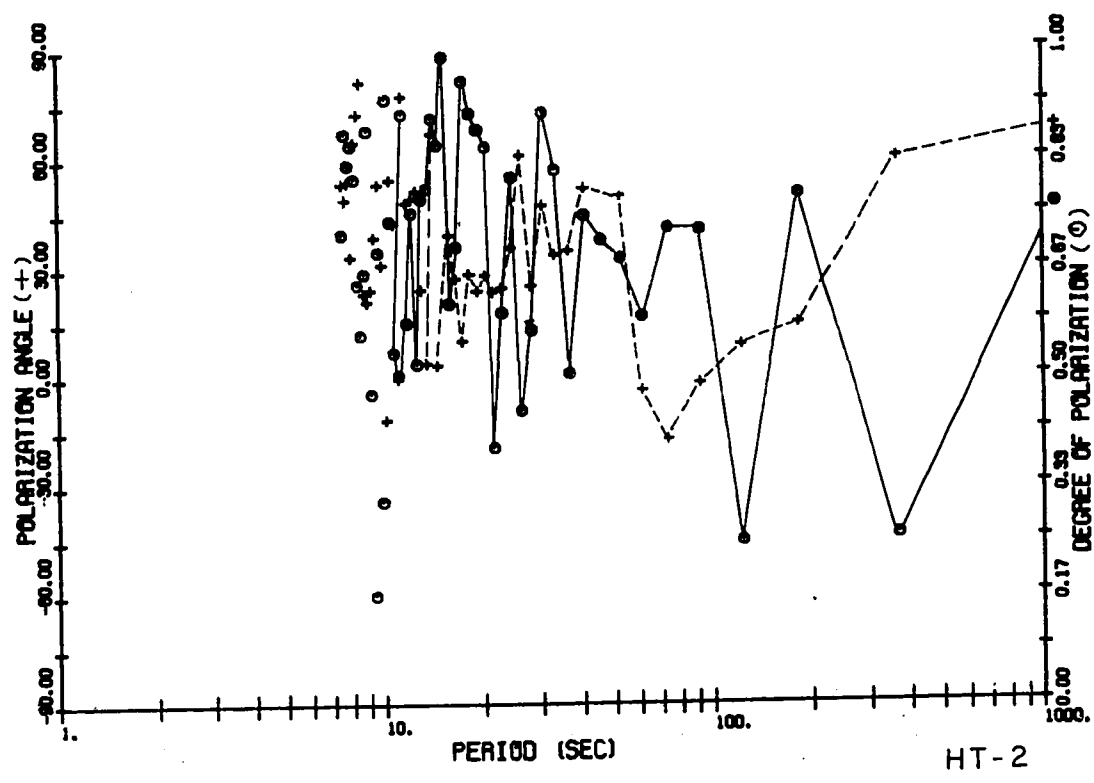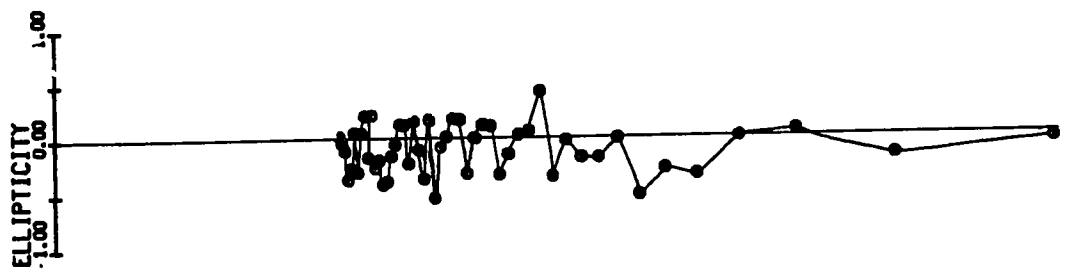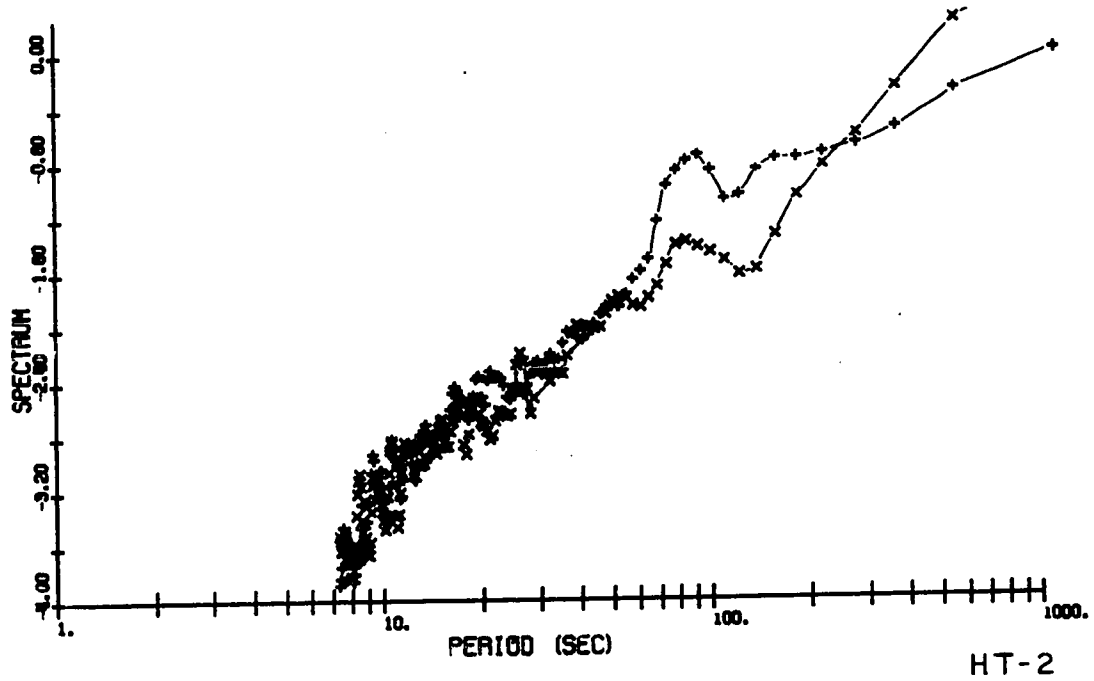
and

$$^{5,6}z_{12}' = z_{12} \bigg/ \left\{ 1 + \frac{\langle H_y^{n*} H_y^{n} \rangle}{\langle H_y^{s*} H_y^{s} \rangle} \right\}$$

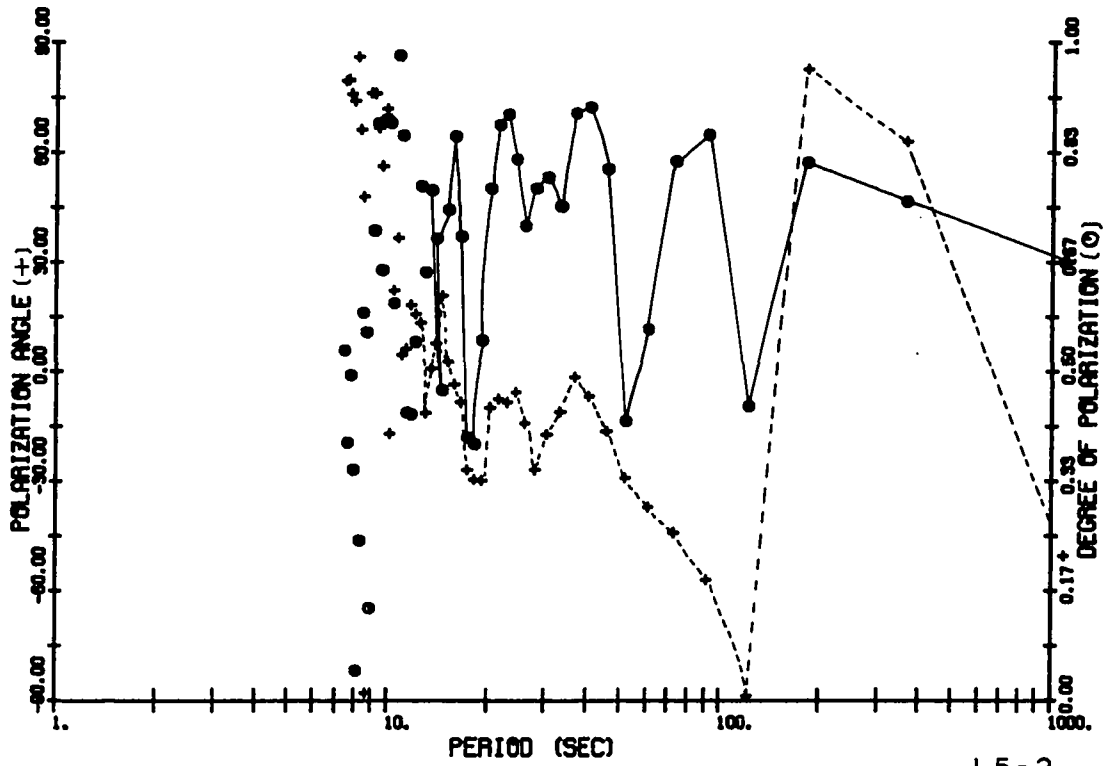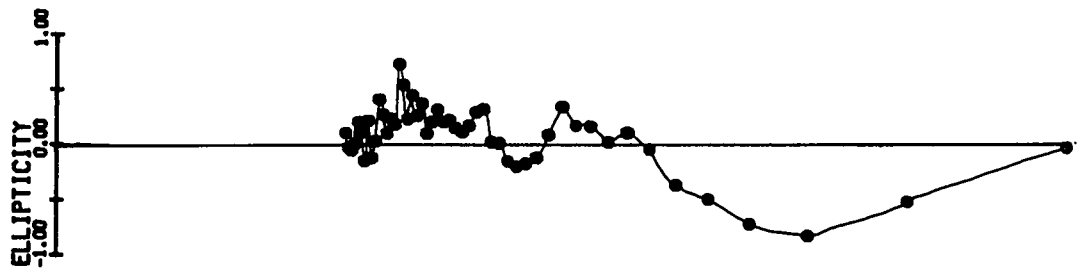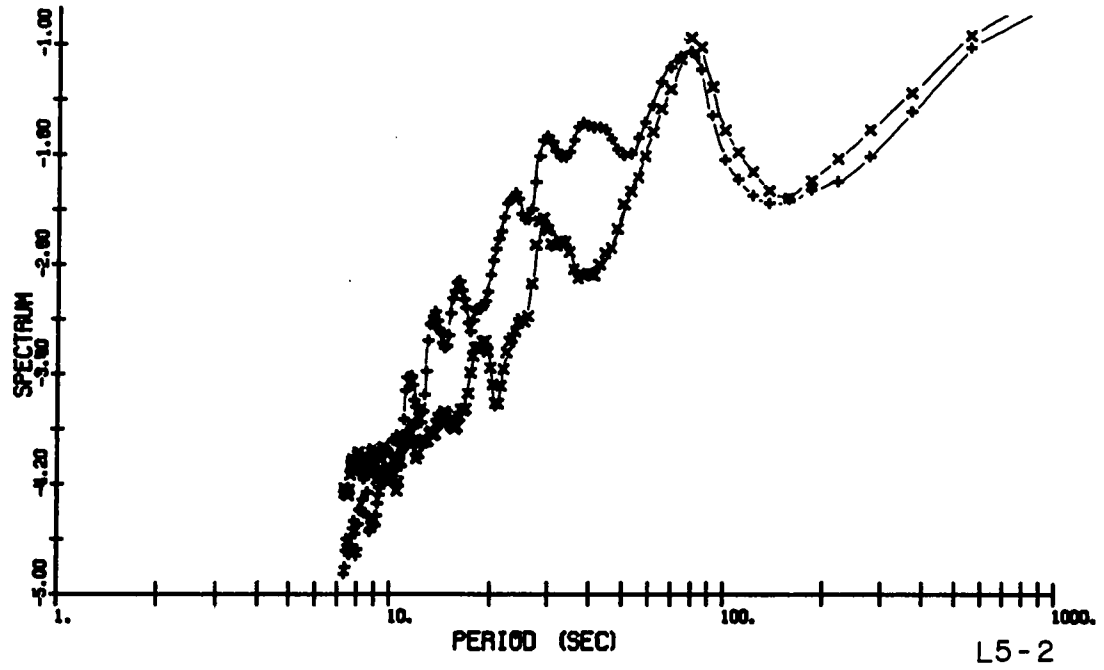Therefore it can be seen that if the magnetotelluric fields are unpolarized, then $^{1,2}z_{12}'$ gives a biased estimate greater than the true value of the impedance element z_{12} due to recorded electric noise while $^{5,6}z_{12}'$ gives a low biased estimate of z_{12} due to recorded magnetic noise. The z_{21} estimates are effected in a similar manner.
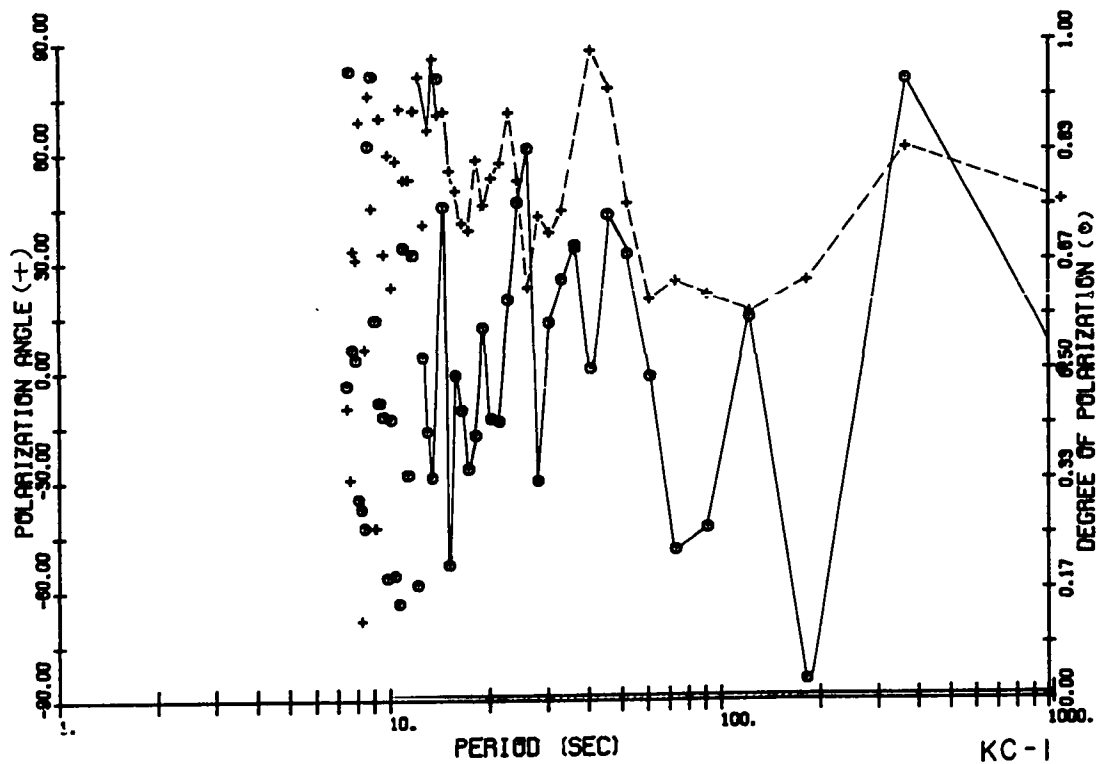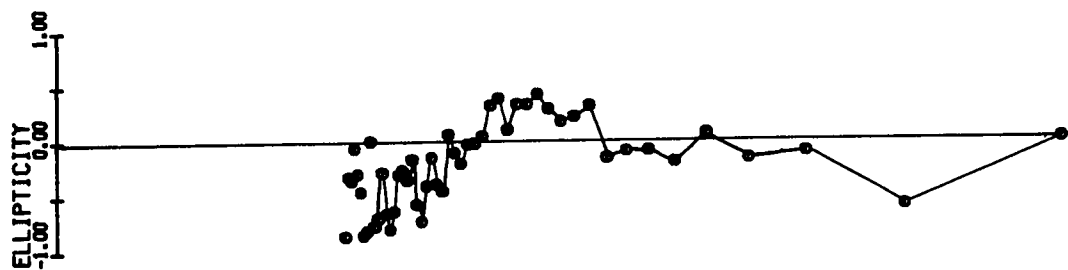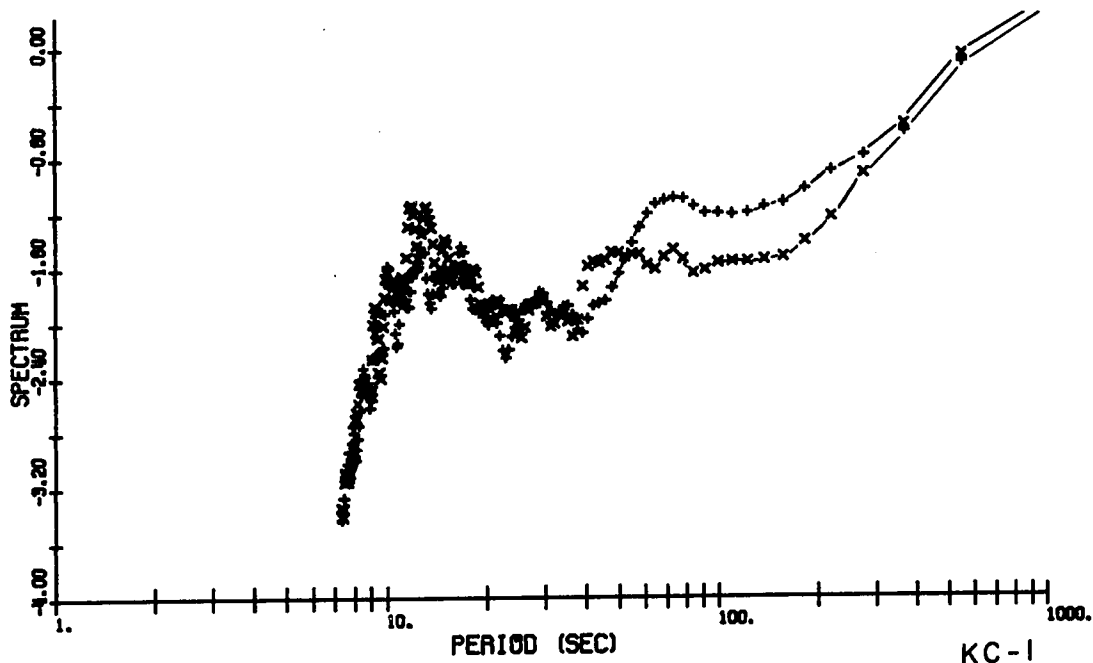
This appendix shows the general form of the magnetic power spectra and the magnetic polarization characteristics for data collected in this survey. The power spectra for Hx and Hy (non-rotated) as presented are instrument pre-whitened spectra (see Chapter 3) and thus are not the actual power spectra in γ^2/Hz. The Hx spectra is denoted by + and the Hy spectra denoted by x.
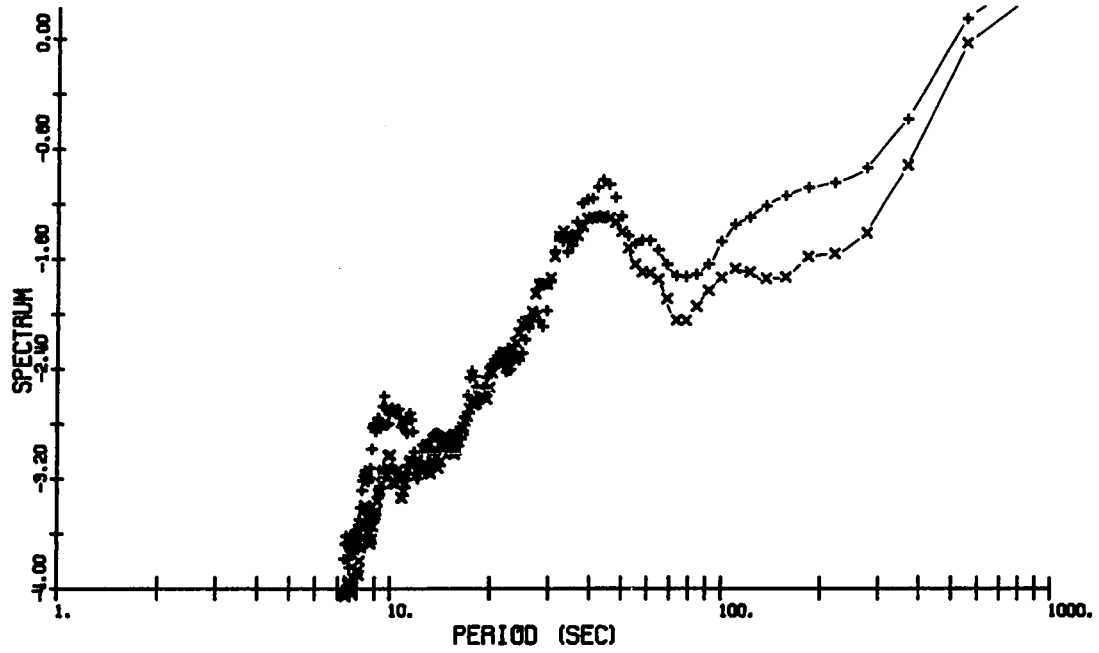
The polarization characteristics of the geomagnetic micropulsations were digitally determined using a quasi-monochromatic wave train theory of physical optics combined with spectral analysis as outlined by Fowler et al (1967). The angle of polarization and the ellipticity are thus calculated for the polarized portion of the signal. The polarization angle is shown as a dashed line and the degree of polarization is a solid line.
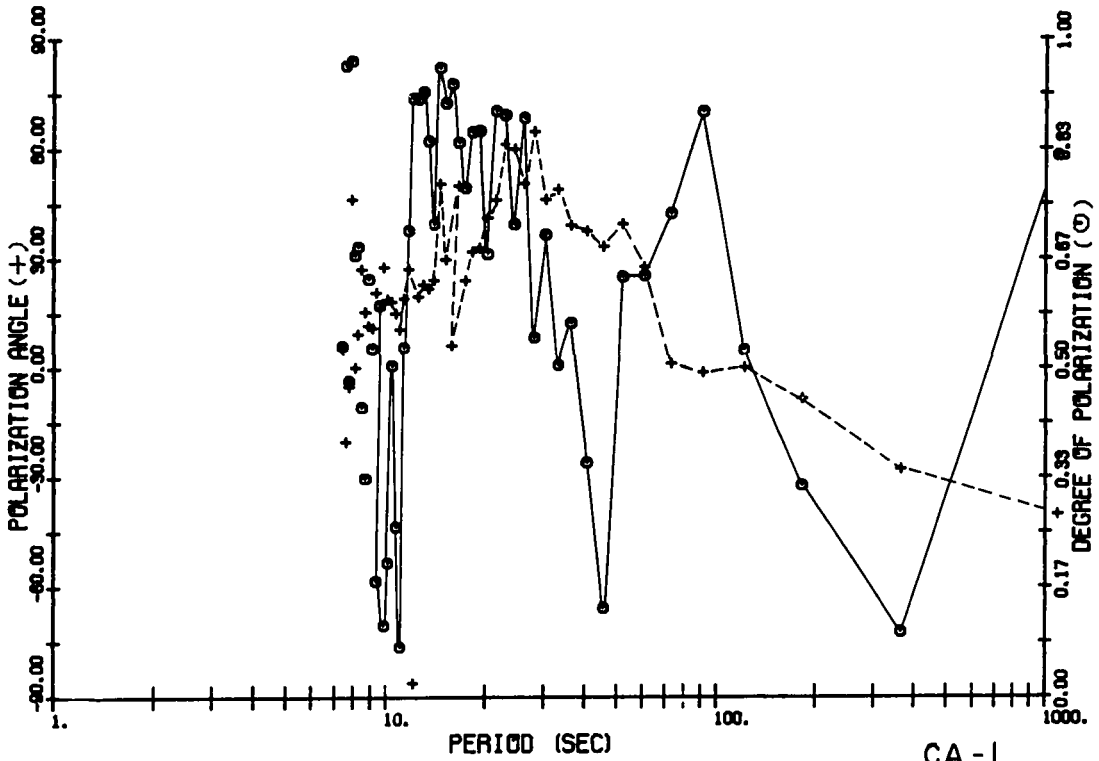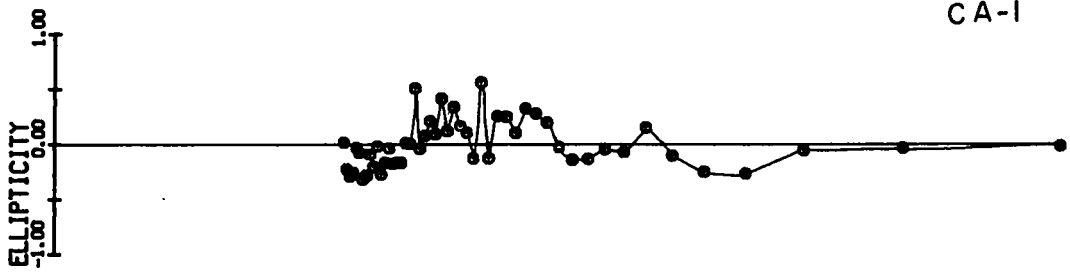
RD-2

RD-2

HT-2

HT-2

SPECTRUM

PERIOD (SEC)

L5-2

ELLIPTICITY

POLARIZATION ANGLE (+)

DEGREE OF POLARIZATION (⊙)

PERIOD (SEC)

L5-2

KC-1

CA-I

CA-I

1291.

TU-2

TU-2